Subaerial volcaniclastic deposits – influences of initiation mechanisms and transport behaviour on characteristics and distributions

Jon J. Major

US Geological Survey, Volcano Science Center, Cascades Volcano Observatory, Vancouver, Washington, USA

0000-0003-2449-4466

Correspondence: jjmajor@usgs.gov

Abstract: Subaerial volcaniclastic deposits are produced principally by volcanic debris avalanches, pyroclastic density currents, lahars, and tephra falls. Those deposits have widely ranging geomorphic and sedimentologic characteristics; they can mantle, modify, or create new topography, and their emplacement and subsequent reworking can have an outsized impact on the geomorphic and sedimentologic responses of watersheds surrounding, and channels draining, volcanoes. Volcaniclastic deposits provide a wealth of information about eruptive histories, volcanic processes, and landscape responses to eruptions. The volcanic processes that produce these deposits, and consequently the character and sedimentary structures of the deposits themselves, are influenced by initiation mechanism. Deposit preservation is affected by deposit magnitude, texture, and composition, depositional environment, and climate regime. Innovative analyses of deposits from several modern eruptions and advancements in physical and numerical modelling have vastly improved our understanding of volcanic processes, interpretations of eruptive histories, and recognition of the hazards posed by volcanic eruptions. This contribution highlights and summarizes major advances that have occurred in the past few decades in understanding of volcaniclastic deposits and linkages with volcanic processes.

Volcanic eruptions, and associated volcanic processes, can generate vast amounts of sediment that can mantle, modify, or create new topography (e.g. Manville *et al.* 2009*a*). Over common lifespans of stratovolcanoes and volcanic centres (*c.* 10^5–10^6 years), deposition and reworking of volcaniclastic sediment greatly affects surrounding terrain (Fig. 1). Depending on the nature of the volcanic processes, local topography, and climate, much of that sediment can remain in subaerial storage for spans of 10^4–10^5 years and some will pass into the geological record over time spans of 10^6–10^7 years (e.g. Roche *et al.* 2016). Volcaniclastic sediments stored over spans of 10^3–10^4 years commonly serve as the basis for understanding pertinent volcanic eruption histories and hazards of concern to society, and for deducing influences of volcanism and climate on sedimentary responses to eruptions. Longer time spans are needed to appreciate tectonic influences on sedimentary responses and storage (e.g. Smith 1991).

In this paper, I examine the influence of the nature of volcanic processes, and their initiation mechanisms and transport, on the character, storage, and preservation of volcaniclastic sediment. It is important to understand how volcanic processes, in conjunction with external influences such as glaciation and fluvial, colluvial, and aeolian reworking, affect volcaniclastic sediment because deposit characteristics and preservation strongly affect our perceptions of the eruptive histories of volcanoes and the hazards they pose. There are many excellent reviews of volcanic processes and deposits (e.g. Fisher and Schmincke 1984; Cas and Wright 1987; Fisher and Smith 1991; Branney and Kokelaar 2002; Ayris and Delmelle 2012; Bonadonna *et al.* 2015; Brown and Andrews 2015; Dufek *et al.* 2015; Houghton and Carey 2015; Vallance and Iverson 2015; Lube *et al.* 2020; Thouret *et al.* 2020; Roverato *et al.* 2021) as well as reviews of the hydrogeomorphic and sedimentologic responses to eruptions (e.g. Manville *et al.* 2007, 2009*a*; Manville 2010; Pierson and Major 2014). Those reviews delve far more deeply into processes and deposits than is possible here. My intention with this paper is to provide a high-level synthesis of major volcanic processes and deposits that compares and contrasts their characteristics and examines how initiation mechanisms and transport can affect the morphology, sedimentology, and distributions of that sediment. Despite extensive work done on submarine eruptions and their deposits, I focus solely on

From: Di Capua, A., De Rosa, R., Kereszturi, G., Le Pera, E., Rosi, M. and Watt, S. F. L. (eds) 2023. *Volcanic Processes in the Sedimentary Record: When Volcanoes Meet the Environment*. Geological Society, London, Special Publications, **520**, 29–100.
First published online July 12, 2022, https://doi.org/10.1144/SP520-2021-142

Fig. 1. Pre-1980 topographic map of Mount St Helens (USA) showing proximal distribution of debris-avalanche, pyroclastic-density-current, lahar, and lava-flow deposits (dashed lines). Base is a composite of pre-1980 US Geological Survey topographic quadrangle maps from 1919. Modified from Clynne *et al.* (2008).

subaerial volcanism and deposition. Furthermore, I focus on processes and deposits associated with eruptions of stratovolcanoes v. eruptions and deposits from more distributed effusive volcanism and mafic cinder cones. Neither do I delve into hydrovolcanism or eruptions of maars, except for occasional brief mention. In the sections to follow, I discuss the major volcanic processes that generate and deliver volcaniclastic sediment during explosive and effusive eruptions – namely volcanic debris avalanches, pyroclastic density currents (PDCs – a generalized term for pyroclastic flows and surges), lahars, and tephra fall – as well as redistribution of that sediment following an eruption.

Several, and sometimes contradictory, terminological schemes have been proposed and used to describe volcanic sediment (see Fisher and Schmincke 1984; White and Houghton 2006; Manville *et al.* 2009*a*). I use the term volcaniclastic in a broad sense to refer to primary deposits that result from eruptive processes (see White and Houghton 2006; Manville *et al.* 2009*a*). Pyroclastic refers to

primary clastic particles formed by volcanic explosions or other fragmentation processes. Some particles in volcaniclastic deposits are eroded from volcanic-conduit walls and, although they are not juvenile particles related to fresh magma, they can be volcanic particles. I do not assign any specific term to such particles but note their potential presence as needed. Other particles in volcaniclastic deposits are eroded along transport paths, and they may be of volcanic or non-volcanic origin. I call out such particles as necessary, but again assign no specific term to them. Primary deposits are those resulting directly from a specific eruption-related volcanic process without having been temporarily stored and subsequently remobilized. During and after deposition, primary deposits may be reprocessed or reworked (e.g. Sohn and Sohn 2019). Deposits of reworked sediment can have characteristics similar to primary deposits, making distinctions difficult. Where deposits have clearly resulted from processes not directly related to eruptions, yet retain characteristics of primary eruption deposits, I refer to them with the prefix 'secondary' (for example, secondary lahars). Several authors use the term epiclastic to refer to deposits that result from sedimentation by water regardless of the origin of the sedimentary fragment (see Manville *et al.* 2009*a*), but in this chapter I avoid this term. Here, I restrict discussion to subaerial volcanism and sedimentation (thus avoiding complications that may arise from terminology involving explosive submarine eruptions), and I further use descriptive phrasing, such as fluvially reworked and deposited sediment, rather than more ambiguous phrasing like epiclastic. The reader is referred to Fisher and Schmincke (1984), White and Houghton (2006), Manville *et al.* (2009*a*), Sohn and Sohn (2019), and Di Capua *et al.* (2022) for more detailed discussions of terminology. Specific volcanic processes also have their own nomenclature (e.g. block facies, bulking, hyperconcentrated flow, megaclasts, surge, etc.), which is defined and used as needed.

Volcanology has a common, but non-intuitive, language for describing and classifying grain-size characteristics of primary volcaniclastic sediment (White and Houghton 2006). In general, particles are classified as volcanic ash, lapilli, blocks and bombs (Table 1). Many sedimentologists, however, use the Wentworth (1922) classification system, which describes particle sizes as clay, silt, sand, granule, pebble, and cobble with various descriptive modifiers (e.g. fine, coarse, etc.). Modern descriptions of debris-avalanche and lahar deposits commonly use sedimentological grain-size terms, whereas descriptions of PDC and tephra-fall deposits typically use volcanological terms. Herein, I retain these conventions for consistency with the literature even though it may make some discussions appear inconsistent. Table 1 lists common volcanological and sedimentological grain-size terms.

In addition to grain-size characteristics, deposit sorting (σ), or the degree of segregation of grains of different sizes, is also used to characterize volcaniclastic deposits. Deposits that consist largely of grains of uniform size are considered very well sorted, whereas those that consist of a broad mixture of grain sizes are considered very poorly sorted. As with grain sizes, sometimes there are differences in the ways that volcanologists and sedimentologists describe deposit sorting (e.g. Cas and Wright 1987). Sorting is based on the deviation of the grain-size distribution about a mean size. Two sets of

Table 1. *Grain-size terminology for volcaniclastic sediment*

Grain size		Primary volcaniclastic deposit	Sedimentary deposit†
(phi)*	(mm)		
>4	<0.63	Extremely fine ash	Silt and Clay
3–4	0.63–0.125	Very fine ash	Very fine sand
2–3	0.125–0.25	Fine ash	Fine sand
1–2	0.25–0.50	Medium ash	Medium sand
0–1	0.50–1	Coarse ash	Coarse sand
−1 to 0	1–2	Very coarse ash	Very coarse sand
−2 to −1	2–4	Fine lapilli	Granule
−4 to −2	4–16	Medium lapilli	Pebble
−6 to −4	16–64	Coarse lapilli	Pebble
−6 to −8	64–256	Block/bomb	Cobble
<−8	>256	Block/bomb	Boulder

Modified from White and Houghton (2006).

*The dimensionless phi scale is a logarithmic transformation of the Wentworth (mm) scale. By definition, $\varphi = -\log_2(d/d_0)$, where d is particle diameter in mm and d_0 is a reference particle diameter (1 mm).

†Particles larger in diameter than sand (larger than 2 mm) are generically referred to as gravel.

Table 2. *Sorting terminology typically used in descriptions of deposits*

Sorting value (σ)	Primary volcaniclastic deposit	Sedimentary deposit
0–1	Very well sorted	Very well to moderately sorted
1–2	Well sorted	Poorly sorted
2–4	Poorly sorted	Very poorly sorted
>4	Very poorly sorted	Extremely poorly sorted

From Cas and Wright (1987).

definitions for this parameter are commonly used: (1) the Inman (1952) graphical standard deviation, defined as $\sigma_\varphi = (\varphi_{84} - \varphi_{16}/2)$, where φ_{84} and φ_{16} are the 84th and 16th percentile phi-scale grain sizes, respectively, and (2) the inclusive graphic standard deviation defined by Folk and Ward (1957) as $\sigma_I = ((\varphi_{84} - \varphi\sigma_{16}/4) + (\varphi_{95} - \varphi\sigma_5/6.6))$, where φ_{95} and φ_5 are the 95th and 5th percentile phi-scale grain sizes, respectively. Regardless of the method used, sedimentologists (and some volcanologists, e.g. White and Houghton 2006) commonly consider deposits having sorting values less than 1 to be very well to moderately sorted and those greater than 1 to be poorly to extremely poorly sorted (Folk and Ward 1957). In contrast, volcanologists sometimes broaden those descriptive categories such that sorting values less than 2 are considered well sorted and those greater than 2 are considered poorly to very poorly sorted (e.g. Cas and Wright 1987) (see Table 2). In this paper, I have adopted the sedimentologists' perspective.

Volcanic processes that generate sediment

Volcanic processes that generate volcaniclastic sediment occur on a variety of scales. Debris-avalanche and PDC deposits can mantle, modify or create new topography. Lahar deposits can bury valley floors and lowland alluvial fans or thinly drape narrow corridors along river channels. Tephra-fall deposits mantle topography but can do so over thousands to tens of thousands of square kilometres. This variety of fill and areal coverage influences the effects of these events on the landscape as well as their subsequent erosion and preservation potential.

Volcanic debris avalanche

Contrary to outward appearances, many volcanoes are perched delicately on the landscape. They commonly consist of stratigraphic mixtures of volcaniclastic sediment, lava flows, and lava domes, which are sometimes highly altered. In some settings the stratigraphic mixtures include glacial sediment. As a result, many volcanoes have grown and collapsed repeatedly over millennia (e.g. Hausback and Swanson 1990; Belousova and Belousov 1995; Cronin *et al.* 1996; Calvari *et al.* 1998; Belousov *et al.* 1999; Cantagrel *et al.* 1999; Tibaldi 2001; Alloway *et al.* 2005; Pareschi *et al.* 2006; Waitt and Begét 2009; Roverato *et al.* 2011; Zernack *et al.* 2011; Tost *et al.* 2015; Cortés *et al.* 2019; Dufresne *et al.* 2021*a*; Zernack and Procter 2021). This tendency for volcanoes to collapse is ubiquitous (e.g. McGuire 1996; Dufresne *et al.* 2021*a*); nearly 600 volcanoes worldwide exhibit evidence of large-scale collapse (Siebert and Roverato 2021). Volcanic collapses can range from segments of lava domes to large sectors of a volcano (Fig. 2). The latter, which can range in size from tenths to hundreds of cubic kilometres, are referred to as volcanic debris avalanches (Voight 1981; Siebert 1984; Glicken 1996; McGuire 1996; Collot *et al.* 2001; Dufresne *et al.* 2021*a*; Siebert and Roverato 2021).

Debris avalanches can greatly alter the morphology of a volcano (Fig. 3). In general, the volume of material composing a debris-avalanche deposit is comparable to the volume of material 'missing' from a volcano. As a result, debris avalanches typically form an 'avalanche crater' (Siebert 1984), commonly manifest as a large, horseshoe-shaped breach of the volcano (Fig. 3a, b). These craters are typically a few kilometres wide, slightly longer in the direction of the breach, and many hundreds of metres deep (Siebert 1984). Ancient volcanic debris avalanches may not easily correlate with present volcano morphology as subsequent eruptions may fill and erase the scar (Fig. 3c, d).

Debris avalanches are exceptionally mobile and can affect large swaths of landscape (Fig. 4). Typically, the horizontal runout distance (L) of a debris avalanche is 5 to 10 times that of its vertical (H) drop ($H/L \sim 0.1$–0.2) (Siebert 1984). Depending on failure size, local topography, and source material characteristics, debris avalanches can travel as little as a few kilometres from a volcano to many tens of kilometres and cover many tens to many hundreds of square kilometres (e.g. Voight 1981; Voight *et al.* 2002; Crandell *et al.* 1984; Wadge *et al.* 1995). They can surmount topographic barriers many tens to hundreds of metres tall (e.g. Voight 1981; Stoopes and Sheridan 1992) and flow across shallowly sloping terrain (e.g. Kelfoun *et al.* 2008). Estimated emplacement velocities are many tens of metres per second (e.g. Voight 1981; Stoopes and Sheridan 1992).

Historical debris avalanches have commonly been associated with magmatic or phreatic eruptions,

Fig. 2. Mount St Helens (USA) debris avalanche of 18 May 1980. Photograph © G. Rosenquist.

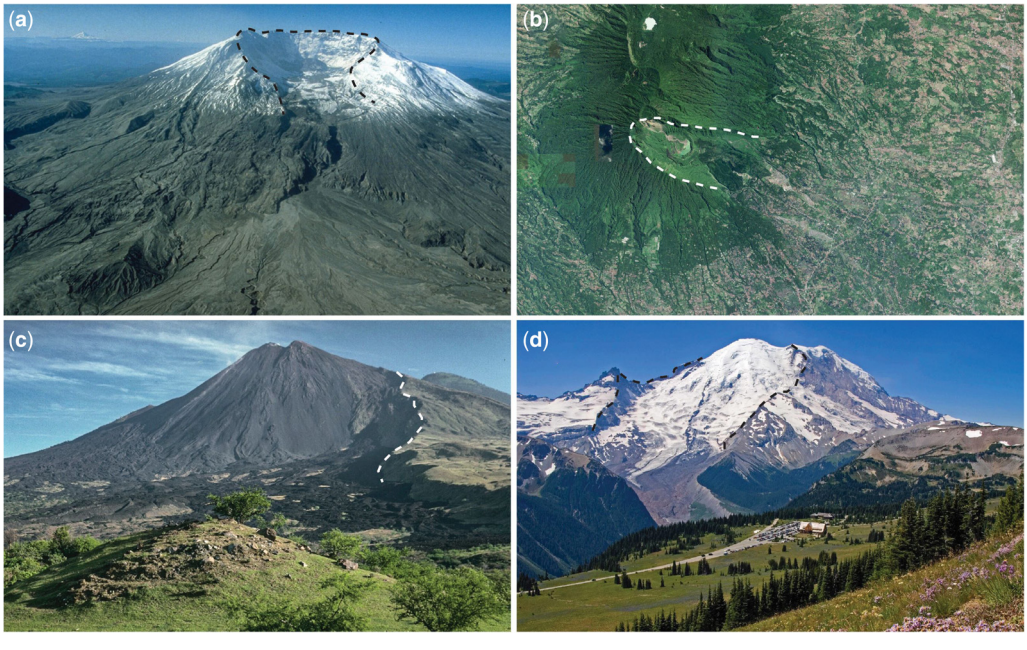

Fig. 3. Volcanic debris avalanches typically form an avalanche crater (delineated by dashed lines), commonly manifest as a large, horseshoe-shaped breach of the volcano. (**a**) Mount St Helens (USA). Photograph by T. Leighley, USGS. (**b**) Galunggung volcano (Indonesia). Google Earth image. Subsequent regrowth of a volcano can obscure prior avalanche craters. (**c**) Pacaya volcano (Guatemala). Photograph by L. Siebert, Smithsonian Institution. (**d**) Mount Rainier (USA). Photograph by J. Chao, National Park Service.

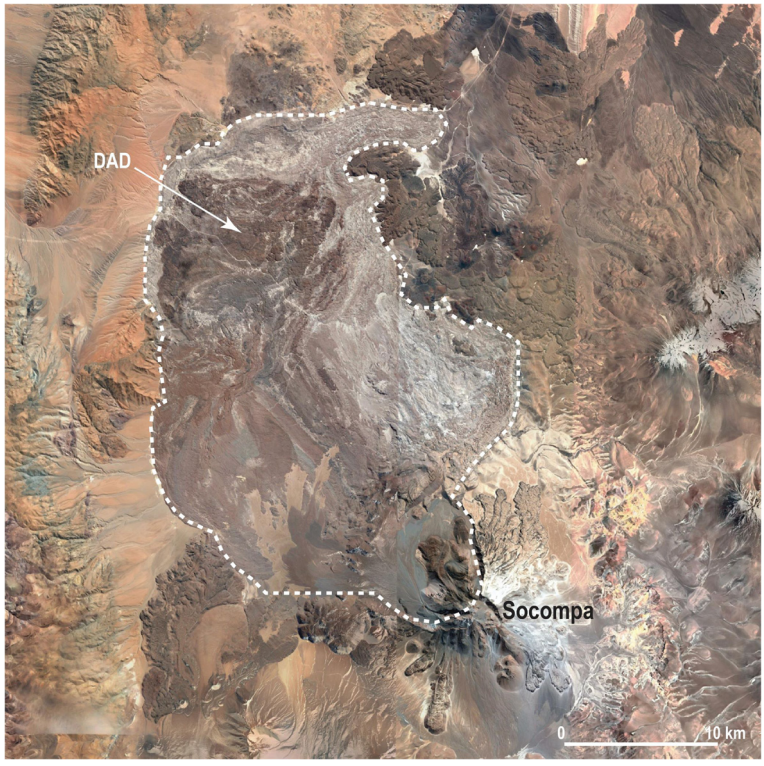

Fig. 4. Google Earth image of debris-avalanche deposit (DAD) from Socompa volcano (Chile). Note the exceptional mobility and area covered by this deposit (highlighted by dashed line), for which H/L ~0.08 (Siebert 1984).

although some may have occurred without an associated eruption (Siebert 1984; Aguila *et al.* 1986; Siebert *et al.* 1987; Paguican *et al.* 2012). If magma intrudes high into a volcanic edifice or is otherwise near the surface of the failure plane when a debris avalanche occurs, the decapitation of the volcano can trigger a magmatic explosion. Such decapitation can produce a violent, laterally directed or low-angle explosion and consequent PDC commonly referred to in the literature since 1980 as a lateral blast, directed blast, or blast PDC (Gorshkov 1959; Hoblitt *et al.* 1981; Waitt 1981; Siebert *et al.* 1987; Belousov 1996; Hoblitt 2000; Sparks *et al.* 2002; Belousov *et al.* 2007, 2020). Laterally directed PDCs associated with such events (see the section 'Directed explosion') can be highly energetic, sweep broadly across rugged topography, and devastate hundreds of square kilometres of landscape (e.g. Lipman and Mullineaux 1981, pl. 1; Bogoyavlenskaya *et al.* 1985; Belousov *et al.* 2007). On the basis of deposit characteristics and stratigraphic associations (see the sub-section 'Deposit characteristics' in the 'Pyroclastic density current' section), directed blasts have been inferred to have occurred in association with some prehistoric debris avalanches (Boudon *et al.* 1984; Francis *et al.* 1985; Siebert *et al.* 1995). Even in the absence of a directed blast, magmatically involved eruptions associated with debris avalanches have produced (Plinian) eruption plumes, PDCs, and subsequent lava domes (e.g. Katsui and Yamamoto 1981; Belousov 1995; Belousova and Belousov 1995; Belousov *et al.* 1999, 2020; Cutler *et al.* 2022). Variations in eruptive behaviour following collapse-driven unloading reflect variations in amounts of eruptible magma, magma storage, and modifications to pressurization of the magma reservoir (Pinel and Albino 2013; Watt 2019). Debris avalanches can also be associated with phreatic explosions that do not involve a magmatic component (Sekiya and Kikuchi 1889; Siebert 1984; Johnson 1987; Siebert *et al.* 1987; Yamamoto *et al.* 1999; Pinel and Albino 2013; Day *et al.* 2015). In those instances, phreatic eruptions occurred when pressure on hydrothermal fluids within the volcano was released suddenly by the debris avalanche. These types of debris-avalanche-triggered phreatic eruptions may also induce laterally directed explosions and PDCs that can devastate the surrounding area.

Precursory activity at some historical eruptions involving debris avalanches has included elevated seismicity, deformation, and minor eruptions (Siebert *et al.* 1987). However, some volcanoes may show little precursory activity or departure from prior styles of activity before an avalanche occurs. At Bandai volcano (Japan), its 1888 debris avalanche and eruption were preceded by substantial seismic unrest, which may have been related to deep magma movement. But it has been inferred that the debris avalanche was triggered by an earthquake well before magma had moved into the edifice (Siebert *et al.* 1987; Yamamoto *et al.* 1999). In 2018, Anak Krakatau (Indonesia) had been active for 6 months prior to flank collapse, but there were no changes in eruptive behaviour that might have signalled incipient failure immediately prior to collapse and consequent formation of a devastating tsunami (Perttu *et al.* 2020; Cutler *et al.* 2022).

Not all debris avalanches induce eruptions. For example, although Unzen volcano (Japan) was active in the late 1700s CE, a debris avalanche occurred on an older part of the volcanic complex at nearby Mayu-yama volcano during an earthquake (in 1792 CE), and this avalanche is not known to have been associated with any explosive activity (Katayama 1974; Siebert *et al.* 1987).

Volcanic debris avalanches pose multiple threats. (1) Because of their size and mobility, debris avalanches pose a severe hazard near volcanoes. They can also pose a hazard far from volcanoes if they are particularly mobile. Their mass and momentum are likely to crush all infrastructure within their paths, and their ability to surmount tall physical barriers minimizes topographic protections. (2) They are commonly associated with explosive eruptions and can trigger complementary volcanic processes (e.g. Hoblitt 2000; Belousov *et al.* 2020), such as PDCs that can sweep beyond the boundaries of the debris avalanche. (3) Debris avalanches from coastal, island, or submarine volcanoes can generate devastating tsunamis (Clark 1977; Katsui and Yamamoto 1981; Moore and Moore 1984; Siebert 1984; Johnson 1987; Tsuji and Hino 1993; Siebert *et al.* 1995; Belousova and Belousov 1995; Satake and Kato 2001; Ward and Day 2003; Giachetti *et al.* 2011; Tinti *et al.* 2011; Paris *et al.* 2014; Day *et al.* 2015; Paris 2015; Sassa *et al.* 2016; Grilli *et al.* 2019; Ye *et al.* 2020). (4) Owing to variations in size, volcanic debris avalanches can mantle or modify existing topography. If sufficiently large they can completely bury existing topography and form new topography. They can block tributary channels and lake outlets, enlarging existing lakes or forming new ones where none existed (Janda *et al.* 1984; Siebert 1984; Meyer *et al.* 1986; Lagmay *et al.* 2000; Pulgarín *et al.* 2001; Waythomas 2001; Capra 2007, 2011; Capra *et al.* 2002; Capra and Macías 2002; Clavero *et al.* 2002). (5) Some debris avalanches, particularly those containing substantial quantities of hydrothermally altered material or those that are particularly wet, can transform directly to lahars. Such transformations, although rare, can extend destruction far from a volcano (e.g. Carrasco-Núñez *et al.* 1993; Vallance and Scott 1997; Capra and Macías 2000; Detienne *et al.* 2017). (6) Subsequent to emplacement, debris avalanches are a source of sediment that, when reworked, poses severe and lasting societal consequences downstream (e.g. Lehre *et al.* 1983; Schuster 1983; Major *et al.* 2000, 2018, 2020; Major 2020). Although debris avalanches are infrequent events at individual volcanoes, on a global basis they have occurred historically a few times per century (Siebert 1984; Dufresne *et al.* 2021*a*).

Initiation mechanisms. Volcanic debris avalanches can form in many ways. Principal initiation mechanisms include: (1) failure owing to magmatic intrusion; (2) failure caused by an earthquake; (3) failure resulting from gradual weakening of an edifice caused by hydrothermal alteration; (4) failure from gradual weakening caused by slope loading; (5) failure of the volcano's substrate; or (6) failure caused by peripheral erosion or debuttressing of a volcano (e.g. Elsworth and Voight 1996; McGuire 1996; van Wyk de Vries and Francis 1997; Voight and Elsworth 1997; van Wyk de Vries *et al.* 2001; Reid *et al.* 2001, 2010; Reid 2004; Paguican *et al.* 2012; Siebert and Roverato 2021). Magmatic intrusions elevate pore-fluid pressures both mechanically and thermally, thus weakening the strength of volcanic rock. Deformation caused by intrusion can steepen volcano flanks, increasing the shear stress exerted on potential slip surfaces within the edifice. These complementary processes can destabilize an edifice and increase the possibility of a large, deep-seated failure (Day 1996; Elsworth and Voight 1996; Voight and Elsworth 1997; Reid 2004). Magmatic intrusions also increase the rate and magnitude of earthquakes, which can generate transient stresses that exceed weakening rock strength and precipitate failure. Over the longer term, hydrothermal alteration gradually weakens segments of a volcano making it more susceptible to failure (e.g. van Wyk de Vries and Francis 1997; Capra and Macías 2000; Reid *et al.* 2001, 2010; Vallance 2005). Stresses on and within a volcano can increase through gradual loading of a volcano slope by repeated extrusion of lava, and the increasing stresses can lead to edifice failure. Gravitational loading of a weak substrate beneath a volcano owing to the weight of a volcano can lead to failure. Loading of substrate materials composed of older, weathered materials, hydrothermally weakened materials, or weak sediments (such as lake sediments) can lead to slow lateral

spreading and eventual structural failure of the substrate, which can cause catastrophic failure of the overlying volcano (van Wyk de Vries and Francis 1997; van Wyk de Vries *et al.* 2001; Cecchi *et al.* 2005). Peripheral erosion at the land–sea interface of coastal and island volcanoes and debuttressing of volcanoes by deglaciation can lead to gradually increasing stresses in an edifice (e.g. Roberti *et al.* 2018). Changing sea levels (in particular sea-level rises) can affect pore-fluid pressures within an edifice and lead to gradual weakening of rock strength (e.g. McGuire 1996).

Deposit morphology. The surfaces of volcanic debris-avalanche deposits commonly are dotted with numerous distinctive mounds known as hummocks or hillocks (e.g. Ui 1983; Siebert 1984; Crandell 1989; Palmer and Neall 1989; Glicken 1996; van Wyk de Vries and Davies 2015; Dufresne *et al.* 2021*b*; Siebert and Roverato 2021) (Fig. 5). These mounds can range in height from a few metres to more than 100 m and have diameters from a few to a few hundreds of metres (e.g. Siebe *et al.* 1992; Glicken 1996; Romero *et al.* 2022). Over time, these mounds may become more gently rounded and surfaces between mounds filled and flattened. The origin of this distinctive morphology was debated for many decades prior to the 1980 eruption of Mount St Helens (USA). Before 1980, these mounds were hypothesized to represent glacial deposits, phreatic 'blisters' on the surfaces of gas-rich lava flows, independent volcanic vents, results of landslides or lahars, or even anthropogenic features (Siebert 1984). Following the 1980 Mount St Helens eruption, it became clear that such mounds are a distinctive feature of volcanic debris avalanches. Voight *et al.* (1981) attributed them to horsts developed in an extending sheet of debris. Glicken (1996) attributed some, especially in distal parts of the deposit, to transport of individual large clasts. Paguican *et al.* (2014) conducted scaled analogue experiments and showed hummocks formed initially by extensional faulting during avalanche motion. They also showed that hummock size depends on position within the flowing mass, and that size can be modified as hummocks disintegrate and coalesce during motion. In their experiments, small hummocks tended to populate the avalanche front whereas larger hummocks remained closer to source, consistent with characteristics of hummocks in natural deposits (Glicken 1996; Yoshida *et al.* 2012; Yoshida 2013). Field studies by Shea *et al.* (2008) of debris-avalanche deposits emplaced over nearly flat, unconfined topography revealed a

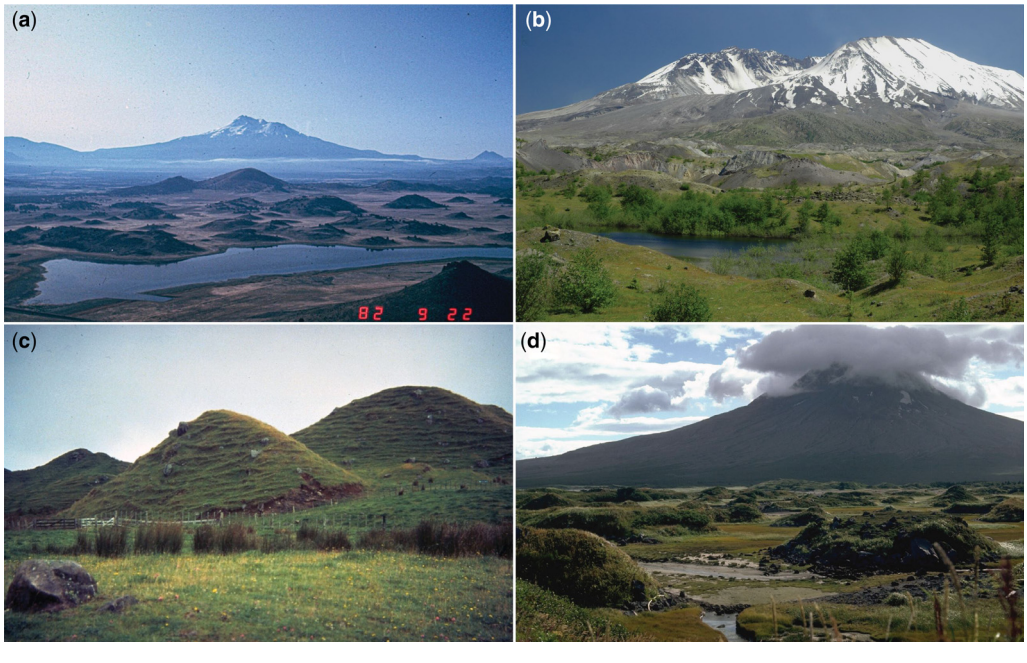

Fig. 5. Examples of hummocky topography of volcanic debris avalanches. (**a**) Mount Shasta (USA). Photograph by H. Glicken, USGS. (**b**) Mount St Helens (USA). Photograph by J. Major, USGS. (**c**) Taranaki volcano (New Zealand). Photograph by D. Swanson, USGS. (**d**) Augustine volcano (USA). Photograph by L. Siebert, Smithsonian Institution.

predominance of extensional structures among hummock fields consistent with experiments by Paguican *et al.* (2014). Particularly large blocks that preserve stratigraphy that is intact but tilted relative to its source, known as toreva blocks, may be present at the bases of failure scars (e.g. Clavero *et al.* 2002; Paguican *et al.* 2014; Dufresne *et al.* 2021*b*; Romero *et al.* 2022).

Surface morphologies of volcanic debris-avalanche deposits may also be characterized by ponds, marginal levees, and ridges (Fig. 6; see also Siebe *et al.* 1992; Romero *et al.* 2022). Extensional faulting and spreading of a debris avalanche not only isolate mounds but can form closed graben that can fill with water. Deposit extension and internal shearing can form linear ridges along the deposit surface. Along valley margins, lateral levees may form, some of which may block outlets of tributary channels and form new lakes.

Deposit composition and texture. Debris-avalanche deposits typically are composed of a chaotic mix of particles, from large intact or deformed blocks of a volcano to an extensively disaggregated mixture of volcanic material as well as sediment, rock, and organic debris entrained during emplacement. Deposits can range widely in thickness, from a few metres to more than 150 m. Depending on pre-existing topography and avalanche volume, average thicknesses commonly range from a few to many tens of metres.

A wide range of terminology has been applied to debris-avalanche deposits. Summaries of terminology are provided in Siebert (1984), Glicken (1996), van Wyk de Vries and Davies (2015), and Dufresne *et al.* (2021*b*). In broadest terms, units within volcanic debris-avalanche deposits are categorized and mapped according to their sedimentological and lithological facies (e.g. Glicken 1996). Debris-avalanche deposits are broadly characterized according to one of two principal facies: block or mixed (sometimes called matrix) facies (Fig. 7). Block facies (also referred to in the literature as megablock and axial facies) refers to those characteristics indicative that the deposit represents material transported largely intact from the source. The block facies can be highly brecciated and pervasively shattered such that no individual particle is larger than about a metre, but this facies clearly preserves material transported intact, such as original source stratigraphy (Palmer and Neall 1989; Glicken 1996; Fig. 7a, b). In contrast, the mixed facies represents material that cannot be shown to have been transported completely intact. Instead, this material is highly fragmented and disaggregated, may contain multiple clast lithologies, is generally unsorted, lacks stratification or grading, and typically appears to consist of isolated large particles (clasts) surrounded by or floating in a matrix of finer-grained sediment (dominantly sand) (Fig. 7e, f). The mixed facies is largely inferred to be the result of disaggregation and mixing of material during transport (Glicken 1996; van Wyk de Vries and Davies 2015). At intermediate distances, outcrops can exhibit textural characteristics of incomplete mixing, revealing a transition from block to mixed facies (Fig. 7c, d). If the flow was locally saturated, facies characteristics may show evidence of transition from debris avalanche to lahar, such as thinning

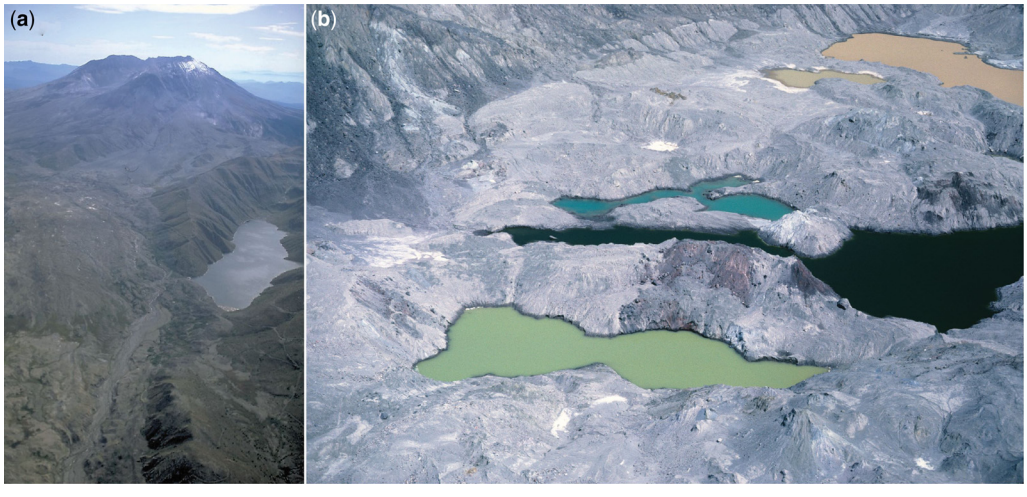

Fig. 6. Examples of lakes and ponds impounded by, or on surface of, a debris-avalanche deposit. (**a**) Castle Lake, impounded when the 1980 Mount St Helens (USA) debris-avalanche deposit blocked Castle Creek. Photograph by S. Brantley, USGS, 1992. (**b**) Ponds on surface of Mount St Helens debris-avalanche deposit. USGS, 1980.

Fig. 7. Examples of textural facies in debris-avalanche deposits. (**a**) Block facies at Mount Shasta (USA) showing clear transport of intact stratigraphic sections from the volcano. Photograph by L. Siebert, Smithsonian Institution. (**b**) Block facies in Mount St Helens (USA) deposit. Photograph by J. Major, USGS. (**c**) Outcrop of Mount St Helens deposit showing preservation of different pieces of the volcano, but not clearly intact stratigraphic units. Note large pieces of mottled-coloured sediment that are distinct but variably intermixed. This texture is reflective of incomplete mixing during transport, revealing a transition from block to mixed facies. Photograph by J. Major, USGS. (**d**) Outcrop showing incomplete mixing in deposit at Tungurahua volcano (Ecuador). Note the mottled coloration of deposit, indicating pieces of the volcano have begun blending together. Photograph by J. Major, USGS. (**e**) Mixed facies in deposit at Parinacota volcano (Chile). Note the more thoroughly dispersed mottled coloration of the deposit compared to (c) and (d) and lack of distinct stratigraphic units. Photograph by J. Major, USGS. (**f**) Mixed facies in debris-avalanche deposit from Misti volcano (Peru). Photograph by C. Harpel, USGS.

of the deposit into a cohesive, matrix-supported flowage deposit with a progressive decrease in primary clasts and increase in secondary entrained particles (Zernack *et al.* 2011).

Many particles within debris-avalanche deposits are highly shattered (Fig. 8). Evidence commonly indicates that particle shattering occurs largely during the initial release of the avalanche, and that subsequent downstream transport disaggregates fragments but causes little additional shattering. For example, Voight *et al.* (1983) and Glicken (1996) found that bulk density of the Mount St Helens debris-avalanche deposit varied little from proximal to distal reaches, indicative that the material was

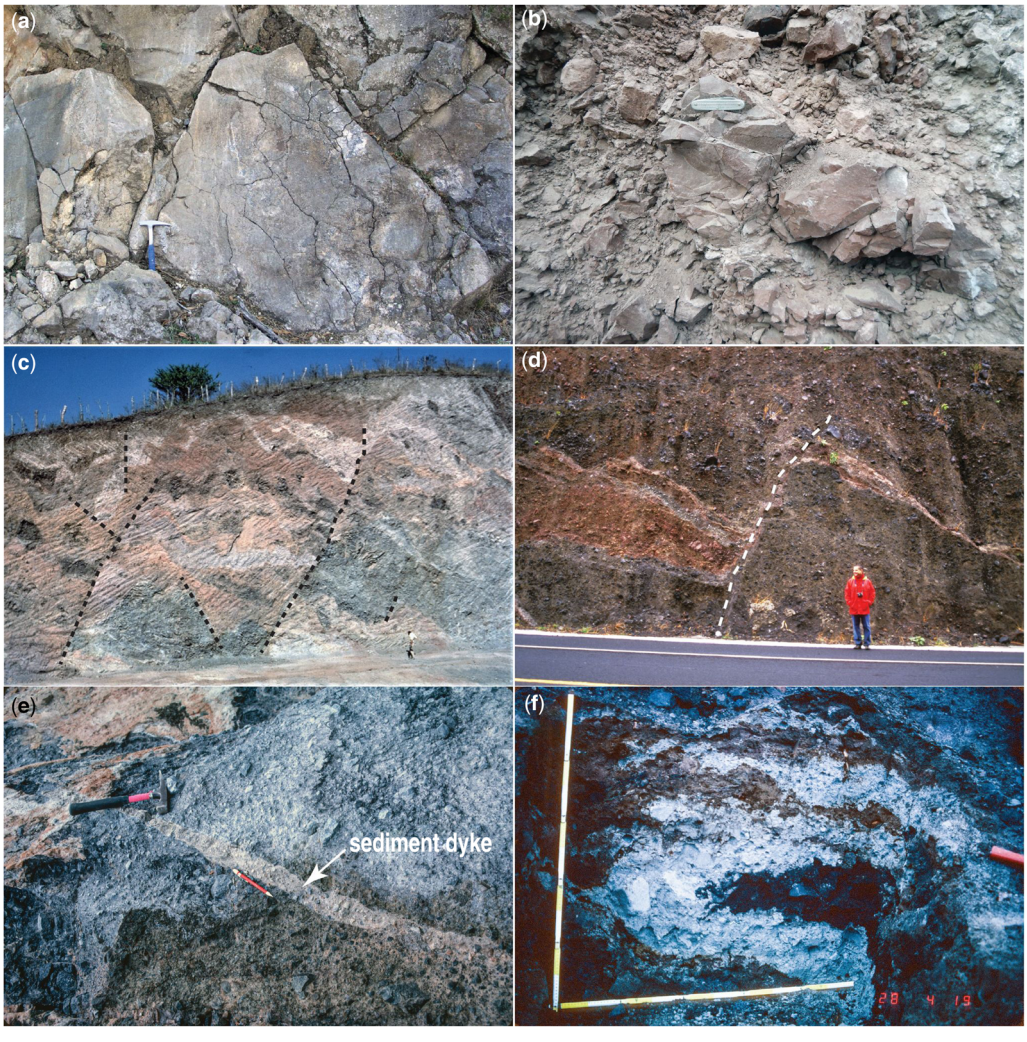

Fig. 8. Characteristic internal textures of debris-avalanche deposits. (**a**) Shattered jigsaw-cracked clast in deposit at Cofre de Perote (Mexico). Photograph by L. Siebert, Smithsonian Institution. (**b**) Shattered clasts in deposit from Misti volcano (Peru). Photograph by C. Harpel, USGS. (**c**) Block-facies deposit showing internal faulting (highlighted by dashed lines) offsetting stratigraphic layers. Avalanche deposit from Fuego or Acatenango volcanoes (Guatemala). Photograph by L. Siebert, Smithsonian Institution. (**d**) Internal faulting (dashed line) in deposit from Popocatépetl volcano (Mexico). Photograph by L. Siebert, Smithsonian Institution. (**e**) Sediment dyke injected within Mount St Helens (USA) avalanche deposit and cross-cutting a shattered volcanic dyke (grey). Injection direction right to left. Photograph by H. Glicken, USGS. (**f**) Material smeared by internal shearing within Mount St Helens avalanche deposit. Photograph by H. Glicken, USGS.

already highly shattered in proximal areas. Inspection of individual clasts shows that in proximal areas, many clasts are shattered but still relatively coherent – called jigsaw-cracked clasts (e.g. Siebert 1984; Glicken 1996; van Wyk de Vries and Davies 2015; Dufresne *et al.* 2021*b*). With distance, debris-avalanche deposits show features of clast disaggregation and separation, internal faulting, smearing of material by internal shearing, fingers of material injected amongst particles, and other evidence to indicate that material is entrained, disaggregated, and mixed with transport distance (e.g. Siebe *et al.* 1992; Glicken 1996; van Wyk de Vries and Davies 2015; Dufresne *et al.* 2021*b*) (Fig. 8). Even at the microscopic level, particles sampled from proximal to distal reaches of debris-avalanche deposits exhibit features indicative of shattering and disaggregation, such as microcracks,

hackly fractures, and fracture separation (e.g. Komorowski *et al.* 1991; Dufresne *et al.* 2021*b*).

Quantitative sedimentological characteristics of debris-avalanche deposits overlap with other volcaniclastic deposits. Analyses of median grain size, sorting, and grain shape show substantial overlap with those from lahar and PDC deposits (e.g. Siebert 1996; Dufresne *et al.* 2021*b*). Indeed, some outcrops of mixed facies of debris-avalanche deposits may be difficult to distinguish from those of PDC and lahar deposits, and correct interpretation may rely on broader morphologic and sedimentary context.

Relations between initiation mechanism and deposit character. Debris-avalanche-deposit textures are likely to be similar despite the nature of the initiation mechanism. Key characteristics of a debris-avalanche deposit are evidence of mass transport from a volcano. This evidence includes distinctive surface morphology (hummocks), transport of intact stratigraphic sections, preservation of jigsaw-cracked clasts, and mottled coloration indicative of incomplete blending of stratigraphic units (Figs 5, 7, 8). There may also be evidence of localized internal shearing and pressured loading (clastic dykes) (Fig. 8). These features, however, do not discriminate a specific initiation mechanism, as the transport process, more than the initiation mechanism, controls these deposit textures. Stratigraphic associations, however, can lend insights into probable, or at least possible, initiation mechanisms. Debris-avalanche deposits with clear association to a magmatic eruption – such as close temporal association with tephra-fall or PDC deposits, especially with deposits from directed explosions rich in juvenile material – provide strong evidence that edifice failure was associated with magmatic intrusion. Debris-avalanche deposits containing substantial amounts of highly deformed subvolcano substrate are suggestive of substrate failure as a precipitating cause, especially if there is structural evidence of failure reaching below the edifice. Debris avalanches caused by earthquakes, slope loading, or debuttressing may or may not be associated with magmatic intrusions or phreatic explosions. Those induced by hydrothermal weakening of an edifice may or may not be associated with an eruption, but close association with deposits containing juvenile material is indicative of magma involvement. Evidence of direct transformation to a lahar along with evidence of inclusion of hydrothermal material may signal that hydrothermal weakening of an edifice was a significant contributing factor to the debris avalanche.

Pyroclastic density current

A pyroclastic density current (a generalized term for a pyroclastic flow or surge) – or PDC – is a hot, gravity-driven, heterogeneous mixture of air, gases, and volcanic particles, which is denser than the ambient atmosphere and flows away from a volcano (Wilson 1986; Druitt 1998; Branney and Kokelaar 2002; Sulpizio *et al.* 2014; Dufek *et al.* 2015; Lube *et al.* 2020) (Fig. 9). It can occur suddenly during an eruption, travel many kilometres across the landscape at high speeds (many tens of metres per second), and burn, bury, and destroy everything in its paths. Its mass, momentum, and temperature (to many hundreds of degrees Celsius) make it particularly destructive and hazardous.

A PDC can have variable particle concentration and be strongly stratified. Dynamic relations among grain interactions, particle densities and settling velocities, turbulent eddies, and fluid drag on solid particles promote particle segregation. Such segregation leads to stratification within the current, creating a dense, high-concentration flow phase, dominated by particle interactions modulated by pore-fluid pressures, underlying a dilute, low-concentration turbulent phase in which particle settling is affected dominantly by fluid drag (e.g. Wilson 1986; Druitt 1998; Burgisser and Bergantz 2002; Sulpizio *et al.* 2014; Dufek *et al.* 2015; Lube *et al.* 2020) (Fig. 10). Although recent experimental work has shown that PDCs can span a spectrum of solids concentrations (Lube *et al.* 2020), two end-member styles of currents are representative of common conceptual models. A coarse-grained, high-concentration current, known as a pyroclastic flow, commonly has a particle concentration of about 50% by volume (e.g. Lube *et al.* 2020). This dense flow generally hugs the ground and is funnelled along topographically low areas. This phase of a PDC commonly constitutes the basal part of a flowing current. In contrast, a swiftly moving, relatively fine-grained, low-concentration flow, known as a pyroclastic surge, commonly has a particle concentration of about 1% by volume or less (e.g. Lube *et al.* 2020). A surge is less constrained by topography and can sweep broadly across the landscape, even surmounting topographic ridges. As a result of these different concentrations and solid–fluid interactions, a PDC develops into a stratified current that can be many tens to hundreds of metres thick (e.g. Druitt 1998; Burgisser and Bergantz 2002; Sulpizio *et al.* 2014; Dufek *et al.* 2015; Lube *et al.* 2020). Because of particle segregation, a PDC can evolve with travel distance. The basal flow can increase in concentration through both substrate entrainment and internal particle settling, and a surge of fine sediment and gas can detach from the underlying coarser flow and travel as a separate entity (e.g. Fisher 1995). Thus, a single PDC can evolve into multiple currents involving different behaviours, sedimentation regimes, and hazards (Branney and Kokelaar 2002; Fisher 1995; Sulpizio *et al.* 2014; Dufek *et al.* 2015; Lube *et al.* 2020).

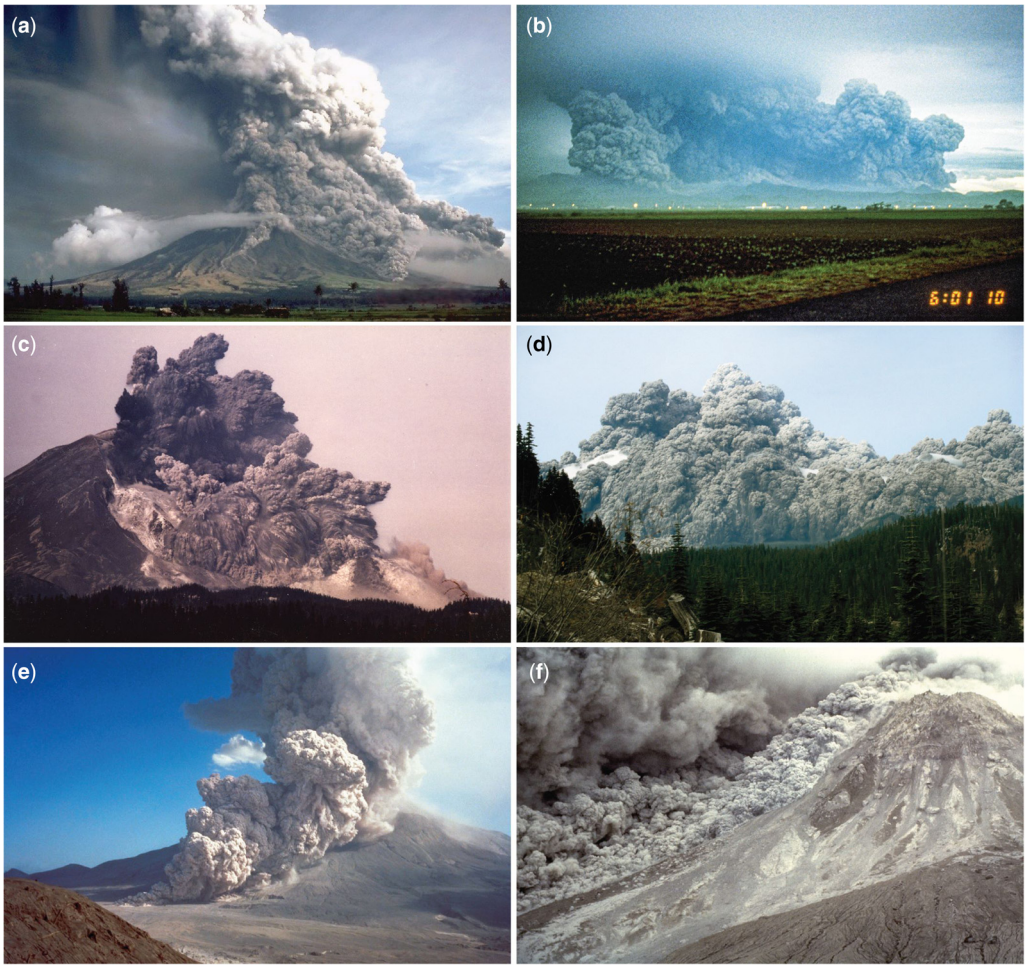

Fig. 9. Examples of pyroclastic density currents (PDCs) generated by various mechanisms. A PDC consists of a dense, ground-hugging phase overlain by a dilute, turbulent phase. (**a**) PDC generated by eruption-column collapse, Mayon volcano (Philippines). Photograph by C. Newhall, USGS, 1984. (**b**) Radial PDC generated by energetic pyroclastic fountaining and collapse during initial phases of cataclysmic eruption of Mount Pinatubo (Philippines). Photograph by R. Hoblitt, USGS, June 1991. (**c**) Initial moments of horizontally directed PDC at Mount St Helens (USA). Photograph © G. Rosenquist, May 1980. (**d**) The directed PDC at Mount St Helens, initially propelled by explosions from the magmatic body unroofed by a preceding debris avalanche, rapidly collapsed under the influence of gravity and spread widely across the landscape irrespective of topography. Photograph © K. Ronnholm, May 1980. (**e**) PDC at Mount St Helens generated by low fountaining of volcanic plume, July 1980. Photograph by P. Lipman, USGS, July 1980. (**f**) PDC generated by dome collapse, Soufrière Hills volcano (Montserrat, British Overseas Territory). Photograph by R. Herd, Montserrat Volcano Observatory, 1997.

In addition to flow stratification that forms within the initial flow mass, hot gases and heating of air ingested into the flow cause buoyant rise and elutriation of fine particles into a cloud above the main flow. If this cloud maintains substantial lateral momentum, it can produce a deposit with evidence of a flowage component, such as cross-bedding or lateral interactions with the substrate and vegetation. In contrast, if deposition from this cloud is predominantly from vertical fall, the deposit will exhibit characteristics of a fall process (see 'Tephra fall' section). Ash clouds emanating from PDCs (called co-PDC ash clouds) can be substantial and produce abundant fall deposits (e.g. Hoblitt 2000) (Fig. 11). They can emerge from a widespread footprint (in contrast to volcanic plumes that rise from discrete vents) and rise many tens of kilometres in altitude (e.g. Sparks *et al.* 1986; Waitt 2015).

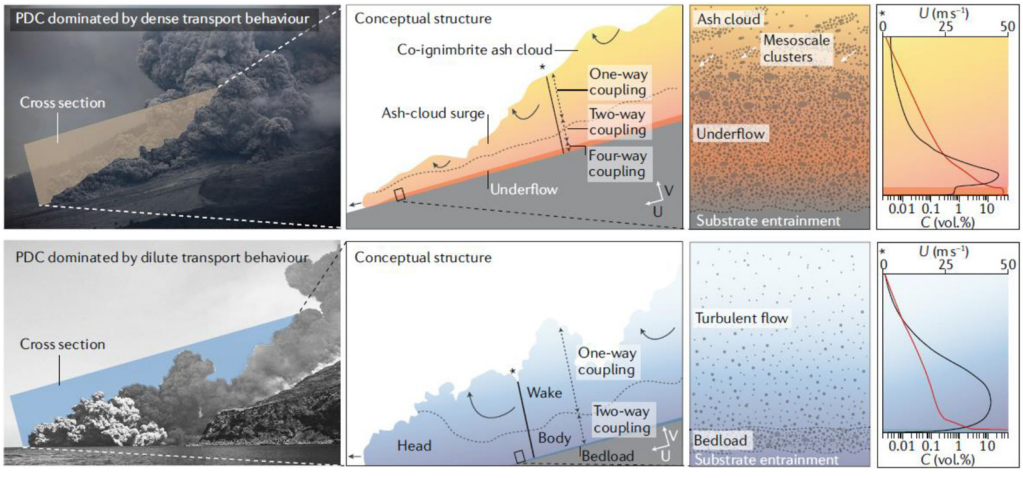

Fig. 10. Schematic depiction of a pyroclastic density current (PDC) illustrating a density-stratified current with a dense basal underflow and an overlying, dilute, turbulent phase. Characteristics of currents having two different particle-concentration structures are depicted. The centre left panels depict height-variant density with different gas-particle coupling regimes. In the most dilute regions of the PDC, particle motion is affected only by the flow of gas past particles (one-way coupling). In more concentrated, intermediate regions, particle motion is affected by the flow of gas past particles, and gas flow is affected by particle presence (two-way coupling). In the most concentrated regions of the current, two-way coupling is further affected by gas compressed between particles as well as by collisional and frictional interactions among particles (four-way coupling). Note the variation in generalized sediment concentration and velocity profiles between the currents (right-hand panel: red line is particle concentration, black line is velocity) and thus thickness of mass flow at base of current v. traction load transport. Reprinted by permission of Sprinter Nature from Lube *et al.* (2020).

Condensation and electrostatic forces within a co-PDC ash cloud may cause aggregation of fine ash and formation of wet accretionary lapilli or dry-ash aggregates (see sub-section 'Deposit characteristics' in the 'Tephra fall' section).

Initiation mechanisms. Multiple initiation mechanisms generate PDCs (Figs 9 & 12). The most common initiation mechanisms include: (1) collapse of parts or all of an eruption column; (2) sustained fountaining of volcanic ejecta that do not fully rise into a lofting eruption plume; (3) laterally or low-angle-directed explosions; (4) collapses of columns from fissures, ring fractures, or multiple vents during caldera collapse; (5) collapses of growing lava domes; (6) collapses of fronts of advancing lava flows; and (7) interactions of magma and water during hydrovolcanic eruptions. In addition, PDC sediment deposited precariously on steep hillsides can spontaneously remobilize and form secondary PDCs (e.g. Hoblitt *et al.* 1981; Fisher 1990). A less common mechanism is slumping of valley-fill PDC deposits, which result in secondary PDCs (Scott *et al.* 1996; Robinson *et al.* 2017).

Eruption column collapse, fountaining, and boiling over. The largest and most hazardous PDCs form during explosive eruptions. PDCs that form during explosive eruptions commonly result from gravitational collapse of an eruption column, although some are the result of directed explosions. Although initiation of PDCs from eruption columns spans a gradational spectrum of processes, this spectrum is captured by three principal variations: eruption-column collapse from a tall column, volcanic fountaining, and boiling over (Fig. 12a–c).

Explosive eruptions commonly thrust volcanic particles vertically into the atmosphere forming an eruption column. Magmatic water content, vent radius, particle size and density, exit velocity, mass flow rate of the ejected material, and entrainment of ambient air influence the height to which ejected material is thrust, the behaviour of the column, and the partitioning of mass between convection and collapse (e.g. Sparks and Wilson 1976; Wilson *et al.* 1980; Neri *et al.* 2002; Shea *et al.* 2011; Carey and Bursik 2015) (Figs 9a & 12a, b). As ejected material rises, there are two conceptual end members that characterize its behaviour: (1) the column can efficiently entrain ambient air, become fully buoyant, convect to great height, and the ejecta are dispersed largely downwind and return to the ground surface as tephra fall, or (2) the column fails to entrain, or entrains insufficient, ambient air to become fully

Fig. 11. A pyroclastic density current (PDC) can generate a substantial plume of fine ash (co-PDC ash cloud). This photograph is of a co-PDC plume generated during 18 May 1980 eruption of Mount St Helens (USA). Note the widespread footprint of this rising plume and the height to which it is rising. View is from the NW. Photograph © M. Huntting.

buoyant and collapses gravitationally, forming PDCs (e.g. Sparks and Wilson 1976; Wilson *et al.* 1980; Neri *et al.* 2002). In reality, convection and collapse usually attain some intermediate hybrid state, such that some of the eruption column becomes buoyant while parts of it collapse (e.g. Taylor 1958; Moore and Melson 1969; Nairn and Self 1978; Hoblitt 1986; Clarke *et al.* 2002; Saucedo *et al.* 2002; Neri *et al.* 2007; Dufek *et al.* 2015; Miyabuchi *et al.* 2018; Roche *et al.* 2021). Depending on how much of the eruption column collapses, the geometry of the collapse, and the topography of the volcano, PDCs can be spatially focused or radial in nature and affect many drainages of a volcano simultaneously (e.g. Moore and Melson 1969; Sigurdsson *et al.* 1984, 1985; Hoblitt *et al.* 1996; Scott *et al.* 1996; Neri *et al.* 2007).

Collapse of large portions of an eruption column can transfer large fluxes of mass and momentum into a highly energetic PDC (e.g. Taylor 1958). However, even partial collapse of an eruption column can generate a substantial PDC. Individual collapses generate unsteady, single-pulsed currents whereas sustained, nearly continuous collapses feed prolonged, quasi-steady currents (Fig. 12a, b). A collapse-triggered PDC can consist of multiple phases and undergo a transformation as it travels (e.g. Fisher 1983). A column-collapse PDC can form a pyroclastic surge at its leading edge followed by pyroclastic flow, which is then followed by a surge from higher in the flow (e.g. Fisher 1979; Sigurdsson *et al.* 1984, 1985). Surges spawned by column collapses commonly outrun the footprint of pyroclastic flows and expand the area of impact.

If an eruption column is unsteady or not particularly energetic, ejected material may rise to only a modest height above the vent before it collapses. Modest column rise is especially common in low fountains of ejecta that contain relatively little magmatic water content (less than 1% by volume; e.g. Sparks and Wilson 1976; Neri *et al.* 2002). As a result, the column lacks buoyancy or rises only weakly and collapses quickly into a PDC. Eruption columns can also be laden with dense juvenile clasts and entrained wall-rock material, which inhibit buoyancy (e.g. Shea *et al.* 2011). Such eruptions may occur in pulses or may be sustained for prolonged periods of time. Thus, volcanic fountaining can feed a transient or sustained PDC that can travel several kilometres from its source. This process of PDC initiation has been observed and modelled at several volcanoes (e.g. Hoblitt 1986; Voight *et al.*

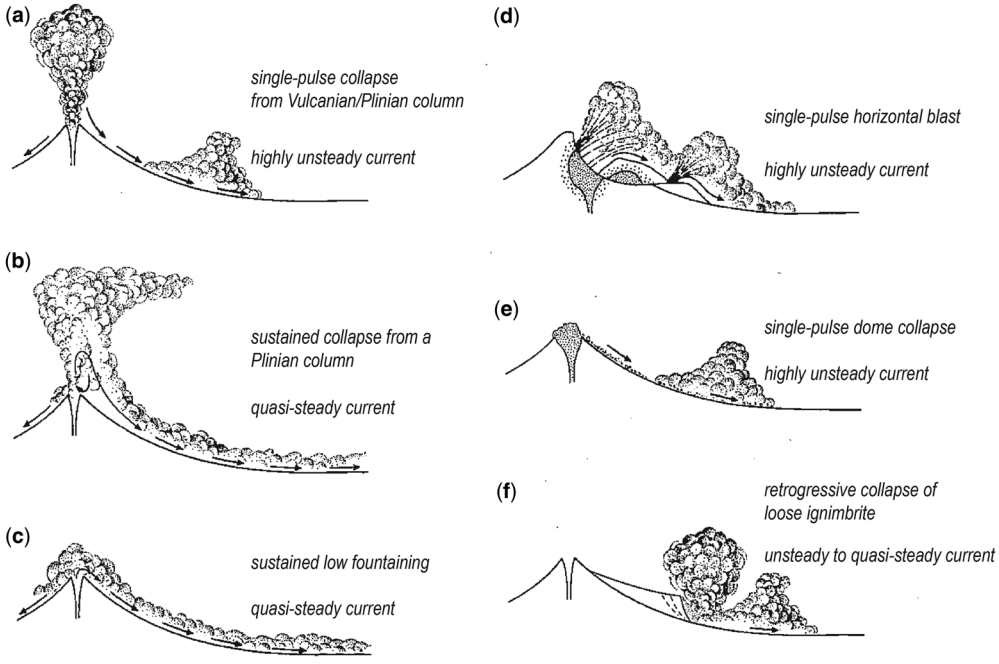

Fig. 12. Primary initiation mechanisms of a pyroclastic density current (PDC). Note that initiation mechanism can influence whether passage of a PDC is transient or sustained, directed or radial, and spatially restricted or widespread. Such behaviours can influence deposit characteristics. Not illustrated is an ash cloud that can rise directly from a moving PDC. From Branney and Kokelaar (2002).

2000*a*; Clarke *et al.* 2002; Cole *et al.* 2005; Maeno *et al.* 2016) (Fig. 9b, e).

Sluggish, transient eruption columns that barely rise above the vent before collapsing have been described as appearing like a pot that is boiling over (e.g. Wolf 1878; Hoblitt 1986; Clarke *et al.* 2002; Hall and Mothes 2008; Rader *et al.* 2015). Such boiling over is merely a gradation of volcanic fountaining (e.g. Hoblitt 1986; Clarke *et al.* 2002).

Directed explosion. Rapid exposure of volatile-rich magma to the atmosphere or sudden reduction of confining pressure on a shallowly emplaced magmatic body can lead to an explosion that is directed laterally or at low angle (Gorshkov 1963; Voight 1981) (Figs 9c, d & 12d). A directed explosion occurs most commonly following a debris avalanche or failures of a lava dome. Rapid decompression permits swift exsolution of magmatic volatiles and generation of a fragmentation wave, perhaps augmented by flashing of heated groundwater to steam, which results in rapid fragmentation of magma and surrounding wall rock and an energetic explosion that spawns a PDC (e.g. Woods *et al.* 2002). The PDC is initially propelled by decompression of the magmatic system, but swiftly becomes negatively buoyant and forms a gravitationally driven flow as the ejected material collapses (e.g. Esposti Ongaro *et al.* 2012; Figs 9c, d & 12d). Perhaps the most renowned laterally directed PDC occurred during the 18 May 1980 eruption of Mount St Helens (Hoblitt *et al.* 1981; Hoblitt 2000; Voight 1981). In that eruption, a debris avalanche rapidly decompressed dacitic magma that had risen high into the volcano. The debris avalanche (Fig. 2), ensuing directed blast, and consequent PDC were observed and well documented by many eyewitnesses (e.g. Voight 1981; Waitt 2015; Figs 9c, d & 13). The PDC spread rapidly (Fig. 13), swept over multiple ridges, and devastated nearly 600 km^2 of rugged landscape in a 180° arc north of the volcano. A similar event occurred during the 1956 eruption of Bezymianny volcano (Russia) and devastated some 500 km^2 of rugged landscape (Gorshkov 1959).

Phreatic explosions may also generate directed PDCs. The 1888 eruption of Bandai volcano included an earthquake-triggered debris avalanche that rapidly decompressed a pressured hydrothermal system. Rapid decompression triggered several brief phreatic explosions and spawned a PDC that travelled about 6 km and devastated 13 km^2 (Yamamoto *et al.* 1999). The PDC that resulted from these explosions had been thought to result from a directed explosion, but Yamamoto *et al.* (1999) suggested

Fig. 13. Images of rapid expansion of pyroclastic density current caused by directed explosion at Mount St Helens (USA) on 18 May 1980, and its large associated ash plume (see also Fig. 11). Total time elapsed in these photographs is about 5 minutes. View is looking south from Mount Rainier. Photographs © R. Decher.

the PDC resulted from fountaining of dense, transient, vertical explosion columns rather than from a directed explosion. Nevertheless, directed explosions can occur during phreatic eruptions.

Directed explosions have been reported for other eruptions, but they are largely inferred based on deposit characteristics (discussed in the sub-section 'Deposit characteristics' in the 'Pyroclastic density current' section). Those deposit characteristics, sometimes showing close association in time with debris-avalanche deposits, have been used to infer directed-blast origins for PDC deposits (Boudon *et al.* 1984, 1990; Ritchie *et al.* 2002; Sparks *et al.* 2002; Komorowski *et al.* 2013; Major *et al.* 2013; Pallister *et al.* 2019).

Distinguishing a directed-blast origin of a deposit from one resulting from an otherwise energetic PDC can be complex. Even a close association with a debris avalanche and significant impact on vegetation do not necessarily indicate a low-angle-blast origin. At Lamington volcano (Papua New Guinea), characteristics of volcanic deposits and impacts on vegetation were used to infer that its 1951 eruption included a directed-blast PDC (Taylor 1958). Belousov *et al.* (2020) reanalysed the deposits and eyewitness accounts and concluded a debris avalanche likely decapitated a magmatic body that nearly reached the surface. Because decapitation exposed the top of the magmatic body rather than its steep side, the directed explosion was high-angle rather than lateral or low-angle. This high-angle-directed explosion generated a dense eruption column that collapsed and formed a transient but very energetic PDC having many hallmarks of a laterally directed PDC. The directionality of the PDC was controlled largely by the pre-existing topography of the volcano rather than being horizontally propelled. At Mont Pelée (Martinique, French Department Territory), eyewitness accounts and distributions of deposits have been debated as to whether the devastating 8 May 1902 PDC was caused primarily by a directed blast or column collapse (LaCroix 1904; Fisher and Heiken 1982, 1990; Boudon *et al.* 1990). Numerical modelling of the event by Gueugneau *et al.* (2020) concluded there were likely elements of both. They concluded a sudden decompression of the lava dome growing in the volcano's crater led to a brief blast-like event and a low, dense vertical eruption column that quickly collapsed into an energetic PDC that was directionally focused owing to the geometry of the crater and downslope topography. As this PDC moved downslope it developed into a powerful pyroclastic surge that spread widely. These analyses and reinterpretations of the

Lamington and Pelée volcanic eruptions show that there is clear gradation among initiation mechanisms of PDCs and that inferences of a specific initiation mechanism from deposit characteristics must be approached with caution.

Caldera collapse. The largest PDCs result from collapses of columns or intense fountaining formed during eruptions leading to caldera collapses. Some of these PDCs are formed during voluminous eruptions from single, central vents prior to caldera collapse as vent-wall erosion increases vent diameter and air entrainment is insufficient to produce a buoyant plume (e.g. Wilson *et al.* 1980). Others occur from eruptions along caldera ring vents that form as the caldera roof founders (e.g. Bacon 1983; Wilson 1985; Self 1992; Wilson and Hildreth 1997; Kandlbauer and Sparks 2014). Multiple-pulsed or prolonged and sustained PDCs resulting from caldera collapses produce deposits that can fill and smooth rugged topography (e.g. Punongbayan *et al.* 1996). Cumulative accumulations of PDC deposits from caldera-collapse eruptions have volumes that range from as little as a few cubic kilometres dense rock equivalent (DRE) to thousands of cubic kilometres (e.g. Bacon 1983; Wilson 1985; Hildreth and Mahood 1986; Self 1992; Scott *et al.* 1996; Allen 2001; Christiansen 2001; Cas *et al.* 2011; Chesner 2012; Hildreth and Fierstein 2012; Kandlbauer and Sparks 2014; Marti *et al.* 2016; Takarada and Hoshizumi 2020; Valentine and Cole 2021).

PDCs produced during caldera-collapse eruptions affect widely ranging areas, are emplaced within minutes to days, and produce deposits having widely variable thicknesses. These PDCs have commonly spread radially from volcanic centres, covered hundreds to a few tens of thousands of square kilometres in area, and reached travel distances of many tens to nearly 200 km from source. PDCs associated with caldera collapses are commonly sustained and emplaced over hours or days' duration (e.g. Scott *et al.* 1996; Wilson and Hildreth 1997; Hildreth and Fierstein 2012). However, they can be emplaced more quickly. Wilson (1985) estimated that the 10 km^3 (DRE) deposit emplaced by the 186 CE eruption of Taupo volcano (New Zealand), which spread over some 20 000 km^2 to distances of 80 km from source, was emplaced within 400 s – a scant 6.5 minutes! Caldera-collapse-generated PDCs can be emplaced as turbulent surges that overrun rugged topography and leave thin veneers (less than 1 m thick) that drape pre-existing topography (e.g. Wilson 1985; Scott *et al.* 1996; Hildreth and Fierstein 2012). They can also form dense pyroclastic flows that follow low topography and thickly bury valleys. Valley deposits from many caldera-collapse PDCs are commonly tens to a few hundreds of metres thick (Bacon 1983; Self *et al.* 1984; Wilson 1985; Self 1992; Fisher *et al.* 1993; Scott *et al.* 1996; Christiansen 2001; Maeno and Taniguchi 2007; Cas *et al.* 2011; Chesner 2012; Takarada and Hoshizumi 2020), but may be as little as a few metres thick (e.g. Hildreth and Fierstein 2012).

The initiation mechanisms of PDCs associated with caldera collapses are no different than described previously for smaller volume eruptions, they merely happen on a much grander scale. Caldera-collapse PDCs have been inferred to result from high mass-feeding rates from quasi-continuous collapse of parts of sustained eruption columns, by repeated brief collapses of entire eruption columns, and by intermittent partial collapses of eruption columns much as occur during smaller eruptions (e.g. Scott *et al.* 1996; Cas *et al.* 2011; Valentine and Cole 2021). Intracaldera fill, however, can affect the style of PDC emplacement (Valentine and Cole 2021). Large amounts of PDC sediment can become trapped within developing calderas. As a result, eruptions must penetrate the accumulating deposits. This behaviour, termed a gargling eruption (Wilson and Hildreth 1997; Valentine and Cole 2021), increases grain size along the margins of the eruption column and extracts momentum from the central jet. As a result, PDCs are generated from a column that might otherwise rise buoyantly and produce fall deposits (Valentine and Cole 2021). Furthermore, material along the edges of the eruption column collapses from a range of heights producing transient pulsing behaviour. The thickness and grain-size composition of the intracaldera fill strongly influence the behaviour of the erupting jet even if mass flow rate is constant, which can affect PDC behaviour and deposit characteristics (Valentine and Cole 2021).

Dome collapse. Explosions from, or collapses of, actively growing lava domes can generate PDCs. Collapses can involve either minor segments of the dome (e.g. Mellors *et al.* 1988) or nearly an entire dome (Sparks *et al.* 2002) and they can be gravitationally or explosively driven. Upon collapse, failed dome rock rapidly disintegrates and fragments into flowing mixtures of coarse rock and finer-grained particles (Figs 9f & 12e). Commonly known as block-and-ash flows (BAFs), these types of PDCs form transient, unsteady currents. They occur most often during active extrusions, particularly if extrusion rates are high (several to a few tens of cubic metres per second; e.g. Komorowski *et al.* 2013; Pallister *et al.* 2013, 2019), domes are perched on steep slopes, there is substantial seismicity that can trigger dome failure, or if domes are overpressured and explosions occur during extrusion (e.g. Voight and Elsworth 2000). The style of dome growth – endogenous or exogenous – as well as magma composition, fluid pressure, dome volume, and

mechanisms of collapse influence the style and size of collapse and formation of a subsequent PDC (e.g. Sato *et al.* 1992; Woods *et al.* 2002; Harnett *et al.* 2019). In general, dome-collapse PDCs are small in volume (10^4–10^6 m^3), travel short distances (a few to several kilometres), and are spatially focused. However, some dome-collapse PDCs, such as those at Soufrière Hills volcano (Montserrat, British Overseas Territory) in 1997, can be large (10^7 m^3) and cover many square kilometres (Calder *et al.* 1999; Sparks *et al.* 2002). In most instances, drainages likely to be affected by these types of PDCs can be anticipated based on location of the lava dome and volcano topography, but overlying surges can detach from the coarser parent flow and affect a broader footprint (Fisher 1995). Dome-collapse PDCs, although small compared to column-collapse PDCs, can nevertheless substantially impact landscapes close to volcanoes (e.g. Sato *et al.* 1992; Yamamoto *et al.* 1993; Gardner *et al.* 1994; Calder *et al.* 1999; Voight *et al.* 2000*b*; Carn *et al.* 2004; Thouret *et al.* 2010; Vallance *et al.* 2010; Major and Lara 2013; Reyes-Dávila *et al.* 2016; Pallister *et al.* 2019; Darmawan *et al.* 2020). Repeated collapses produce abundant sediment that can later be remobilized as lahars and transported farther downstream. Collapses of older lava domes that are no longer active typically generate flows akin to cold rockfalls that are more restricted in volume and travel shorter distances than those that occur when a dome is actively growing.

Collapse of advancing lava flow. If extrusion rates are sufficiently high, cooling rates sufficiently low, viscosity sufficiently low, and slopes sufficiently steep, actively extruding silicic lava domes can transition into slowly advancing lava flows. These dome-transition lava flows can extend several kilometres. On occasion, the front or sides of those advancing flows can fail, exposing gas-rich lava that can rapidly vesiculate, explode, and generate a PDC. Although less common than those from dome collapses, PDCs generated in this manner are similar to dome-collapse BAFs. Like those spawned by dome collapses, these PDCs can travel several kilometres at speeds of a few tens of metres per second (e.g. Rose *et al.* 1976; Harris *et al.* 2002; Saucedo *et al.* 2002; Pallister *et al.* 2019). However, because these PDCs form by collapse of lava flows, those lava flows displace the source of the PDC from the volcanic vent, possibly up to several kilometres. If the lava is sufficiently pressurized, the collapse of the front or side of the lava flow can spawn a directed-explosion PDC that can have severe societal and ecological consequences (e.g. Pallister *et al.* 2019).

Phreatomagmatic explosion. Near-surface interactions of magma and groundwater can produce energetic explosions that generate PDCs. Rapid conversion of thermal to mechanical energy and generation of shock waves within a conduit cause extensive fragmentation and pulverization of both magma and wall rock (Zimanowski *et al.* 2015). This rapid conversion of energy can generate pyroclastic surges (known as base surges) rich in fine ash. Examples of phreatomagmatic eruptions producing PDCs include eruptions of Ontake volcano (Japan) (Kaneko *et al.* 2016), Kuchinoerabujima volcano (Japan) (Geshi and Itoh 2018), Aso volcano (Japan) (Miyabuchi *et al.* 2018), Ukinrek Maars (USA) (Self *et al.* 1980), the Oruanui eruption of Taupo volcano (Wilson 2001), and the Table Rock complex (USA) (Brand and Clarke 2012).

Depositional processes. Deposition by PDCs is conceptually bounded by two end members: *en masse* deposition in which the flow stops abruptly and progressive deposition in which sediment at the flow base gradually accumulates during flow passage (e.g. Branney and Kokelaar 1992, 2002; Brown and Andrews 2015; Dufek *et al.* 2015; Lube *et al.* 2020). Through *en masse* deposition, a deposit represents the structure and texture of the entire dense underflow of the current at the instant of deposition. In contrast, progressive deposition reflects the time varying characteristics of the base of the current as it passes a location, which reflects only a limited part of the structure and texture of the entire flow. In this concept, deposition is a sustained but time-varying process with deposit characteristics determined by the nature of a flow-boundary zone – the region that encompasses the basal part of the current and the uppermost part of the aggrading deposit (Branney and Kokelaar 1992, 2002) (Fig. 14).

The nature and character of the PDC influences the nature of particle support, transport, and deposition at the flow-boundary zone (Branney and Kokelaar 1992, 2002). If a current is fully dilute with little intergranular particle support, then the flow-boundary zone is dominated by direct particle fallout from higher in the current and a strong shear gradient is developed near the deposit surface. Strong shear stress at the current–deposit interface facilitates tractional transport and leads to a stratified and moderately to well-sorted deposit. In contrast, in a highly segregated current with a dense basal underflow, the flow-boundary zone is dominated by particle–particle interactions modulated by interstitial fluid pressure. As a result, this flow-boundary zone is dominated by granular-flow processes commonly resulting in non-stratified deposits that can exhibit variable sedimentary textures with respect to clast composition and orientation, fluidization structures, and particle grading. As clasts settle through this concentration-stratified flow-boundary zone, they are subject to selective filtering (Branney and

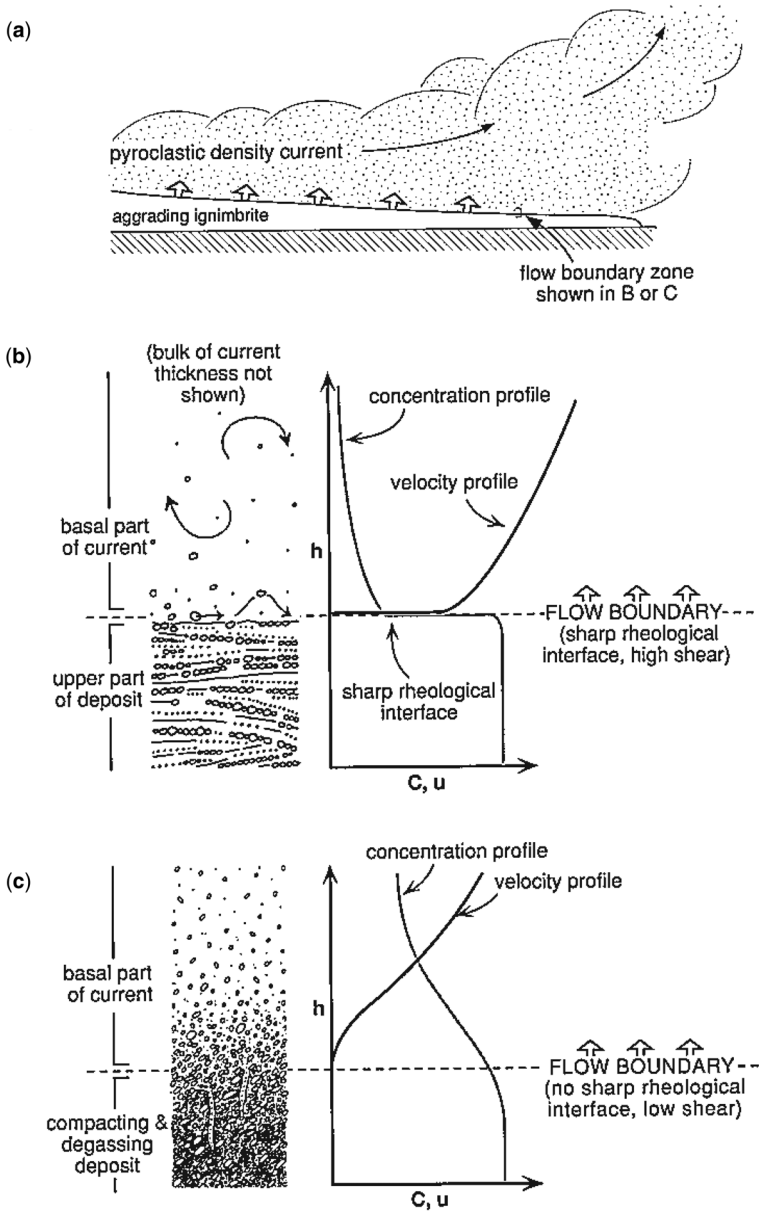

Fig. 14. Schematic of model of progressive aggradation of a pyroclastic-density-current deposit from a sustained current. (**a**) Instantaneous position of flow-boundary zone, which constitutes the lowermost part of current, the flow boundary, and uppermost part of aggrading deposit. (**b**, **c**) Conceptual end-member types of flow-boundary zones: (b) flow-boundary zone at base of a low-concentration current showing development of a strong shear gradient owing to abrupt changes in velocity (u) and particle concentration (c) at the sharp interface between the current and deposit; (c) flow-boundary zone at base of a high-concentration current. Near the interface, flow velocity and particle concentration vary gradually. The concentration of the lowest part of current and deposit are similar, thus forming a non-stratified deposit when current is relatively steady. From Branney and Kokelaar (2002). Also see Figure 10.

Kokelaar 2002). For example, dense lithic particles may pass downward and be deposited, whereas less-dense pumice particles may be unable to penetrate the flow-boundary zone locally and are transported farther downcurrent and deposited in clast-supported lobes and levees (e.g. Brown and Andrews 2015).

Selective filtering of the flow-boundary zone can vary in space and time. PDCs are, however, more complex and gradational than these two conceptual end members, and thus PDC deposition is more complex. Variations in source emissions that produce unsteady source behaviour, longitudinal variations in topography, internal current stratification, flow-boundary zones, interactions with the substrate, and local accelerations and decelerations result in a complex interplay of forces among particles and gases, particle concentration, particle sedimentation, and ultimately the texture of PDC deposits (e.g. Druitt 1998; Branney and Kokelaar 2002; Brown and Andrews 2015; Dufek *et al.* 2015; Lube *et al.* 2020). Even single currents can produce deposits having broad temporal and spatial diversity.

Particle settling within and deposition by a PDC ultimately affects its behaviour and runout distance. PDCs are driven largely by their density difference with respect to the atmosphere (e.g. Branney and Kokelaar 2002; Dufek *et al.* 2015; Lube *et al.* 2020). Eventually, there is sufficient particle settling and deposition such that the density of the current becomes less than that of the atmosphere; consequently, it lifts and ceases forward flow. This buoyancy-induced change in current behaviour can occur abruptly, as seen by sharp changes in distal effects on vegetation and observed by eyewitnesses (e.g. Lipman and Mullineaux 1981, pl. 1; Major *et al.* 2013; Waitt 2015).

Topography can strongly influence PDC behaviour. The dense, basal part of a PDC is commonly focused in valleys and topographic lows whereas the overlying turbulent part of a PDC can overrun ridges and divides. Slope gradient influences the turbulence of a current and affects its erosivity and depositional regime (e.g. Brand *et al.* 2016). Topographic ruggedness can affect flow direction and local flow detachment, causing a single current to exhibit spatially variable directionality (e.g. Lipman and Mullineaux 1981, pl. 1; Fisher 1990).

Deposit characteristics. PDC deposit characteristics are influenced by initiation mechanism, the nature of particle transport by the current, and particle composition. Single-pulse events consist of both dense and dilute flow phases that can leave superposed deposits that are gradational, or they can leave singular deposits if the dilute-flow phase outruns or detaches from the dense-flow phase. Sediment concentrations in PDCs can fluctuate with distance as the current entrains, deposits, and elutriates sediment. As a result, deposits can have textures that range from non-stratified, non-graded, and poorly sorted, to well sorted, cross-bedded and cross-stratified. Pumice and lithic particles can exhibit different size and sorting characteristics both spatially and within an outcrop owing to their different densities. Co-PDC fall deposits are a unique depositional phase that represents fall from a plume that originated from a flow phase. PDCs can be stratified both vertically and laterally; thus, deposit textures and compositions can vary not only along a flow path but also at a single site during passage of the current, leaving varied morphologic and sedimentologic signatures.

Despite insufficient understanding of the details of particle transport and depositional processes by PDCs, broad and simplified relations can be established between deposit properties and flow character. From a lithofacies perspective, PDC deposits are broadly categorized as one of two types: ignimbrites and block-and-ash flows (e.g. Wilson 1986; Branney and Kokelaar 2002). An ignimbrite is defined as the deposit of a PDC rich in pumice and pumiceous ash with dominant particle compositions having densities less than 1000 kg m^{-3}. In an ignimbrite, clasts of pumice and subordinate lithic fragments are supported in an ashy matrix of vitric shards and crystal fragments (Fig. 15). Some lithic fragments within ignimbrites may show a distinctive stretched-crack texture known as breadcrusting, indicative of magmatic fragments having skins that cooled rapidly but having interiors that were still hot and expansive. In contrast, a block-and-ash flow is typically dominated by dense, juvenile lithic fragments that are poorly to moderately vesicular and supported in a non-pumiceous ashy matrix (Fig. 16). They can also contain prismatically jointed clasts indicative of high fragment temperature.

Deposit relations with topography. PDC-deposit thicknesses and textures may show relations with topography. High-concentration flow phases tend to follow topographic lows, are focused along valleys, and can leave deposits that are a few to many metres thick. Deposits from high-concentration flows can form individual lobate deposits (Fig. 15a) or fans of debris at bases of lava domes or volcanoes (Fig. 15b). Valley-fill deposits thin laterally and terminate against valley walls or transition to deposits from a more dilute flow phase (e.g. Scott *et al.* 1996; Hildreth and Fierstein 2012; Brown and Andrews 2015). Thicknesses of deposits from high-concentration PDCs can reflect progressive aggradation of sediment during flow passage and are not necessarily representative of the depth of flow that passed. Progressive aggradation is particularly evident where chemical compositions of juvenile components change vertically within a deposit (e.g. Bacon 1983; Branney and Kokelaar 2002; Hildreth and Fierstein 2012) (Fig. 15c). Low-concentration PDCs are less constrained by topography and can flow well beyond the boundaries of channels and other topographic lows. Indeed, low-concentration currents can pass across rugged terrain surmounting multiple ridges and valleys (e.g. Fisher 1990).

Fig. 15. Textures of pyroclastic-density-current (PDC) deposits known as ignimbrites. (**a**) Lobate PDC deposit (tan) at Mount St Helens (USA). Note person and helicopter for scale. Photograph by R. Hoblitt, USGS, July 1980. (**b**) Ignimbrite sheet that overlies debris-avalanche deposit at Mount St Helens. The smooth, relatively flat-surfaced sheet is composed of multiple PDC deposits emplaced from May–October 1980. Note how this sheet mantles and fills rugged topography of the debris-avalanche deposit. Also note the secondary explosion pits formed when hot material contacted water or glacier ice in deposit. Pit on left is about 40 m wide; that on right is about 75 m wide. Photograph by J. Pallister, USGS, 2004. (**c**) Non-stratified, non-graded PDC deposit from the caldera-forming eruption of Crater Lake (USA). Note the compositional change in the deposit, which represents eruption from a compositionally zoned magma chamber. Rhyodacite (tan colour), which composed upper part of magmatic body, erupted first and was followed by eruption of andesite. Deposit is capped by a reddish oxidized zone. Outcrop is about 100 m thick. Photograph by S. Brantley, USGS. (**d**) Faintly stratified to non-stratified PDC deposits from 18 May 1980 eruption of Mount St Helens. Outcrop is about 20 m tall. Photograph by J. Major, USGS. (**e**) Non-stratified PDC deposits from eruption of Katmai volcano (USA). Note conformable contact between units at about 2/3 height of exposure, implying little break in time between emplacements. Exposure is capped by thin tephra-fall layer. Exposure is about 12 m tall; deposits overlie glacial and fluvial deposits. Photograph by W. Hildreth, USGS. (**f**) Non-stratified, poorly sorted, non-graded texture of the F-4 ignimbrite unit at Cotopaxi volcano (Ecuador). This deposit is distinguished by its mixture of rhyolite and obsidian clasts in a pumice-rich matrix. Field of view about 1 m wide. Photograph by J. Major, USGS. (**g**) Diffusely stratified, thinly laminated PDC deposit from eruption of Katmai volcano. Exposure is about 8 m tall. Note how laminae are continuous throughout exposure height. Deposit is about 15 km from vent source. Photograph by W. Hildreth, USGS.

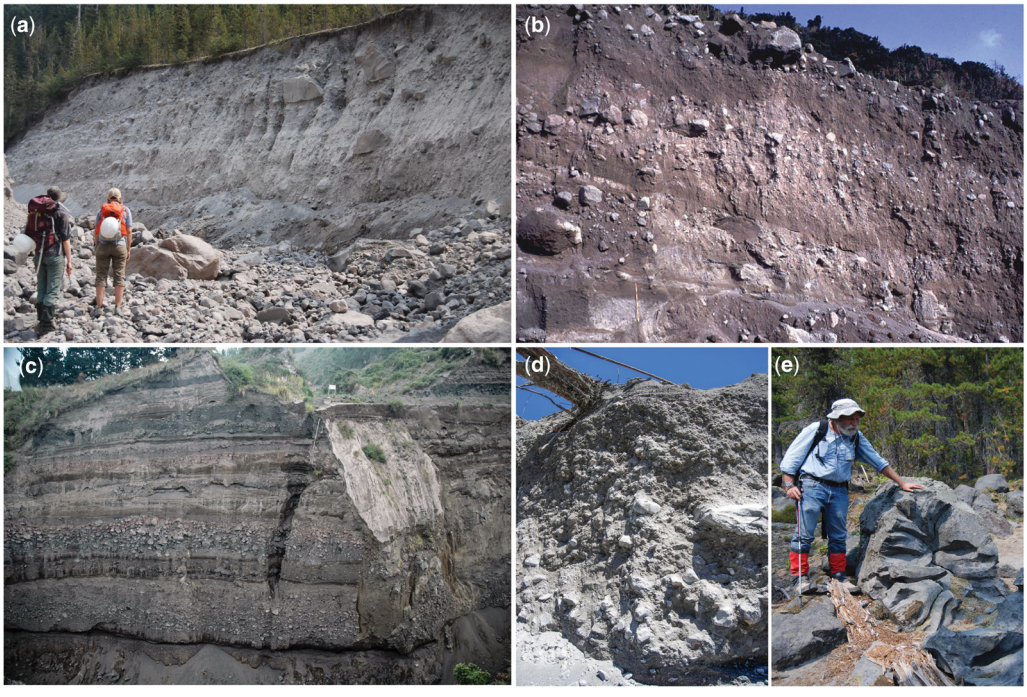

Fig. 16. Textures of block-and-ash-flow (BAF) deposits. Note poor sorting of deposits and angularity, size, and general lack of grading of the dense, coarse clasts transported. (**a**) Multiple BAF deposits along Butte canyon, Mount St Helens (USA). Photograph by J. Major, USGS. (**b**) BAF deposits emplaced by 1991–95 eruption of Unzen volcano (Japan). Outcrop about 4 m tall. Photograph © Y. Miyabuchi, Japan Ministry of Agriculture. (**c**) Sequence of multiple BAF deposits exposed along Rea Ravine, Tungurahua volcano (Ecuador). Note road sign for scale. Photograph by J. Major, USGS. (**d**) BAF deposit from 2009 dome collapse at Chaitén volcano (Chile), exposed along Chaitén River valley. Outcrop about 5 m tall. Photograph by J. Major, USGS. (**e**) Prismatically jointed block in BAF deposit from fifteenth–eighteenth century eruptions of Mount St Helens. Photograph by J. Major, USGS.

Deposits of these currents are thin (centimetres to tens of centimetres thick), and they can become thinner and finer with distance from source. Thicknesses of PDC deposits resulting from caldera collapse can vary from tens of centimetres to hundreds of metres, and stratigraphic sequences can exhibit time transgressions of currents having varied texture and thickness within a single large event. Particularly energetic PDCs that sweep across the landscape can leave deposits that are thin relative to deposit volume and coverage area (e.g. Hoblitt *et al.* 1981; Wilson 1986; Fisher *et al.* 1987). Non-stratified deposits related to concentrated parts of the current are commonly more prevalent and thicker along valley floors whereas thinner but stratified deposits from the same current may be found at higher elevations along valley walls and ridges (e.g. Scott *et al.* 1996; Charbonnier and Gertisser 2008).

Slope angle can influence longitudinal variations in deposit textures within a single current. Brand *et al.* (2016) showed that non-blast-origin PDCs from the 18 May 1980 eruption of Mount St Helens produced non-stratified, poorly sorted deposits on low-gradient slopes and generally stratified to cross-stratified deposits on steeper slopes leading from the volcano's crater, indicating that currents were more turbulent with less internal stratification on steeper-gradient slopes.

Deposit textures and sedimentary structures. Because of the variety of initiation mechanisms, particle support mechanisms, and particle compositions, PDC deposits can exhibit a variety of textural characteristics and sedimentary structures (e.g. Branney and Kokelaar 2002; Brown and Andrews 2015). Ignimbrites are usually coarse grained and consist of angular to subangular lithic clasts and subangular to rounded pumice clasts, with clasts as large as metres in diameter, within an ashy matrix, whereas BAFs are dominated by angular to subangular lithic fragments up to metres in diameter in an ashy matrix (Figs 15 & 16). Both types of deposits are typically non-stratified and poorly sorted, although they can show textural variety (e.g. Wilson 1986; Branney

and Kokelaar 2002; Hildreth and Fierstein 2012; Major *et al.* 2013; Brown and Andrews 2015; Douillet *et al.* 2015; Brand *et al.* 2016; Báez *et al.* 2020; Gillies *et al.* 2020).

Varying clast density within PDCs affects particle grading and sorting. Within ignimbrites, pumice and lithic clasts may be strongly segregated and exhibit different styles of grading (for example lithic clasts may be normally graded whereas pumice clasts may be inversely graded). However, clast segregation may be suppressed and particles non-graded. An extreme form of particle segregation in PDCs is recorded by lithic-rich, co-ignimbrite lag deposits (e.g. Druitt and Bacon 1986). Those deposits typically are coarse grained, fines depleted, lithic-and-crystal enriched, and they can extend several kilometres from a volcano. They are distinguished from fall or other lithic-rich deposits through evidence of lateral flow and association with ignimbrite deposits. They represent exceptional lithic-particle segregation and sedimentation within proximal reaches of a column-collapse PDC and are commonly associated with caldera-collapse events. Overall, the grading of lithic and pumice particles reflects relations between size and density (e.g. Wilson 1986; Choux and Druitt 2002). Within BAFs, lithic fragments may exhibit some grading, but they are most commonly non-sorted and non-graded.

Vesicularity of juvenile lithic particles can vary within PDC deposits. Highly vesicular particles within ignimbrites are the result of magmatic explosions or column collapse, whereas denser juvenile particles are more likely the result of BAFs induced by dome collapse or reflect inclusion of fragments of largely degassed magma. Other lithics may include conduit material entrained during ejection or eroded during flow.

Particle composition and texture have been used to infer volcanic processes. For example, some ignimbrite deposits associated with caldera collapse show sudden onset of abundant lithic fragments within vertical sections of deposits, especially in proximal deposits. This sudden onset of lithic material, especially of non-juvenile lithics, reflects abrupt entrainment of conduit wall rock within the eruption column. Its appearance is generally inferred to represent onset of ring-vent development and caldera collapse (e.g. Bacon 1983; Druitt and Bacon 1986; Scott *et al.* 1996). PDC deposits rich in vesicular, cauliflower-head-shaped clasts have been inferred to have formed by a boiling-over mechanism at Cotopaxi volcano (Ecuador) (Hall and Mothes 2008), Tungurahua volcano (Ecuador) (Hall *et al.* 2013; Rader *et al.* 2015), and Citlaltépetl volcano (Mexico) (Carrasco-Núñez and Rose 1995) among others, but may not be diagnostic of such an origin.

PDC deposits can display a variety of sedimentary structures. Ignimbrite and BAF deposits are commonly massively textured but may show diffuse stratification, indicative of unsteady flow behaviour or amalgamation of multiple pulses of flow (e.g. Branney and Kokelaar 2002; Brand *et al.* 2014). Clast compositions and basal boundaries may show evidence of substrate erosion, such as clasts and other debris clearly entrained from the substrate. Deposits may exhibit internal channel erosion and other cross-cutting relations indicative of self-channelization during sustained flow (e.g. Brand *et al.* 2014) or of time breaks between flows, soft-sediment deformation structures indicative of sediment fluidization, and fines-depleted pipe structures related to degassing (e.g. Branney and Kokelaar 2002; Douillet *et al.* 2015; Valentine *et al.* 2021). Lithic-rich BAF deposits (Fig. 16) may exhibit textures and structures similar to other breccias, and can be difficult to distinguish. However, BAF deposits contain clues to their origin. Uniform remanent magnetism of originally hot clasts, slightly reddish coloration owing to iron oxidation from percolating gases, an ashy or a less dense and more friable matrix owing to elutriation of some fines by gases and ingested air, evidence of pipes along which fine material has been removed, and inclusion of prismatically jointed clasts can signal that the deposit is from a PDC (e.g. Crandell 1987). Lahar deposits may sometimes contain pipe or dish structures related to escape of water (e.g. Scott *et al.* 1995), which can mimic gas-pipe structures in PDC deposits. But lahars may show small voids in the matrix related to air bubbles trapped within water-saturated sediment. Such voids are not present in PDC deposits. In some instances, deposit origin may be difficult to identify until or unless detailed field mapping is conducted. Fisher and Schmincke (1984) provide a table of deposit characteristics (table 11-3) that may help distinguish breccia-deposit origin.

Deposits from pyroclastic surges, in which transport and deposition are strongly influenced by turbulence, are commonly moderately sorted to well-sorted, distinctly stratified to cross-stratified and may show evidence of bedform development (e.g. Waitt 1981; Sigurdsson *et al.* 1984; Scott *et al.* 1996; Sulpizio *et al.* 2007; Brown and Andrews 2015; Brand *et al.* 2016) (Fig. 17). However, they can also be non-stratified if deposited rapidly (e.g. Fisher *et al.* 1987). These deposits typically form subordinate facies within ignimbrite and BAF successions, although some successions may be dominated by this type of deposit. Phreatomagmatic eruptions, in which near-surface magma interacts with water, can produce very energetic surges. Because of the interaction with water, the magma and conduit wall rock can become highly fragmented, and that fragmentation can produce abundant fine ash. Surge deposits from phreatomagmatic eruptions are commonly highly enriched in fine ash whereas

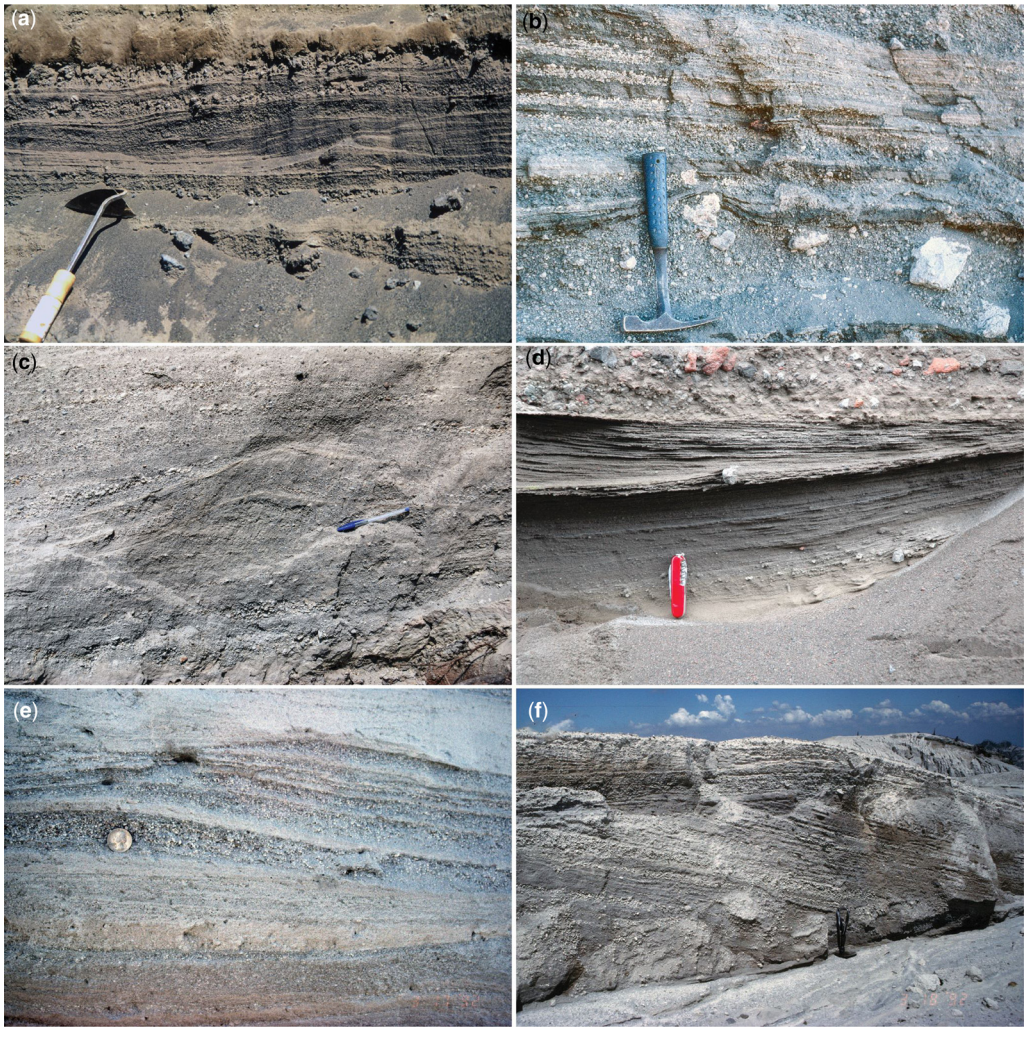

Fig. 17. Deposit textures and sedimentary structures of low-concentration (surge) pyroclastic density currents (PDCs). Note the predominantly stratified to cross-bedded nature of the deposits and local formation of bedforms. Some deposits are poorly to moderately well sorted and rich in fine to extremely fine ash (fine sands and silts); others are moderately to well sorted and dominated by medium to coarse ash (medium to coarse sand). (**a**) Deposit from phreatomagmatic explosions of Batur volcano (Indonesia). Deposit is rich in fine ash. Flow direction left to right. Photograph by J. Major, USGS. (**b**) Deposits from phreatomagmatic explosions of Laguna de Aramuaca volcano (El Salvador). Surge deposits are rich in fine ash and interbedded with coarser fall deposits. Photograph by J. Major, USGS. (**c**) Laminated PDC deposit from ancestral eruption of Mount St Helens volcano (USA). Note well-developed bedforms. Flow direction is left to right. Photograph by J. Major, USGS. (**d**) Stratified PDC deposits from eruption of Tungurahua volcano (Ecuador). Photograph by J. Major, USGS. (**e**) Cross-bedded, stratified deposits with small-scale bedforms, Mount Pinatubo (Philippines). Flow direction is left to right. Photograph by W. Scott, USGS. (**f**) Stratified deposit with large-scale bedforms. Foreset (dipping) beds are overlain by topset (subhorizontal) beds. Those topset beds transition into foreset beds at right, Mount Pinatubo. Flow direction is left to right. Photograph by W. Scott, USGS.

deposits of surges caused by other mechanisms are commonly poorer in fine ash owing to elutriation caused by ingestion of air and magmatic gases.

Deposits of particularly high-energy PDCs, such as at Mount St Helens in 1980 and Lamington volcano in 1951, and especially those that result from directed explosions, exhibit characteristics of deposits resulting from flow, surge, and fall (Hoblitt *et al.* 1981; Fisher *et al.* 1987; Belousov *et al.* 2007). Like flow deposits, they can contain poorly sorted

units that are thicker in topographically low areas and taper against valley walls, can contain juvenile rock fragments having variable density and vesicularity, and those fragments commonly constitute 50% or more of the particle composition. Like surge deposits, they can have units that are moderately sorted to well sorted and bedded to cross-bedded. Overall, the deposits are thin compared to the area they cover, typically are thinner on ridges and thicker in topographically low areas at any given distance from source, and are less sensitive to topography than pyroclastic flows in that they can be spread broadly over rugged topography. Like fall deposits, they become thinner and finer grained with distance from source. Topographic grain can affect deposit character depending on whether the current moves parallel or perpendicular to topographic trends (Fisher 1990).

High-energy PDC deposits are normally graded overall, but are commonly subdivided into a bipartite or tripartite stratigraphic layering with layers exhibiting variable grading, sorting, and stratification (e.g. Hoblitt *et al.* 1981; Waitt 1981; Fisher *et al.* 1987; Belousov *et al.* 2007, 2020; Major *et al.* 2013) (Fig. 18). Typically, they consist of a basal layer of friable, poorly sorted, non-graded to normally graded angular gravel and coarse sand (blocks, lapilli, and ash) admixed with soil and organic debris. This layer commonly has an erosive contact and may be smeared across the ground surface. It typically grades into a layer of moderately sorted, fines-depleted angular gravel and sand (lapilli and ash), which may be non-stratified to indistinctly bedded. These two layers may be stratigraphically distinct, or the basal layer may form the lower part of a single stratigraphic subunit. Commonly, the fines-depleted unit grades into, or transitions abruptly into, a less friable, poorly sorted layer rich in fine material and commonly consisting of a normally graded sand (ash), which may be non-stratified to laminated or distinctly bedded with evidence of translational bedforms. Commonly, but not always, this depositional sequence is capped with a normally graded sandy silt (fine to extremely fine ash) rich in accretionary lapilli. Contacts and stratigraphic relations indicate that these diverse layers were deposited rapidly by a single event.

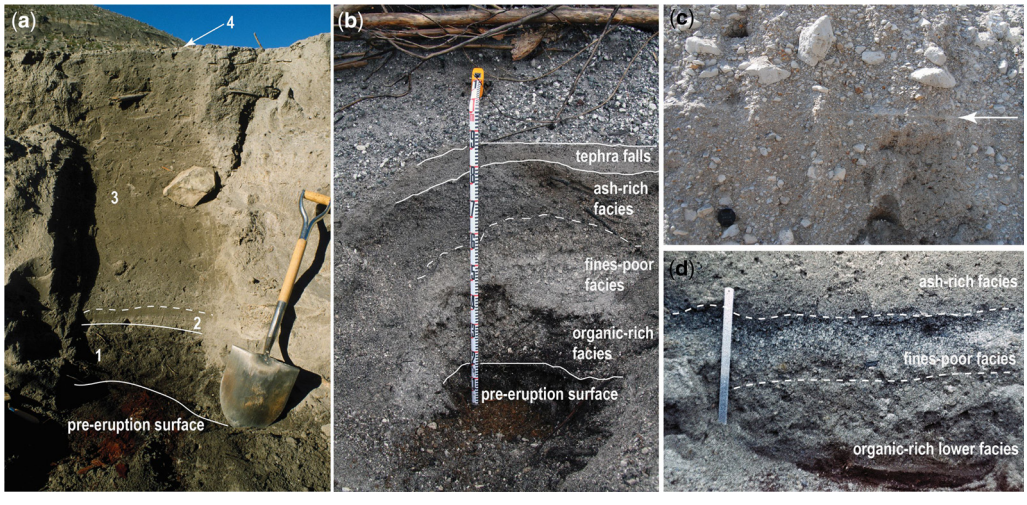

Fig. 18. Deposits from pyroclastic density currents (PDCs) initiated by horizontally or low-angle-directed explosions. (**a**) Deposit from 18 May 1980 Mount St Helens (USA) eruption. Layer 1 is an organic and soil-rich layer with clear basal erosional contact. Layer 2 is a non-stratified, fine-grained unit (coarse to fine ash) deposited by dilute part of PDC. Layer 3 is a non-stratified, generally poorly sorted unit that accumulated largely in topographically low areas. Layer 4 is an overlying fall unit rich in accretionary lapilli. In this exposure, layers 1 and 2 are equivalent to the lower organic-rich, fines poor and ash-rich layers that compose similar deposits elsewhere. Layer 3, a deposit from a dense flow unit that developed through continued settling of the stratified PDC and which is found only in isolated topographically low areas, is not commonly observed in other deposits from directed explosions. Its presence illustrates the complexity of deposition by such events. Photograph by C.D. Miller, USGS. (**b**) Deposit from directed explosion during 2008 eruption of Chaitén volcano (Chile). Photograph by R. Hoblitt, USGS. (**c**) Proximal exposure of coarse, poorly sorted, fines-poor facies of Mount St Helens 18 May 1980 deposit at base of volcano. Note possible evidence of two pulses of flow separated by thin fine-grained layer (arrow). Photograph by J. Major, USGS. (**d**) Deposit from directed explosion during 1956 eruption of Bezymianny volcano (Russia). Photograph © A. Belousov, Russian Institute of Volcanology and Seismology.

Effects of temperature and vapour-phase alteration. PDCs can deposit sediment under a variety of temperatures. Those deposited at low temperatures (<550°C) are commonly loose to weakly compacted unless altered by hydrothermal activity or vapour-phase mineralization, and deposits have textural characteristics essentially identical to those at the time of deposition (Wilson 1986). They may show varying shades of pink and red coloration related to deposition of iron oxides from percolating gases (Wilson 1986). In contrast, high-temperature PDC deposits may be fully or partly indurated, a textural characteristic known as welding (e.g. Smith 1960; Wilson 1986). Welding results from cohesion and deformation of particles at temperatures above the glass-transition threshold, first at local contacts between particles and ultimately through complete fusion of particles by elimination of pore space. Deformed pumice particles known as fiamme are common in welded ignimbrites (e.g. Wilson 1986). The degree of welding in high-temperature PDC deposits is largely a function of chemical composition (which affects viscosity of glassy particles), temperature, and deposit thickness, which affects contact pressure at any point within the deposit and rate of cooling (Smith 1960; Wilson 1986; Brown and Andrews 2015). As a result, welding tends to be most intense within, but near the base of, an ignimbrite deposit. Exceptionally intense welding can lead to glassy deposits that are difficult to distinguish from lava flows. On steep slopes, intensely welded ignimbrites can continue to deform and flow, forming what are known as rheomorphic ignimbrites (Wilson 1986; Brown and Andrews 2015). In addition to fusing of particles by welding, vapour transfer through deposits can lead to crystallization within pore spaces and densification and induration of deposits. Textures such as columnar jointing, primarily attributed to cooling of welded deposits, can also develop in high-temperature, vapour-phase-altered, non-welded PDC deposits (Wilson 1986; Wright *et al.* 2011).

Lahar

A lahar is a mobile, saturated mixture of water and sediment that flows swiftly along a channel that drains a volcano or a volcanically impacted landscape (Fig. 19). Unlike a water flood, a lahar is a coherent mixture of water and sediment that can transport abundant rocky and organic debris. As a result of its mass, momentum, and sediment competence, it poses a serious threat to people and property, and typically deposits a sheet or lobe of muddy sand and gravel, which ranges from many centimetres to many metres thick (e.g. Thouret *et al.* 2020).

A lahar spans a spectrum of sediment–water flows having varying sediment concentrations; thus, no single sediment concentration defines a lahar. Instead, a lahar is a flowing sediment–water mixture that is different from normal sediment-laden streamflow (Smith and Fritz 1989; Vallance and Iverson 2015). Lahar characteristics can evolve in time and over travel distance. Two basic styles of lahar are commonly identified: a debris-flow lahar, here called a type-1 lahar, contains roughly equal proportions of sediment and water and looks very much like flowing, wet cement. This type of flow is poorly sorted and transports sediment ranging in size from clay to boulders. A hyperconcentrated-flow lahar, here called a type-2 lahar, is more dilute and composed of more water than sediment (Pierson 2005). The proportion of water and sediment can vary broadly, and as a result a type 2 lahar takes on a more liquid-like appearance than does a type-1 lahar. A type-2 lahar is broadly transitional between sediment-laden streamflow and a type-1 lahar. A type-2 lahar is composed dominantly of moderately to poorly sorted sand but can transport larger particles as bedload.

A lahar can form in many ways, and it can occur both during and after an eruption (Fig. 20). A lahar commonly forms in one of five principal ways: (1) by scour and melt of snow and glacier ice during passage of a PDC to form a mixture of water and sediment; (2) by liquefaction and direct transformation of a volcanic debris avalanche; (3) by an explosive eruption or other mechanism that releases a crater lake to form a flood that erodes sediment; (4) by other floods that erode sediment (such as glacier outburst floods or when groundwater is released during an eruption or intrusion); and (5) by rainfall that erodes and mobilizes fresh volcanic ash (tephra) or triggers a shallow landslide from the flank of a volcano. On rare occasions, a lahar can be triggered by a phreatic eruption that directly ejects a mixture of water and sediment (e.g. Sasaki *et al.* 2016). A primary lahar is directly associated with co-eruptive processes, such as snow and ice melt by PDC or explosive ejection of a crater lake. A secondary lahar occurs after primary volcanic sediment has been deposited. It can occur during or after an eruption or during a quiescent period between eruptions. A secondary lahar results from remobilization of volcanic sediment by heavy rainfall, landslide, lake breach, or water released from a glacier, and it can occur days, weeks, months, or even centuries after initial sediment deposition. More rarely, a lahar can be initiated by an earthquake that generates a failure of a segment of a volcano or many shallow landslides that liquefy and coalesce into a larger flowing mass (e.g. Scott *et al.* 2001; Worni *et al.* 2012). Close association with an eruption, but not direct association with eruptive processes, can blur distinction between primary and secondary lahars and make interpretation of the geological record challenging.

Fig. 19. Examples of lahars. (**a**) Flow along Whangaehu River, Mount Ruapehu (New Zealand). Concrete pillar is about 4 m tall. Photograph © J.R. Grant, 1995. (**b**) Lahar from Mayon volcano (Philippines), 1984. Boulders in flow range from about 0.3–1 m in diameter. Photograph by E. Corpuz, PHIVOLCS, 1984. (**c**) Lahar along Sacobia River, Mount Pinatubo (Philippines). Flow wave is about 1 m tall. Photograph © M. Dolan, Michigan Technological University, 1992. (**d**) Mudflow along White Salmon River (Washington, USA). This flow was initiated by a dam removal rather than a volcanic eruption, but it shows well the texture of a high-concentration flow. Inset shows samples of sediment-to-water ratio of this flow. Channel is about 35 m wide. Photograph by J. O'Connor, USGS, 2011.

For example, the North Fork Toutle River lahar caused by the 1980 eruption of Mount St Helens was not associated directly with the eruption, but rather formed over a span of hours as the large debris avalanche locally dewatered. Thus, the original source sediment for this lahar was temporarily stored and subsequently remobilized. Yet, in the geological record, it will largely be interpreted as a primary lahar owing to its close association with the eruption. Broader sedimentologic and geomorphic context and relative position and timing in the stratigraphic record must be scrutinized when deciphering primary from secondary origins of lahars.

Initiation mechanism affects the nature, size, and composition of a lahar. A lahar formed during an explosive eruption by snow-and-ice melt, by release of a crater lake, by failure of wet, weak rock from a volcano, or by sudden release of water from a large lake dammed by volcanic debris commonly is large, fast, and very destructive far downstream from a volcano. Lahars formed by rainfall erosion of volcanic ash or by release of modest volumes of subglacial water are likely to be smaller and travel shorter distances, but they may occur more frequently. These smaller but more frequent lahars can gradually fill river channels close to volcanoes with thick amounts of sediment. A lahar formed when groundwater is released during an eruption or intrusion can vary in size depending upon the volume of water released. A secondary lahar formed by transformation of a shallow landslide commonly is small (typically to a few hundreds of thousands of cubic metres) compared to an eruption-triggered lahar and is largely restricted to an area close to a volcano.

Melting of snow and ice and mixing with volcanic debris. Pyroclastic density currents commonly trigger lahars at glaciated volcanoes. These hot currents sweep across snow- and ice-covered slopes, scour and mix with snow and glacier ice, and produce watery floods or slurries. As these floods sweep downhill, they erode additional sediment from the volcano's flanks and surrounding river channels, grow in volume, and become sediment-rich lahars. Notable lahars of this type have formed during

Fig. 20. Examples of lahars triggered by various initiation mechanisms. (**a**) Lahar at Redoubt volcano (USA) triggered by melting of snow and ice. Photograph © M. Fulle, http://www.stromboli.net, April 2009. (**b**) Lahar triggered by release of subglacial water and groundwater, Huila volcano (Colombia). Photograph by B. Pulgarín, Servicio Geológico Colombiano, Observatorio Vulcanológico y Sismológico de Popayán, November 2008. (**c**) Lahar triggered by snowmelt during a minor explosion, Mount St Helens (USA). Photograph by T. Casadevall, USGS, March 1982. (**d**) Lahar triggered by explosive ejection of water from crater lake, Ruapehu volcano (New Zealand). Photograph © G. Jolly, GNS Science/EQC (image VML 190924), September 2007. (**e**) Lahar triggered by rainfall-induced shallow landslide, San Vicente volcano (El Salvador). Photograph by J. Major, USGS, June 2010. (**f**) Lahar triggered by rainfall erosion of tephra-fall and pyroclastic-density-current deposits, Mount Pinatubo (Philippines). Photograph by W. Scott, USGS, July 1991.

many eruptions (e.g. Wolf 1878; Gorshkov 1959; Murai 1960; Gorshkov and Dubik 1970; Pierson 1985; Eppler 1987; Fairchild 1987; Scott 1988*a*; Major and Newhall 1989; Pierson *et al.* 1990; Doravа and Meyer 1994; Branney and Gilbert 1995; Mothes *et al.* 1998; Vallance *et al.* 2010; Waythomas *et al.* 2013; Waythomas 2015).

Lahars caused by PDCs scouring and melting snow and ice range widely in size (Pierson 1985; Pierson *et al.* 1990; Vallance *et al.* 2010; Waythomas *et al.* 2013). Some are relatively small and localized (Vallance *et al.* 2010) whereas others can be as large as hundreds of millions of cubic metres (e.g. Worni *et al.* 2012; Waythomas *et al.* 2013). At Mount St

Helens in 1980, PDC-generated lahars had volumes of about 15×10^6 m^3 and travelled many tens of kilometres down valley (Fairchild and Wigmosta 1983; Pierson 1985; Scott 1988*a*). At Nevado del Ruiz (Colombia) in 1985, small PDCs swiftly melted snow and ice on the volcano's summit and produced abundant meltwater (Naranjo *et al.* 1986). The resulting floods eroded sediment from several steep, narrowly confined valleys, and transformed to lahars ranging in volume from $1–40\times10^6$ m^3 (Pierson *et al.* 1990). Those lahars descended nearly 5000 m in elevation from the summit and travelled more than 100 km (Pierson *et al.* 1990). During the 2009 eruption of Redoubt volcano (USA), PDC-triggered lahars had volumes of $10^7–10^8$ m^3 (Waythomas *et al.* 2013). Field studies at Cotopaxi volcano revealed that the Holocene Chillos Valley Lahar, possibly formed in part by PDC melt of the volcano's icecap, had a volume of *c.* 3.8 km^3, flowed more than 300 km from the volcano, and had local depths of 80–160 m (Mothes *et al.* 1998).

Transformation of landslides. A volcanic debris avalanche can produce a lahar directly if the avalanche is particularly wet, clay rich (many weight-percent clay), and transforms from a slide to a flow as it sweeps downslope. Lahars caused by transformations of debris avalanches are not known to be common, but, where documented, they have been large, commonly on the order of 0.1–1 km^3 (MacPhail 1973; Carrasco-Núñez *et al.* 1993; Vallance and Scott 1997; Capra and Macías 2000; Detienne *et al.* 2017). A classic example of this type of lahar is the Osceola Mudflow from Mount Rainier (USA), which formed during an eruption 5600 years ago. High on the volcano's flank, weak, water-saturated rock collapsed. That material transformed to a deep, valley-filling lahar within a few kilometres of its source. This lahar, nearly 4 km^3 in volume, funnelled into and filled mountain valleys 75–150 m deep, travelled more than 100 km to Puget Sound (Washington, USA), and continued some 15 km underwater (Vallance and Scott 1997).

Most large debris avalanches from collapses of volcanoes do not transform immediately, if at all, to lahars. For example, the 2.5 km^3 debris avalanche that initiated the 18 May 1980 eruption of Mount St Helens slid off the volcano and came to a complete stop within 30 km. Then, over the next hours, water-saturated parts of its deposit liquefied and began to flow (Janda *et al.* 1981; Fairchild and Wigmosta 1983). Several small flows coalesced to produce the 140×10^6 m^3 North Fork Toutle River lahar. That lahar was the largest of the 1980 eruption, flowing some 100 km from the volcano (Janda *et al.* 1981; Schuster 1983).

Heavy rainfall and snowmelt can trigger relatively small ($10^3–10^5$ m^3) landslides at volcanoes. Such meteorologically triggered landslides are generally shallow slope-failures (a few tens of metres thick). Unlike large debris avalanches, these smaller landslides can transform to lahars that range from a few thousands to a few hundreds of thousands of cubic metres in volume. For example, intense rainfalls at San Vicente volcano (El Salvador), Mount Hood (USA), and Izu Oshima volcano (Japan) triggered shallow landslides that evolved into lahars (Gallino and Pierson 1985; Major *et al.* 2004; Miyabuchi *et al.* 2015; Smith *et al.* 2015).

Sediment erosion by floods. Floods resulting from mechanisms other than by scour of snow and ice during an eruption can also entrain sediment and transform into lahars. These floods can form by release of water from a summit crater lake, breaching of a valley-margin lake dammed by volcanic sediment, release of abundant groundwater from a volcano, or sudden release of stored water from a volcano glacier (e.g. Suryo and Clarke 1985; Scott 1988*b*; Umbal and Rodolfo 1996; Cronin *et al.* 1997*a*; Capra and Macías 2002; Rodolfo and Umbal 2008; Massey *et al.* 2010; Worni *et al.* 2012; Gudmundsson 2015; Pagneaux *et al.* 2015; Johnson *et al.* 2018). Depending on the volume of water released and the rate at which it is released, these lahars can vary in size, speed, and travel distance. A 2008 phreatomagmatic eruption of Huila volcano (Colombia) triggered an estimated 300×10^6 m^3 lahar (Worni *et al.* 2012; Pulgarín *et al.* 2015). Subsequent inspection showed the glacier on the volcano's west flank to be heavily fractured, but the exact source of the large amount of water needed to produce this lahar is not entirely clear (Worni *et al.* 2012; Pulgarín *et al.* 2015).

The largest known lahar at Mount St Helens occurred about 2500 years ago when a large lake dammed by volcanic debris breached its blockage. Sudden release of lake water produced a series of flood surges that entrained channel sediment through bed incision and lateral erosion over many kilometres of valley. The largest lahar had a volume of about 1 km^3 (Scott 1988*b*) and inundated now-urbanized areas 80–100 km downstream with a coarse-sediment-rich flow to depths of 5–10 m (Chan 2008). The largest lahar at Mount St Helens since its great 1980 eruption happened when a temporary meltwater lake formed and spilled from the crater. In 1982, an explosion from a growing lava dome sprayed hot rock across the volcano's crater walls, which melted snowpack and formed a transient lake (Waitt *et al.* 1983). Released lake water produced a flood that eroded sediment and transformed into a 15×10^6 m^3 lahar that flowed at least 80 km downstream (Pierson 1999).

Release of water from existing crater lakes can occur during an eruption. Kelut volcano (Indonesia)

is notorious for expelling water from its crater lake during eruptions and generating large floods that scour sediment from the volcano's flanks and form lahars. Such lahars occurred in 1919 and 1966 during explosive eruptions through its crater lake (Suryo and Clarke 1985). Drainage tunnels now limit the volume of the crater lake, reducing the amount of lake water available to form lahars. A month-long series of explosions through the crater lake at Ruapehu volcano (New Zealand) in 1995 emptied the lake, causing some 26 lahars having a cumulative volume of 10^6 m^3 at a distance 56 km from source (Cronin *et al.* 1997*b*).

Crater lakes can also release water during periods of inactivity. During dormant periods between eruptions, the summit crater lake at Ruapehu volcano has breached its volcanic sediment dam (formed by heavy ash fall during eruptions) and produced notable lahars. The most recent instance in 2007 released 1.3×10^6 m^3 of lake water (Procter *et al.* 2010). The consequent flood mobilized roughly 3×10^6 m^3 of sediment from the initial 5 km of downstream channel, forming a nearly 4.5×10^6 m^3 lahar. As this lahar travelled farther downstream, it alternately eroded and deposited sediment along the channel, which maintained a nearly 3×10^6 m^3 lahar for more than 60 km (Massey *et al.* 2010; Procter *et al.* 2010).

A sudden release of water stored within or beneath glaciers or released from moraine-dammed lakes can also produce flood surges that spawn lahars. Glacier-outburst floods can occur during eruptions when subglacial lava flows, pyroclastic eruptions, or increased heat flux melt glacier ice. But they can also occur during non-eruptive times, such as during spells of hot weather or heavy rainfall when subglacial and intraglacial storage cavities link, pressurize, and release. In Iceland, for example, lahars – or at least sediment-laden floods – can form from large glacier outburst floods (jökulhlaups), which are common when eruptions occur beneath massive glacial ice caps that overlie many of its volcanoes (Gudmundsson 2015). Lahars caused by glacier-outburst floods also occur on much smaller scales. In the Cascade Range (USA), small (typically 10^4 m^3) lahars formed by outburst floods are common. For example, outburst-flood-triggered lahars occur frequently at Mount Rainier and Mount Shasta, and have also been witnessed at Glacier Peak and Mount Hood (Richardson 1968; Crandell 1971; Walder and Driedger 1994, 1995; Blodgett *et al.* 1996). Most of these lahars travel only a few kilometres. Other interactions between glaciers and streams can also trigger small lahars. At Mount Rainier, for example, a meltwater stream along the margin of a glacier spilled through a notch in a moraine, eroded and entrained sediment, and transformed into a small lahar (Vallance *et al.* 2002). Glacial-lake-outburst floods occur when a moraine-dammed lake is released through dam failure or displacement of lake water over the dam or when a summit meltwater lake is displaced by collapsing ice and debris. Similar to breachings by lakes dammed by volcanic debris, these breakout floods can cause lahars of varying size depending on volume and rate of water released (e.g. Coombs *et al.* 2006; George *et al.* 2019).

Rainfall-runoff erosion of volcanic ash and other pyroclastic sediment. Heavy rainfall on freshly deposited volcanic ashfall can promote surface runoff that can lead to flash-flood-like events that transform into lahars by eroding and entraining sediment from both hillsides and river channels (e.g. Waldron 1967; Barclay *et al.* 2007; de Bélizal *et al.* 2013; Pierson and Major 2014). These types of lahars occur frequently and can persist for many years, especially if the landscape is repeatedly recharged with ashfall or deposits from PDCs during prolonged eruptions (e.g. Waldron 1967; Barclay *et al.* 2007). Although individual lahars may not be large, their frequency can have significant cumulative effects downstream; cumulated deposits can overwhelm channels and cause rivers to change course (e.g. Crittenden and Rodolfo 2002; Pierson *et al.* 2013). Furthermore, rainfall lahars can occur well after eruptions end if rainfall intensities, durations, and sediment supply are sufficient (e.g. Crittenden and Rodolfo 2002; Capra *et al.* 2018; Tsunetaka *et al.* 2021).

Rainfall-triggered lahars are distributed across many environmental settings, from tropical- to high-latitude volcanoes. The most devastating rainfall-generated lahars in modern times occurred at Mount Pinatubo (Philippines) during and following its 1991 eruption. There, multiple drainages around the volcano were affected for many years (Pierson *et al.* 1996; Umbal 1997; Crittenden and Rodolfo 2002). Notable rainfall lahars, many in just the past few decades, have been documented in varied environmental settings including at tropical volcanoes (Waldron 1967; Rodolfo and Arguden 1991; Thouret *et al.* 1998; Harris *et al.* 2006; Barclay *et al.* 2007; Paguican *et al.* 2009; Capra *et al.* 2010; Doyle *et al.* 2011; de Bélizal *et al.* 2013; Vázquez *et al.* 2014; Dibyosaputro *et al.* 2015; Cando-Jácome and Martínez-Graña 2019), low-latitude, high-altitude volcanoes (Jones *et al.* 2015), mid-latitude volcanoes (Hodgson and Manville 1999; Miyabuchi 1999; Pierson *et al.* 2013; Miyabuchi *et al.* 2015; Kataoka *et al.* 2018; Hayes *et al.* 2019; Mosbrucker *et al.* 2019; Baumann *et al.* 2020), and even heavily glacier-clad, high-latitude volcanoes (Jensen *et al.* 2013).

Depositional processes. Conceptual understanding of lahar deposition has evolved over the past several

decades. In the late 1960s and 1970s, Johnson (1970) proposed that non-volcanic debris flows could be modelled as Bingham fluids having yield strength. As long as applied stresses exceeded the inherent yield strength of the mixture, it remained in motion. When stresses dropped below the inherent yield strength of the mixture (for example when flows reached shallow gradients or spilled across flood plains) the flow stopped *en masse*, essentially 'freezing' in place. In this view of deposition, the deposit reflects the characteristics of the flow at a given instant in time. In the 1980s, field examinations of lahar deposits in the aftermath of eruptions of Mount St Helens and studies of ancient lahar deposits began to document vertical variations in deposit textures that were incompatible with a model of flow instantaneously freezing in place (e.g. Pierson and Scott 1985; Vallance and Scott 1997). In addition, large-scale flume experiments with debris flows in the 1990s showed that complex deposition by waves of flow could produce deposits that appeared to have textural characteristics identical to those attributed to *en masse* instantaneous deposition (e.g. Major 1997). These observations and experiments, coupled with emerging ideas regarding deposition by PDCs (Branney and Kokelaar 1992, 2002), spurred the hypothesis that lahars can deposit sediment progressively from flow-front to tail. Thus, deposits can reflect progressive changes of flow character over time and not simply a snapshot of flow character at an instant in time (e.g. Vallance and Iverson 2015; Fig. 21).

Many lahars evolve by varying their sediment load through erosion or deposition of sediment. Although nearly all lahars are the result of sediment erosion, evidence of the sources of sediment and how those sources evolve along flow paths may be subtle or obvious depending on the textural and lithological characteristics of the entrained sediment. For example, a lahar that forms on the flank of volcano will commonly contain large proportions of angular to subangular clasts composed of volcano lithologies.

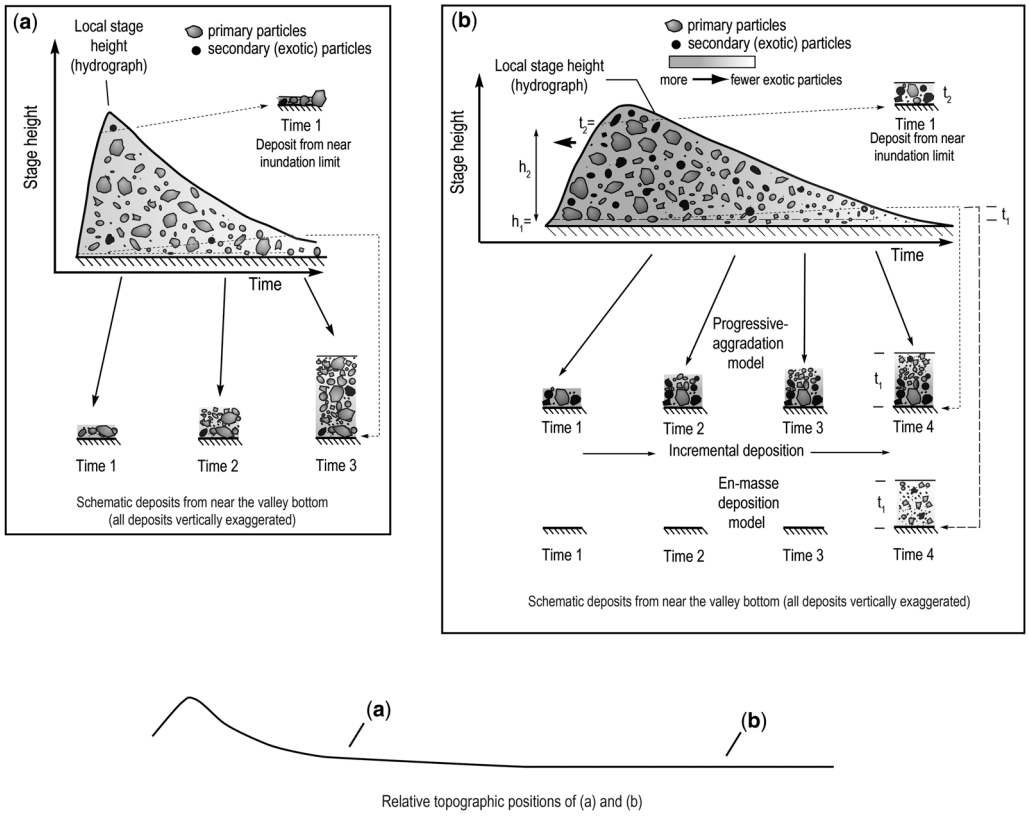

Fig. 21. Schematic depiction of relations between character of lahar flow and consequent deposits in space and time during progressive sediment accumulation. Bottom profile represents a view looking downstream, with relative topographic position of (**a**) and (**b**) within channel cross-section identified; (b) is closer to channel centre. From Vallance and Iverson (2015).

But as it travels downstream, a lahar can erode and entrain channel sediment that is dominantly subrounded to rounded, composed of lithologies not found on the volcano, and include intact stratigraphic sections of bank sediment. As a result, the amounts of rounded and exotic particles in its deposit can provide information on the degree of sediment entrainment along the flow path and offer clues to its origin and transport behaviour (e.g. Scott 1988*a*, *b*; Vallance and Scott 1997; Thouret *et al.* 1998; Capra *et al.* 2002; Scott *et al.* 2005). Aside from entraining sediment, a lahar can mix with streamflow, deposit sediment, and evolve toward a less sediment-rich flow with distance, ultimately transforming into a type-2 lahar or sediment-laden flood (Fig. 22). A flow that contains less than a few percent clay-sized or clay mineral particles is more likely to transform into a type-2 lahar or sediment-laden water flow with distance and can do so comparatively quickly. In contrast, a flow that contains a greater amount of clay-sized and clay mineral particles commonly maintains its textural character as a type-1 lahar over many tens of kilometres of travel distance.

Deposit characteristics. A lahar deposit can exhibit a variety of characteristics related not only to flow initiation mechanism but also to the ability of the flow to interact with the channel and streamflow and evolve along its flow path. As a lahar moves downstream, it can entrain and deposit sediment, sometimes repeatedly, allowing its volume and composition to fluctuate with distance (e.g. Scott 1988*a*; Pierson *et al.* 1990; Hodgson and Manville 1999; Capra *et al.* 2010; Procter *et al.* 2010; Doyle *et al.* 2011). Furthermore, flow duration at a given point along a channel can vary from swift passage as a flash flood to prolonged flow at maximum stage, and characteristics of the passing flow can vary from head to tail (Vázquez *et al.* 2014; Vallance and Iverson 2015). Consequently, a lahar can leave a deposit that has morphologic and sedimentologic characteristics that vary both in space and time.

Deposit thickness. Deposit thickness can vary widely along the flow path, is greatly influenced by flow initiation process and topography, and commonly is thin in relation to flow depth. Flood-plain deposit thickness can vary from centimetres to a few metres. The channel deposit, however, results largely from progressive accumulation during flow passage and its thickness can vary considerably, from a few to many metres. Initiation process can greatly affect deposit thickness. For example, a flow that results from transformation of a debris avalanche or from a break-out flood from a large lake, which can entrain immense amounts of sediment, can form a deep flow that leaves a thick (many metres) deposit. In contrast, rainfall-runoff generated lahars are shallow and although cumulative deposit thicknesses from multiple flows can be substantial, individual deposits are thin (metre-scale). Topography, however, commonly exerts a greater control on deposit thickness than does flow genesis. Along unchannelled fans at the bases of volcanoes, or beyond the mouths of canyons, flows can spread widely and leave thin deposits. In more confined reaches, thick deposits can accumulate on channel floors, flood plains, and terraces. Metre-thick

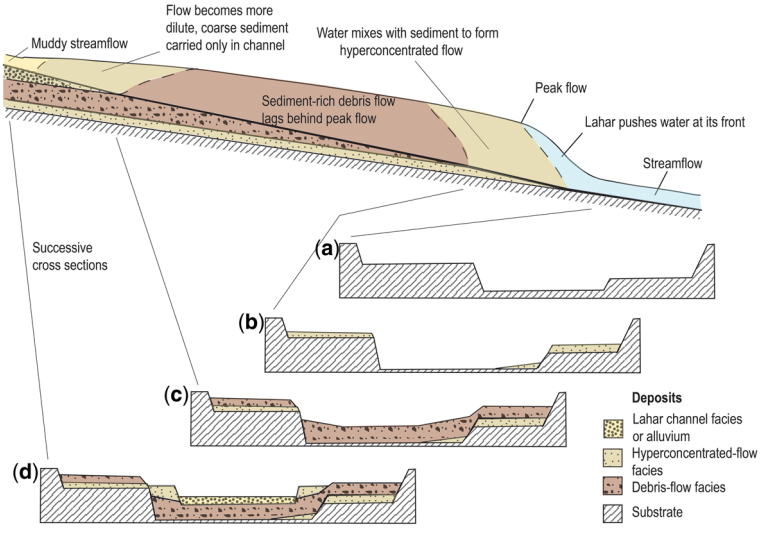

Fig. 22. Schematic depiction of spatial and temporal relations between lahar flow and lahar deposits. From Vallance and Iverson (2015).

deposits of type-1 lahars on flood plains and terraces many tens of kilometres from volcanoes attest to great sizes and mobilities of many lahars.

Deposit thickness, however, provides an incomplete picture of the nature of a flow. Flow depths of moderate to large flows can be much greater than deposit thickness (Fig. 23). Deposits of smaller flows may also be misleading indicators of original flow depth. As noted, deposits can accumulate progressively, yet appear to be deposited *en masse*. Caution should be exercised when inferring relations between deposit thickness, flow depth, and the nature of the depositional process.

Deposit texture. Textures of lahar deposits can vary considerably depending on sediment concentrations and compositions of lahar flows. Nevertheless, there are many common and distinctive traits. A type-1 lahar deposit is commonly non-stratified, poorly sorted, and consists of particles ranging in size from clay to boulders (Fig. 24). Clasts larger than about 2 mm are commonly supported within a matrix of finer particles, especially in flood-plain deposits. Locally, coarse clasts may be in clast-to-clast contact, especially at deposit margins. Channel deposits of a type-1 lahar are typically coarser grained than flood-plain deposits and may exhibit abundant clast-contact texture that may look similar to gravel-rich flood deposits. Clast angularity can provide clues to the dominant transport process; gravel-rich flood deposits will be composed mainly of rounded particles whereas those resulting from lahars will likely be composed of angular or a mix of angular and rounded particles. However, if the dominant source of sediment for a lahar is channel sediment (such as for a lahar triggered by a lake breakout along valley margins), then channel and flood-plain deposits can be dominated by rounded particles, and other evidence is needed to decipher deposit origin.

Clasts within a type-1 lahar deposit can exhibit wide variation in size, grading, and dispersal (Fig. 24). Some deposits may consist of a relatively narrow range of sizes, with the coarsest clasts only a few to several centimetres in diameter, whereas others may contain clasts many tens of centimetres to a metre or more in diameter. Coarse clasts may be normally graded, fining upward, or inversely graded, coarsening upward. Deposits can exhibit inverse grading of clasts near the base, little grading in the middle section, and normal grading above. In contrast, the finer (<2 mm) matrix particles commonly exhibit little grading and are distributed uniformly through the deposit. Internal sorting and grain migration allow large clasts to accumulate along flow fronts and margins producing bouldery snouts and levees (Johnson *et al.* 2012; Vallance and Iverson 2015). Vertical grading of clasts can reflect longitudinal variations in flow composition (see Fig. 21). Thus, vertical variations in clast grading may be influenced more by progressive aggradation than by internal sorting processes.

Clast shapes and compositions are indicative of predominant sediment sources. Angular to subangular clasts composed of volcano lithologies are indicative of lahars forming at a volcano or of flows that

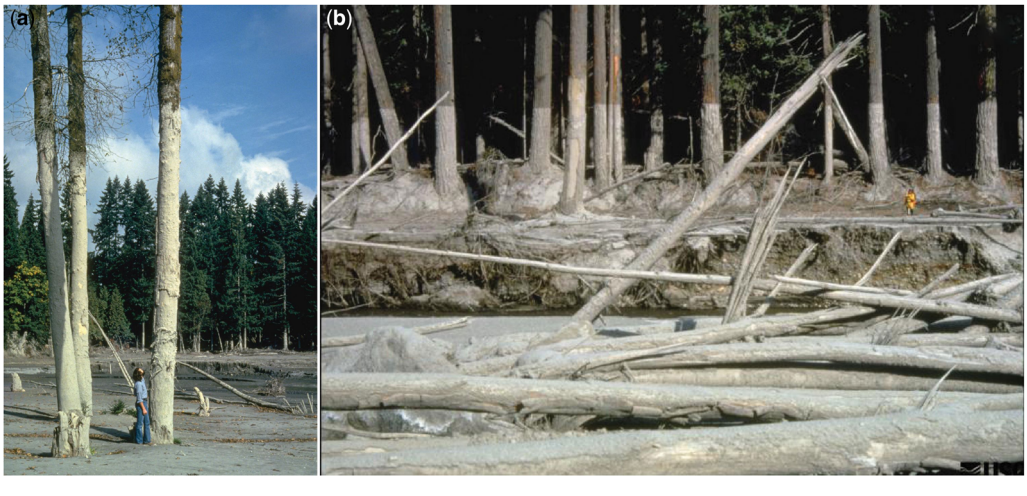

Fig. 23. Physical evidence of relations between peak flow depth and deposit thickness from large lahars triggered by 18 May 1980 eruption of Mount St Helens (USA). (**a**) Inundation depth of North Fork Toutle River lahar in Toutle River valley shown by mud coating on trees. Photograph by L. Topinka, USGS. (**b**) Inundation depth of Muddy River lahar on SE side of Mount St Helens shown by mud coating on trees. Note person (upper right quadrant) for scale. Photograph by L. Topinka, USGS.

Fig. 24. Deposit textures of type-1 (debris flow) lahars. Note the non-stratified nature of the deposits, poor sorting, range of particle sizes transported, and variations in grading of coarse clasts. (**a**) Lahar deposits from Mount St Helens (USA), 1980. Note the variation in textures between the two lahar deposits. The lower deposit (SFT) is from the 1980 Mount St Helens South Fork Toutle River lahar which was triggered by a pyroclastic density current melting snow at the volcano. At this location, the flow was undergoing transition to a type-2 (hyperconcentrated flow) lahar. Note its relative fine-grained texture. The upper deposit (NFT) is from the 1980 North Fork Toutle River lahar, which was triggered by dewatering of the debris-avalanche deposit. Because this lahar contained a higher percentage of clay-sized sediment than did the SFT lahar, it maintained its type-1 character for much longer distance. Note its coarse-grained texture. Site is near confluence of North Fork Toutle and South Fork Toutle Rivers, 50 km downstream from Mount St Helens. Note hat (circled) for scale. (**b**) Type-1 lahar deposit containing dominantly subrounded particles entrained from channel bed and banks. Note poor sorting and non-stratified texture of deposit. Shovel about 1 m tall. (**c**) Ancestral type-1 lahar deposits along lower North Fork Toutle River draining Mount St Helens. Particles are volcanic lithologies but dominantly rounded river alluvium, and deposits contain eroded pieces of debris-avalanche sediment. Deposits resulted from floods caused by breaching of a valley-margin lake, which entrained channel sediment (Scott 1988*b*). Note poor sorting and non-stratified textures of deposits. (**d**) Type-1 lahar deposit exhibiting inverse (coarsening-upward) grading of coarse clasts. All photographs by J. Major, USGS.

entrained sediment from older primary volcanic deposits. In contrast, clasts that are dominantly rounded to subrounded and/or composed of mixtures of volcano lithologies and exotic lithologies are indicative that stream alluvium was an important sediment source.

Clasts in type-1 lahar deposits can also consist of large intact fragments of older deposits. Such clasts, commonly referred to as fragile megaclasts, may be composed of fragments of sediment entrained from a single deposit, or of stratigraphic sections entrained largely through bank erosion (Fig. 25). Fragile megaclasts, in conjunction with other deposit characteristics, have been inferred as evidence that the lahar entrained substantial channel sediment along its flow path (Scott 1988*b*; Major and Scott 1988). In some instances, entrained fragments of debris-avalanche sediment provide possible evidence for lake blockage by a debris-avalanche deposit (Fig. 25a, d).

In contrast to the compositions and textures of a type-1 lahar deposit, a type-2 lahar deposit is composed dominantly of moderately sorted sand. Because type-2 lahars span a range of sediment concentrations, their deposits can exhibit a variety of textures. They can consist of non-stratified to laminated and stratified sand (Fig. 26) or of moderate to poorly sorted mixtures of sand and small gravels. A key feature of type-2 lahars is that they transport large amounts of sand both in suspension and as bed load (Pierson and Scott 1985; Cronin *et al.* 1999; Pierson 2005). The coarse sediment in transport is commonly deposited rapidly and progressively whereas the fines (silt and clay) remain in

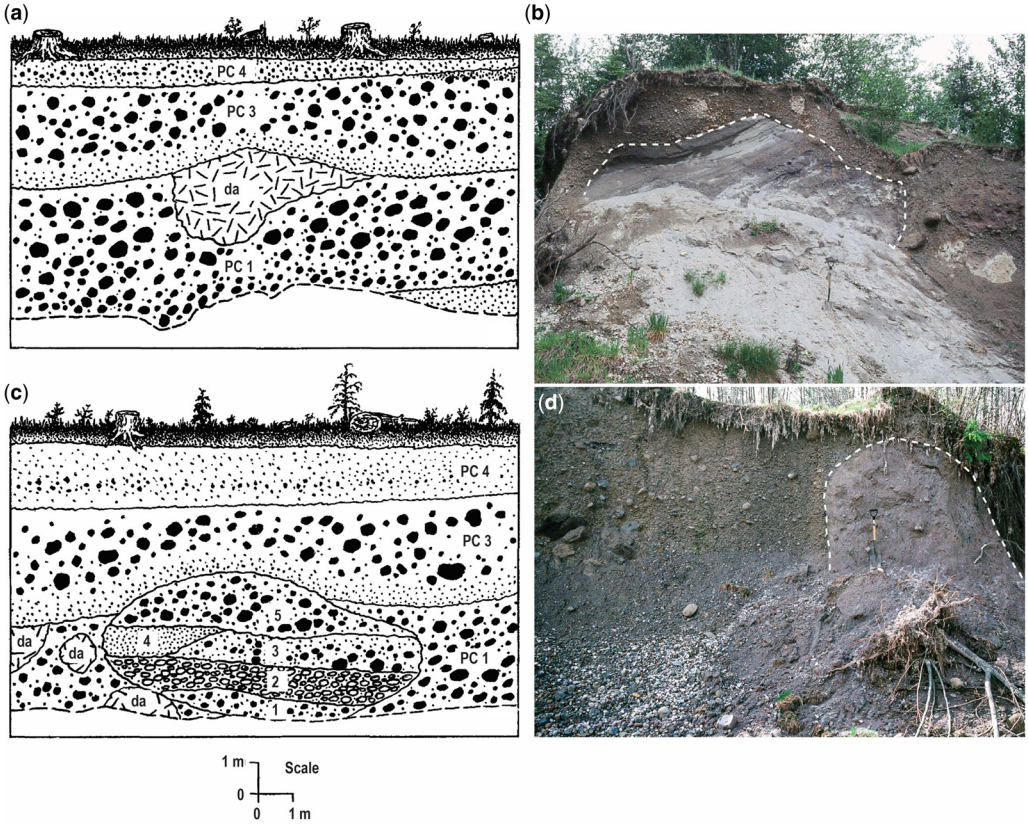

Fig. 25. Fragile megaclasts in ancient lahar deposits at Mount St Helens (USA). (**a**) Dacitic sediment megaclast (da; eroded debris-avalanche material), formerly exposed along North Fork Toutle River valley, entrained within and extending above lahar deposit surface. (**b**) Megaclast of intact stratified sandy alluvium (outlined). (**c**) Megaclast composed of pre-lahar flood-plain stratigraphy, formerly exposed along North Fork Toutle River valley. The stratigraphic section includes older lahar (1, 3, 5) and fluvial (2, 4) deposits. (**d**) Megaclast of poorly sorted debris-avalanche sediment (outlined). Panels (a) and (c) from Scott (1989). Megaclasts shown in (b) and (d) are preserved within an ancient lahar deposit along Lewis River valley near Yale Dam, Cougar, Washington. Shovel is 1 m tall. From Major and Scott (1988).

Fig. 26. Textures of type-2 (hyperconcentrated flow) lahar deposits. Note non-stratified to laminated textures, dominantly sand composition, and occasional coarse clasts. (**a**) Deposit from lahar that was relatively highly concentrated and near transition to type-1 lahar, Chaitén River, Chaitén volcano (Chile). Photograph by T. Pierson, USGS. (**b**) Horizontally bedded deposit from a dilute type-2 lahar, possibly verging on sediment-laden streamflow, Chaitén River, Chaitén volcano. Photograph by T. Pierson, USGS. (**c**) Non-stratified, normally graded type-2 lahar deposit (unit 3), underlying tephra fall (unit 2) and reworked tephra fall (unit 1), Abacan River, Mount Pinatubo (Philippines). Photograph by J. Major, USGS. (**d**) Deposit of non-stratified to indistinctly laminated coarse sand with entrained pumice particles within and atop deposit, Toutle River valley, Mount St Helens (USA). Photograph by T. Pierson, USGS. (**e**) Deposits from type-1 (unit 1) and type-2 (unit 3) lahars. The deposit juxtaposed with axe head (unit 2) represents a type-1 lahar in basal part and grades upward to sandy facies deposited by a type-2 lahar phase, Nisqually River valley, Mount Rainier (USA). Photograph by J. Major, USGS. (**f**) Non-volcanic hyperconcentrated-flow deposit emplaced by flow having a sediment concentration of about 26% by volume, White Salmon River (Washington, USA). This deposit resulted from flow shown in Figure 19d, a flow generated by a dam removal. Photograph by J. O'Connor, USGS. (**g**) Stratified fine to medium sand deposited by a type-2 lahar from April 2009 eruption of Redoubt volcano (USA). Convoluted bedding (arrow) indicates rapid loading of water-saturated sediment. Photograph by T. Pierson, USGS.

suspension and are transported farther downstream. Consequently, resulting deposits consist mainly of moderately sorted sand (Pierson and Scott 1985; Cronin *et al.* 1999; Pierson 2005; Pierson *et al.* 2013; Wilcox *et al.* 2014). Deposits may show some vertical grading of sand-sized particles. Dispersed lithic or pumice clasts may be sporadically embedded within type-2 lahar deposits, or they can be abundant, producing fines-depleted gravel lenses. Pebble-sized clasts largely reflect particles transported as bed load.

Deposit textures can evolve down valley if a lahar undergoes distal transformation. If a lahar progressively entrains sediment, it can evolve from a low-concentration flood or type-2 lahar to a type-1 lahar. In contrast, a lahar that mixes with streamflow can drop sediment and transform from a type-1 to type-2 lahar and ultimately to sediment-laden streamflow. As a result, deposit characteristics can change longitudinally from non-stratified, poorly sorted gravelly sand that contains dispersed large clasts to crudely stratified, moderately sorted sand lacking coarse clasts (e.g. Pierson and Scott 1985), and ultimately to well-stratified, cross-bedded, well-sorted sand indicative of alluvial transport. Deposits may show inconsistent longitudinal variations in texture if flows undergo episodic erosion and deposition along transport paths (e.g. Procter *et al.* 2010).

Relations among deposit textures and initiation and flow processes. Deposit textures, clast shapes and compositions, and the characteristics of megaclasts provide an array of information regarding lahar initiation and transport processes. The amounts of rounded clasts and exotic lithologies can be used to distinguish a lahar that entrained sediment at or near a volcano from one that largely scavenged sediment from channels and entrained bed and bank sediment farther along its flow path. A lahar that eroded sediment at or near a volcano contains abundant angular debris of volcanic lithologies, whereas one caused by a flood that entrained abundant channel sediment commonly contains dominantly rounded alluvium composed of a mix of volcano and exotic lithologies. It may also contain megaclasts of alluvium. Although a lahar that forms at or near a volcano can contain entrained stream gravels, the amount of such clasts typically is subordinate. Such a criterion for distinguishing initiation mechanism is generalized, however. For example, at Mount St Helens in 1980, a large debris-avalanche deposit blocked the outlet to a large lake at the foot of the volcano. Had that lake breached and released a large flood surge that ultimately transformed into a lahar, that surge would have entrained sediment from the nearly 30 km-long debris-avalanche deposit – a deposit composed predominantly of angular volcanic debris. The distal lahar deposit would therefore be composed largely of angular to subangular volcanic clasts. This hypothetical texture is considerably different from the lahar deposit related to an ancient breakout of the same lake, a breakout that also followed blockage by a debris-avalanche deposit (Scott 1988*b*). That ancestral lake-breakout lahar deposit is dominated by rounded volcanic clasts that represent stream alluvium (Fig. 24c). The abundance of entrained stream alluvium and paucity of angular clasts indicates that the predominant sediment source for that ancient lahar was the stream channel beyond the debris-avalanche blockage. That predominant sediment source suggests that the ancient debris-avalanche(s) deposit that blocked the lake was not as extensive down valley as the 1980 debris-avalanche deposit.

Amounts and types of clay within lahar deposits have been used to distinguish possible origins of lahars. A lahar that forms at a volcano as a result of a large slope failure is more likely to contain greater amounts of clay-sized and clay-mineral material than one formed by another mechanism. A lahar containing a few to several percent clay-sized and clay-mineral material commonly contains volcanic debris that may be hydrothermally altered or debris from which the finest particles had not been sorted. Abundant hydrothermally altered clay minerals may provide evidence for a debris-avalanche origin of a lahar (Scott *et al.* 1995). In contrast, a lahar formed from sediment entrainment by runoff and flood erosion typically contains little clay, which indicates that the source sediment contained little clay. Channel-sediment entrainment by flood surges, transformations of small surficial landslides, and remobilization of tephra fall by rainfall runoff are some of the most likely causes of such lahars. Clay-poor lahars commonly transform toward dilute sediment-laden floods as they move down valley (e.g. Zehfuss *et al.* 2003). Although some clay-poor lahars can maintain their type-1 flow character for many tens of kilometres, others transform to type-2 lahars or sediment-laden floods over distances of a few to a few tens of kilometres (e.g. Scott 1988*a*).

In summary, multiple lines of evidence, including clast compositions, shapes, percentages of volcanic v. non-volcanic lithologies, morphologic and stratigraphic position, and sedimentary textures such as grain size, sorting, grading and bedforms must all be considered when assessing potential initiation mechanisms.

Tephra fall

The most widespread volcaniclastic deposits result from tephra fall – the rain of particles from volcanic plumes that drift downwind (Fig. 27). These particles consist of angular fragments of rock, pumice, crystals, and glass. The size distribution of

Fig. 27. Examples of volcanic plumes that produce tephra fall. (**a**) Eruption of Calbuco volcano (Chile) 2015. View from Puerto Montt. Photograph © C. Barría Kemp/CC BY-SA 2.0. (**b**) Eruption of Shinmoedake volcano (Japan) 2011. Photograph © Kyodo News Images. (**c**) Eruption of Redoubt volcano (USA) 1990. Photograph by R. Clucas, courtesy of Alaska Volcano Observatory, United States Geological Survey.

particles within tephra-fall deposits, and local deposit thicknesses, can range broadly as functions of mass eruption rate, distance from a volcano, particle aggregation, particle composition and density, wind speeds and directions, and atmospheric dynamics at various altitudes.

Fall deposits provide information about volcanic eruptions and eruptive processes. They record eruptions and thus help delineate eruptive histories, record changes in magmatic compositions within and between eruptive periods, and serve as crucial regional time-stratigraphic marker beds (Mullineaux 1986). Grain characteristics (size, shape, and density) and textural compositions provide insights into fragmentation and collisional processes operating within volcanic conduits (e.g. Dufek *et al.* 2012) as well as processes operating within volcanic plumes (e.g. Van Eaton *et al.* 2015). Fall-deposit preservation, and its reliability as a time-stratigraphic marker and eruption record, is affected by depositional environment. Nevertheless, preservation of primary fall can be substantial, especially within tens of kilometres of a volcano. Although tephra fall can induce significant changes to a landscape's hydrogeomorphic regime and result in substantial erosion (see the 'Posteruption sediment erosion, transport, and deposition' section), recent studies have estimated that some 50–80% of primary fall can remain uneroded within proximal watersheds for at least decades or longer (Collins and Dunne 1986, 2019; Manville and Wilson 2004; Pierson *et al.* 2013). Even thin tephra-fall deposits (less than 30 cm thick) can be well preserved at great distances downwind for centuries or longer (Blong *et al.* 2017). But tephra preservation becomes less consistent the greater the distance from a volcano and under variable surface covers (e.g. Cutler *et al.* 2018). Tephra preservation is common in peatlands and lakes (e.g. Hardardóttir *et al.* 2001; Kuehn and Negrini 2010; Moreno *et al.* 2015; Jensen *et al.* 2021), but whereas peatlands typically preserve primary tephra (and cryptotephra) fall, deposits in lakes reflect a combination of primary fall and reworked tephra washed in from erosion of the surrounding catchment (e.g. Hardardóttir *et al.* 2001; Watson *et al.* 2016). Tephra falls are also preserved in continental glaciers, notably in the Greenland Ice Sheet and Antarctica, and provide not only time-stratigraphic horizons within the ice but also facilitate correlations of various climatic archives (Abbott and Davies 2012; Jensen *et al.* 2021; Narcisi and Petit 2021).

Depositional process. Tephra fall is the outcome of competing influences of volcanic plume behaviour, particle characteristics, atmospheric dynamics, and the nature of volcanic processes. Volcanic plumes fall into three major classes – those driven by volatile exsolution and fragmentation of magma, those resulting from near-surface interactions of magma and water, and those resulting from material lofting from PDCs (Bonadonna *et al.* 2015; Carey and Bursik 2015). Plume character represents interactions between eruption (e.g. plume rise velocity) and wind characteristics (Bonadonna *et al.* 2015). When plume rise velocity exceeds horizontal wind velocity, a strong vertical column develops and feeds an umbrella cloud that advects downwind at the level of neutral buoyancy (Figs 27a, c & 28a). As a result, downwind fall deposits are broadly distributed in a wide, elongate pattern, perhaps with some upwind deposition. In contrast, weak plumes form when horizontal wind velocities exceed plume rise velocities (Figs 27b & 28b). Weak plumes commonly develop narrow, elongate fall deposits with little upwind deposition.

Sedimentation from volcanic plumes is affected by particle settling, aggregation, and plume dynamics (Bursik *et al.* 1992; Bonadonna *et al.* 2015). In general, tephra fall results from sedimentation along the margins of a rising turbulent volcanic plume and settling from a horizontally drifting cloud. It can also result from co-PDC ashclouds. Particle settling is related to particle size, shape, and density. Relations between particle settling velocities and plume vertical velocities cause particle segregation within a plume. Larger and denser particles separate quickly from the plume and fall near the vent whereas smaller and less dense particles are carried higher in the

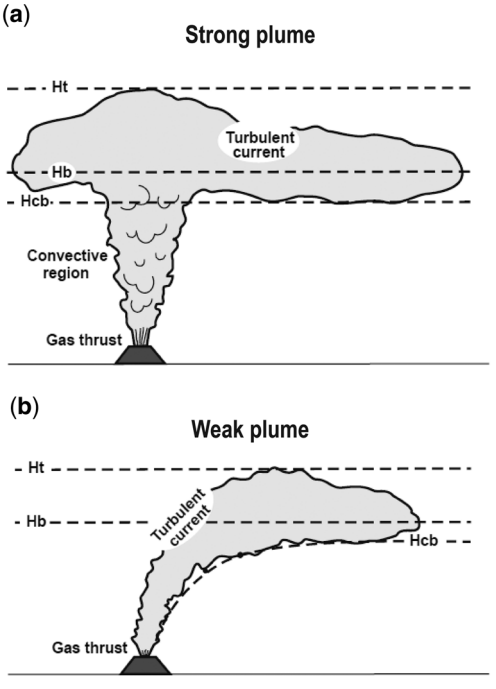

Fig. 28. Schematic representation of strong and weak volcanic plumes. Plume character represents a competition between plume rise velocity and horizontal wind speed. H_t is maximum plume height, H_b is the height of the neutral buoyancy level where plume density equals atmospheric density, and H_{cb} is the height of the base of the downwind-advecting plume. Reprinted from Bonadonna *et al.* (2015), with permission from Elsevier.

plume and farther downwind. Strong density differences between pumice and lithic particles greatly affect their fall behaviour. Particle aggregation affects fall of fine ash. Moisture within a volcanic plume causes fine ash to cluster in dense, coherent aggregates known as accretionary lapilli. Electrostatic forces can draw fine ash together into porous, fragile dry aggregates. Aggregation increases the effective size of particles within a volcanic plume and causes fine ash to fall out much more rapidly than it would otherwise. Aggregation of fine ash can be effective at removing these particles from a plume. During the 2009 eruption of Redoubt volcano, Van Eaton *et al.* (2015) estimated that more than 95% of deposited fine ash fell as aggregates and less than 5% remained in the plume as single particles. Eruption dynamics, such as mass eruption rate, eruption duration, total grain-size distribution within the plume, downwind plume dynamics such as gravitational instabilities, and atmospheric dynamics affected by local topography also affect tephra fall (e.g. Bonadonna *et al.* 2015; Watt *et al.* 2015).

Fall deposits blanket the landscape and typically fine and thin exponentially with distance from source (Pyle 1989; Houghton and Carey 2015), an observation consistent with predictions from tephra sedimentation models (Bursik *et al.* 1992; Bonadonna *et al.* 2015). Relations between fall-deposit thickness and distribution, grain size, and grain-size distribution are commonly used to estimate mass eruption rates, plume heights, and eruption volumes (e.g. Carey and Sparks 1986; Pyle 1989; Fierstein and Nathenson 1992; Bonadonna and Costa 2013). However, these relations are affected by variations in eruption source parameters, aggregation of fine particles, wind speeds, variations in plume conditions, interactions among sediment sources (e.g. fallout from central volcanic plumes co-mingled with fallout from a co-PDC plume), and deposit preservation (Sigurdsson and Carey 1989; Sparks *et al.* 1992; Eychenne *et al.* 2012; Engwell *et al.* 2013; Bonadonna *et al.* 2015; Houghton and Carey 2015; Van Eaton *et al.* 2015).

Deposit characteristics. Characteristics of fall deposits represent competing influences of volcanic plume behaviour, wind and atmospheric characteristics, and the nature of volcanic processes. As a result, fall deposits can exhibit a variety of bedding and textural characteristics (Fig. 29). Unlike PDC deposits, fall deposits are generally well sorted and drape the pre-existing topography uniformly (Fig. 29b, f), except where locally thickened or thinned by erosion. Topography exerts little influence on deposit distribution (except where it influences atmospheric turbulence and fallout from a volcanic plume; Watt *et al.* 2015). Depending on proximity to source, the nature of the source, eruption vigour, and wind and atmospheric characteristics, fall deposits can range from dominantly coarse lapilli, blocks, and bombs to micron-sized ash. Fall deposits can also range from non-stratified to finely stratified and exhibit normal to inverse size grading (e.g. Houghton and Carey 2015). They can also be diffusely stratified or sharply bedded. Fall deposits are distinguished from pyroclastic surge beds by a lack of internal directional bedding such as cross-stratification or bedforms (Fig. 29).

Accretionary lapilli are formed by wet aggregation of fine ash within a volcanic plume. Water content and residence time of aggregates within a plume affect the size and character of accretionary lapilli (Bonadonna *et al.* 2015; Van Eaton *et al.* 2015). The modal size of aggregated particles in accretionary lapilli is typically around 0.03–0.06 mm (4φ–5φ) (Bonadonna *et al.* 2015), whereas accretionary lapilli are commonly a few millimetres in diameter. Accretionary lapilli (Fig. 29g) are typically spherical, internally massive to weakly layered, and display concentric layering of ash particles (e.g. Bonadonna

Fig. 29. Examples of tephra-fall deposits. (**a**) Cotopaxi volcano (Ecuador) F-4/F-5 rhyolitic to andesitic pumice-fall deposits that are about 4.5 ka. Photograph by J. Major, USGS. (**b**) Tephra-fall layers from Izu Oshima volcano (Japan). Photograph by S. Raczyński, Wikimedia Commons. (**c**) Fall deposits exposed at Mount Rainier National Park (USA). Lower light-yellow ash fall is from 7.7 ka eruption of Mount Mazama (Crater Lake), 435 km south of Mount Rainier. The yellow-brown fall deposit at top of section is the Mount St Helens Y tephra, erupted 3.9–3.3 ka. Mount St Helens lies 80 km south of Mount Rainier. Photograph by D. Mullineaux, USGS. (**d**) Mount St Helens Wn pumice fall (1479 CE) overlying *c.* 920 CE Sugar Bowl eruptive period blast pyroclastic-density-current (PDC) deposit. Exposed section about 1 m tall. Flag denotes contact (dashed line) between fall and PDC deposits. Photograph by J. Major, USGS. (**e**) Tephra fall from 2008 eruption of Chaitén volcano (Chile). Note upward-fining textures of the deposits. Photograph by R. Hoblitt, USGS. (**f**) Blanket of fine ash fall from post-climactic eruption of Mount Pinatubo (Philippines). Photograph by J. Major, USGS. (**g**) Accretionary lapilli from the 18 May 1980 Mount St Helens directed (lateral blast) PDC (co-PDC ashcloud) deposit. Photograph by C.D. Miller, USGS.

et al. 2015; Brown and Andrews 2015; Van Eaton *et al.* 2015). Because they are fragile and often have an ice-particle nucleus, they can break apart upon impact and are thus poorly preserved overall. Dry aggregates formed by electrostatic forces are typically not preserved in deposits; they are observed in rare instances when ash is collected while actively falling (e.g. Sorem 1982; Taddeucci *et al.* 2011) or inferred from grain-size character of the deposit (e.g. Carey and Sigurdsson 1982). Deviations from exponential deposit thinning with distance from source and anomalous abundance of fine ash in

deposits relative to nominal particle-settling velocities may be related to particle aggregation (e.g. Brazier *et al.* 1983).

Unlike PDC deposits, tephra-fall deposits are generally cool at the time of deposition. As a result, tephra-fall deposits are usually not welded. Those that are welded are most commonly the result of deposition of spatter from basaltic and intermediate-composition eruptions (Houghton and Carey 2015). In those instances, welding and agglutination provide an indication of proximity to the source vent.

Relations among deposit textures and depositional processes. Fall-deposit textures provide an array of information about depositional process and eruption characteristics. For example, basic differences in fall-deposit compositions – such as pumiceous fall v. lithic- and crystal-rich fall – have been used to discriminate fall resulting from magmatic explosions v. fall resulting from phreatic explosions or co-PDC ash clouds (e.g. Scott and McGimsey 1994). Average maximum sizes of pumice and lithic fragments are commonly used to estimate plume height (e.g. Carey and Sparks 1986). The presence of fine-scale stratification within fall deposits is used to distinguish fallout from non-sustained eruptions having mass eruption rates that wax and wane v. those from sustained eruptions with constant mass eruption rate, which produce more uniformly textured deposits (Houghton and Carey 2015). Sharp bedding contacts and abrupt changes in grain size have been inferred by some as representing pulsating eruptive behaviour and by others as indicative of column collapses that have generated PDCs, with deposition of fine ash by dilute currents or by co-PDC ashfall (e.g. Paladio-Melosantos *et al.* 1996; Houghton and Carey 2015). Thin, fine-ash partings have been used to infer pauses during an eruption, because fine ash can remain suspended for days; its presence may indicate a pause during which time it settles (Houghton and Carey 2015). Varying amounts of very fine ash within proximal fall deposits may lend insights into dry v. wet eruptions – with large amounts indicative of wet eruptions thought to have greater fragmentation efficiency (Houghton and Carey 2015). Deposit sorting may also provide insights on dry v. wet eruptions. Because wet eruptions contain larger amounts of very fine ash, their proximal fall and surge deposits are more poorly sorted (commonly $\sigma_\varphi > 2$) compared to those of dry eruptions (commonly $\sigma_\varphi \sim 1–1.5$) (e.g. Houghton and Carey 2015). Sorting characteristics and bimodality of grain-size populations in fall deposits have been used to infer that fall deposits reflect synchronous deposition from different volcanic processes (Eychenne *et al.* 2012). Relations among median grain size, sorting, and deposit area have been proposed as ways of distinguishing deposits of different volcanic processes (Walker 1971) as well as distinguishing styles of eruption (Walker 1973). Although there is broad correlation among median particle size, sorting, deposit footprint characteristics and depositional process, subtle complexities preclude discrimination of process solely by these characteristics (Houghton and Carey 2015). Overall, a key question to be answered in the field is whether a deposit results from a flow or fall process. Uniform topographic draping, nearly universal particle angularity, generally well to moderate sorting, and a clear lack of palaeoflow indicators are common hallmarks of fall deposits.

Posteruption sediment erosion, transport, and deposition

The volcanic processes discussed can broadly modify landscapes and disrupt normal hydrogeomorphic functioning (Fig. 30). Much of the following discussion is modified from Pierson and Major (2014). Explosive eruptions affect the hydrological functioning of watersheds in three basic ways: (1) they damage or remove vegetation, which decreases (or eliminates) interception and evaporation of precipitation; (2) volcaniclastic deposits on hillsides commonly reduce surface infiltration, which increases overland flow; and (3) large injections of valley-floor sediment alter hydraulic properties of river channels and enable efficient transport of water and sediment (Pierson and Major 2014). Alterations to the hydrogeomorphic functioning of landscapes by explosive eruptions thus affect the routes and rates of precipitation runoff, which in turn affect erosion and sediment transport.

Volcanic processes can remove, damage, or bury vast tracts of vegetation. Trees can be toppled or defoliated, and understorey can be damaged or buried (e.g. Dale *et al.* 2005; Ayris and Delmelle 2012; Swanson *et al.* 2013, 2016). As a result, more precipitation in the form of rainfall or snowfall reaches the ground surface and, in the case of rainfall, impacts the surface with greater force. Tree canopies intercept, on average, 10–40% of incoming precipitation (Reid and Lewis 2009; Carlyle-Moses and Gash 2011). Furthermore, loss of or damage to vegetation reduces transpiration of soil moisture, which alters subsurface storage and flow of water.

Tephra-fall and PDC deposits draping hillsides commonly alter the rate at which precipitation infiltrates the ground surface (e.g. Teramoto *et al.* 2006; Jones *et al.* 2017; Tarasenko *et al.* 2019). The finer the surface of the deposited sediment, the greater the loss of surface infiltration (Pierson and Major 2014; Fig. 31). As a result, more of the precipitation that reaches the ground surface is partitioned

Fig. 30. Landscape modifications by volcaniclastic processes. (**a**) Upper North Fork Toutle River smothered by Mount St Helens (USA) 1980 debris-avalanche deposit. Thick, hummocky fill contains many ponds but has disrupted interconnected drainage channels. Photograph by A. Post, USGS, June 1980. (**b**) Thick 1991 pyroclastic-flow deposits completely bury Marella River valley, Mount Pinatubo (Philippines). Throughgoing drainage had to redevelop. Photograph by R. Hoblitt, USGS, June 1991. (**c**) Channel fill resulting from dome-collapse block-and-ash flows, Soufrière Hills Volcano (Montserrat). Image P3210088-MVO, British Geological Survey, 1997. (**d**) Deposit of lahar from November 1985 eruption of Nevado del Ruiz volcano, which devastated Armero, Colombia. Photograph by R. Janda, USGS, December 1985. (**e**) Erosion of tephra fall mantling hillsides, Chaitén volcano. Photograph by T. Pierson, USGS, January 2010. (**f**) Tree damage by blast pyroclastic density current, Mount St Helens, 1980. Photograph by USGS, August 1980.

into overland surface flow as opposed to shallow subsurface flow. This change in partitioning of run-off promotes hillside erosion and allows more water to reach river channels faster. These changes in hydrogeomorphic functioning promote the occurrence of larger floods and lahars after an eruption (e.g. Todesco and Todini 2004; Favalli *et al.* 2006; Major and Mark 2006; Alexander *et al.* 2010; also see the 'Rainfall-runoff erosion of volcanic ash and other pyroclastic sediment' section).

Volcaniclastic deposits affect river channels in various ways. Extensive channel deposition by

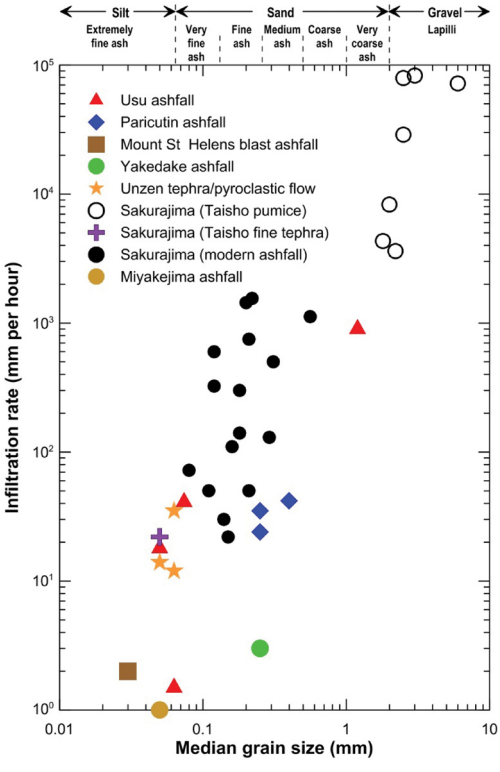

Fig. 31. Relations between infiltration rate and grain size of tephra-fall and PDC deposits. From Pierson and Major (2014).

debris avalanches and large PDCs smothers valleys and disrupts channel networks (Fig. 30). In those instances, unchannelled runoff must concentrate and carve new channels to re-integrate channel networks. Complete integration of channel networks can take years to accomplish (e.g. Daag and van Westen 1996; Simon 1999). Early posteruption channels are commonly straighter, wider, and steeper than their pre-disturbance counterparts (Meyer and Martinson 1989; Gran and Montgomery 2005). In contrast, lahars commonly do not fully bury river channels. Rather, they strip river corridors of vegetation, straighten channels, and pave channel beds with large loads of sand making them hydraulically smoother (Janda *et al.* 1984; Pierson and Major 2014). Such changes enhance the efficiency with which rivers can transport exceptional posteruption sediment loads.

Erosion mechanisms and sediment sources. Sediment reworked after an explosive eruption comes from two basic sources: (1) hillsides where sheet and rill erosion as well as shallow landslides mobilize tephra-fall and PDC deposits, and (2) channels where debris-avalanche, PDC, and lahar deposits are reworked as channels reestablish or react to these perturbations. The sediment eroded from these two sources is delivered from watersheds at different rates and persists for different durations (Major *et al.* 2000; Gran *et al.* 2011). In addition to freshly deposited sediment, older hillside and channel sediments can be remobilized providing additional sediment supply (e.g. Waldron 1967; Pierson *et al.* 1990, 1996; Swanson and Major 2005; Korup *et al.* 2019).

Hillside erosion. Owing to loss and damage of vegetation and to changes in the hydrological regime, sheet and rill erosion are the dominant processes that mobilize hillside volcaniclastic sediment (Segerstrom 1950; Waldron 1967; Kadomura *et al.* 1983; Swanson *et al.* 1983; Chinen 1986; Collins and Dunne 1986; Takeshita 1987; Leavesley *et al.* 1989; Shimokawa *et al.* 1989, 1996; Yamakoshi *et al.* 2002; Waythomas *et al.* 2010; Pierson *et al.* 2013). Sediment erosion from hillsides is typically acute and rapid, but once a rill network is established, rates of erosion diminish swiftly. Diminished erosion occurs once rills incise into coarser, more permeable layers or reach resistant substrates (Collins and Dunne 1986). Once hillside incision ceases, rill networks evolve toward fewer active rills (Swanson *et al.* 1983; Collins and Dunne 2019). Biogenic and cryogenic processes along with wind deflation can coarsen the surface and improve infiltration, which reduces or eliminates surface runoff (e.g. Yamakoshi and Suwa 2000; Major and Yamakoshi 2005). As a result, initially high sediment yields owing to hillside erosion can decrease sharply within just a couple of years, even in the absence of revegetation (Chinen 1986; Collins and Dunne 1986, 2019). However, at some volcanoes, such as Sakurajima (Japan) and Santiaguito/Santa Maria (Guatemala), persistent recharge of tephra-fall deposits by frequent eruptions can maintain high rates of hillside erosion and sediment yield for long durations (e.g. Shimokawa *et al.* 1989; Harris *et al.* 2006).

Rapid reduction of hillside erosion permits large volumes of proximal tephra fall to remain in place. Approximately 80–90% of the tephra fall deposited by eruptions of Usu volcano (Japan) in 1977–78 and Mount St Helens in 1980 is estimated to remain in place decades after deposition (Kadomura *et al.* 1983; Chinen 1986; Collins and Dunne 1986, 2019; Smith and Swanson 1987). As much as 50% or more of tephra fall deposited in proximal areas following eruptions of Irazú volcano (Costa Rica) (1963–65) and Chaitén volcano (Chile) (2008) appeared to remain in place (Waldron 1967; Pierson *et al.* 2013).

Although rill erosion of tephra-fall deposits diminishes rapidly, shallow landslides can emerge

as an effective process delivering sediment to channels. Some landslides occur shortly after an eruption (Swanson *et al.* 1983; Smith and Swanson 1987) as an immediate response to loss of vegetation, deposition of fresh sediment, and increased precipitation throughfall. Others, however, are delayed and can mobilize not only fresh tephra fall, but also older tephra-fall deposits (e.g. Swanson and Major 2005; Korup *et al.* 2019). The efficacy of landslides to mobilize tephra-fall deposits depends on a number of factors, including recurrence and duration of intense precipitation, compositions and structure of hillside strata, and a competition between the timescales of root decay of trees killed by an eruption, reducing strength within deposits, and regrowth of new vegetation sufficient to anchor tephra-fall deposits (Swanson and Major 2005; Korup *et al.* 2019).

Valley and channel erosion. Erosion of valley-filling deposits causes greater-magnitude and more prolonged posteruption sediment delivery than does erosion of hillside tephra or thin valley deposits. This difference in erosion response occurs because rivers can deeply incise and greatly widen channels as they adjust to posteruption water and sediment fluxes. Sediment supply commonly exceeds river transport capacity, and thus sediment shifts about causing channel instabilities that perpetuate channel widening and lateral channel migration. In general, posteruption channels experience complex sequences of incision, aggradation, and widening (e.g. Meyer and Martinson 1989; Daag and van Westen 1996; Simon and Thorne 1996; Gran and Montgomery 2005; Ulloa *et al.* 2016; Major *et al.* 2019).

Initial erosion of valley-filling deposits can be rapid and dramatic. Following the great eruptions of Mount St Helens (1980) and Mount Pinatubo (1991), channels carved into debris-avalanche and PDC deposits were incised tens of metres and widened hundreds of metres within a year (Meyer and Martinson 1989; Daag and van Westen 1996; Simon 1999; Major *et al.* 2019). Following the 1982 eruption of El Chichón (Mexico), valleys buried thickly by PDC deposits were incised up to 20 m, most of that incision occurring within months after the eruption (Inbar *et al.* 2001). But channels need not be thickly buried to experience substantial hydrogeomorphic responses. Even channels relatively thinly paved by lahar deposits can incise by metres and widen by many tens of metres owing to channel instabilities associated with altered water and sediment discharges (e.g. Meyer and Martinson 1989; Lavigne 2004).

Although channel erosion is most dramatic within the first few years after an eruption, persistent channel instabilities and geomorphic adjustments can prolong notable channel erosion for years or decades. Such prolonged channel adjustment, which Gran *et al.* (2011) referred to as phase II adjustment, or the phase that follows initially rapid hillside and channel erosion (Fig. 32), is the result of persistent mining of channel bed and bank sediment. Persistent mining of bank sediment is a result of incision having created tall banks susceptible to

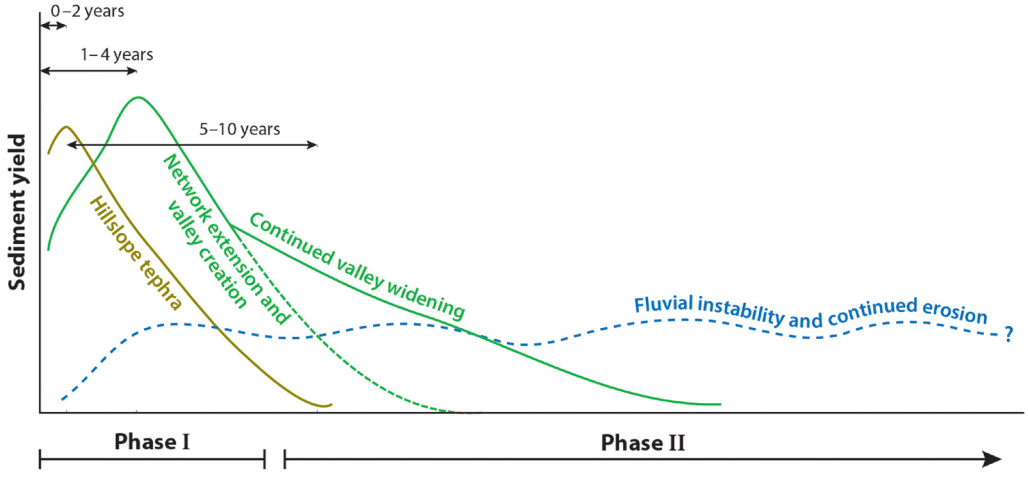

Fig. 32. Conceptual diagram illustrating phases of geomorphic change and sources for sediment yield from volcanically disturbed landscapes, as functions of time and degree of landscape recovery. Phase I is caused by erosion of tephra-fall and pyroclastic-density-current deposits from hillslopes and development of channel networks. This phase produces the greatest peak sediment release but that release declines rapidly. Phase II response is caused by persistent lower-level channel erosion related mainly to bank erosion. From Pierson and Major (2014), modified from Gran *et al.* (2011).

undercutting and mass failure along channels that are highly mobile (Gran 2012; Major *et al.* 2018). Indeed, major sediment sources along rivers in the Cascade Range (USA) are Holocene terraces composed of glacial and lahar sediment subject to small, frequent mass movements induced by inexorable lateral erosion (Scott and Collins 2021).

Eruption effects on sediment transport. Posteruption erosion of volcanically disturbed landscapes increases sediment transport. Because of induced hydrogeomorphic changes, sediment-transport processes and channel geometries evolve and adjust to convey the supplied sediment load. Commonly, sediment concentrations increase over a broad range of discharges (Dinehart 1998), lahars and high-sediment-transporting floods become more prevalent, and channels become smoother, steeper, and straighter to convey these sediment loads (Pierson and Major 2014).

Local climate affects the sediment transporting processes. In tropical and subtropical climates, secondary lahars become more frequent and may continue for many years (Waldron 1967; Rodolfo 1989; Umbal 1997; Suwa and Yamakoshi 1999; Lavigne *et al.* 2000; Lavigne and Suwa 2004; Gran and Montgomery 2005; Harris *et al.* 2006; Barclay *et al.* 2007; Cinque and Robustelli 2009). In temperate, non-tropical climates, early lahars may occur, but fluvial processes subsequently dominate (Major 2004; Manville *et al.* 2009*b*; Pierson *et al.* 2011, 2013; Major *et al.* 2016).

The proportion of volcanic sediment output from a watershed v. that stored within a watershed can be highly variable. As noted above, large amounts of deposited tephra fall commonly remain in hillside storage. Abundant valley sediment can also remain in storage if the area of deposition greatly exceeds the fluvial footprint of channel systems. Large amounts of reworked volcaniclastic sediment commonly move among storage areas within watersheds rather than being exported rapidly (e.g. Pierson *et al.* 1992). The proportion of volcanic sediment output from a watershed v. that moved into storage reflects differences in volcanic process, the amount of sediment input to watersheds, watershed size, hydrology, and the distances and average gradients between the source volcano and watershed outlet (Davies *et al.* 1977; Pierson *et al.* 1992; Manville *et al.* 2009*b*; Pierson and Major 2014).

Despite differences in sediment output and storage among volcanic landscapes, posteruption sediment yields (mass output per unit watershed area) can be extraordinary. Erosion and transport of fresh volcanic sediment, as well as of older sediment from storage, can generate sediment yields that rival those of Earth's greatest sediment-transporting rivers. Common values range from 10^3–10^7 Mg km^{-2} (Fig. 33). When converted to average rates of landscape denudation, erosion rates of volcanically disturbed landscapes typically exceed those of other landscapes by 3–4 orders of magnitude (see Pierson and Major 2014, supplemental table 1). Even though releases of reworked sediment from volcanically disturbed landscapes are largely transitory, they can still dominate geomorphic and sedimentologic functioning of landscapes over decadal- to century-scale timeframes – timeframes critical to human societies (Umbal 1997; Manville and Wilson 2004; Cinque and Robustelli 2009; Manville *et al.* 2009*b*; Gran *et al.* 2011; Pierson *et al.* 2011; Major *et al.* 2020).

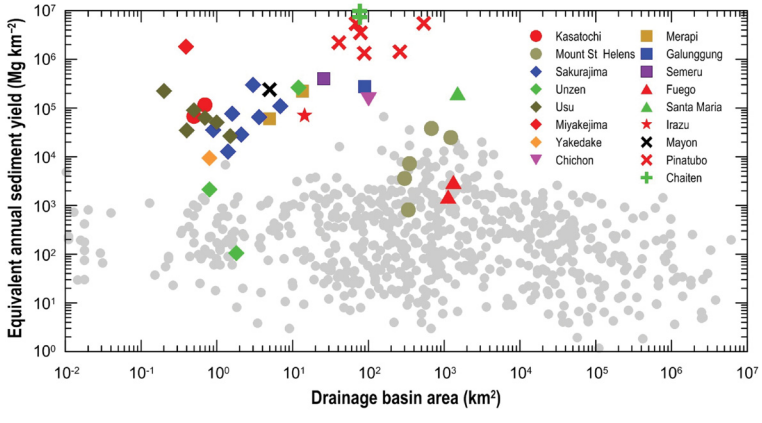

Fig. 33. Average annual (mainly suspended) sediment yield as a function of drainage-basin area. Note the extraordinary releases of sediment caused by volcanic disturbance (coloured data points). Grey data points are for non-volcanic terrain, or drainage basins in volcanic terrain where eruptions have not occurred for centuries or millennia. From Pierson and Major (2014).

Durations of exceptional sediment yield from volcanically disturbed landscapes vary with nature of disturbance. Delivery from disturbed channels is commonly greater and more prolonged than that from disturbed hillsides. Nevertheless, exceptional sediment delivery diminishes rapidly within a few years of disturbance (Chinen 1986; Simon 1999; Suwa and Yamakoshi 1999; Major *et al.* 2000, 2016, 2021; Lavigne 2004; Yamakoshi *et al.* 2005; Gran *et al.* 2011) (Fig. 34). Even so, ongoing adjustments of disturbed channels can maintain prolonged, elevated sediment delivery for decades (e.g. Major *et al.* 2021), and modelling projections suggest they can last for centuries (e.g. Meadows 2014).

Geomorphic and sedimentologic responses to altered hydrology and excess sediment. Changes to the hydrogeomorphic regime of a volcanically disturbed landscape trigger geomorphic adjustments in fluvial systems. Extraordinary sediment mobility can induce net storage where sediment supply exceeds transport capacity. That accumulation of sediment induces channel aggradation (e.g. Smith 1987; Gran and Montgomery 2005; Kataoka *et al.* 2009; Manville *et al.* 2009*b*; Pierson *et al.* 2011, 2013; Zheng *et al.* 2014; Major *et al.* 2021), which affects channel pattern. When sediment supply wanes, the balance between supply and transport capacity adjusts and streams can re-incise channel beds (e.g. Gran and Montgomery 2005; Cinque and Robustelli 2009; Pierson *et al.* 2011; Major *et al.* 2019). Channels can undergo cycles of aggradation and incision as diffuse waves of sediment pass through fluvial systems (e.g. Janda *et al.* 1984; Tanarro *et al.* 2010). Channel aggradation can occur rapidly – hours to days – especially when sediment is transported by secondary lahars or sediment-laden floods (e.g. Punongbayan *et al.* 1996; Lavigne *et al.* 2000; Pierson *et al.* 2013; Fig. 35). Channel aggradation and degradation are not synchronous along the longitudinal profile; rather, they reflect interactions among channel morphology, streamflow, sediment supply, sediment size, and sediment transport (e.g. Lisle *et al.* 2001; Pierson and Major 2014; Major *et al.* 2021).

Aggradation of volcanic sediment induces changes in channel patterns. In particular, aggradational channels invariably evolve from single-thread to braided channel patterns (e.g. Davies *et al.* 1977; Kuenzi *et al.* 1979; Janda *et al.* 1984; Smith 1987; Manville *et al.* 2009*a*, *b*; Gran 2012; Ulloa *et al.* 2015) (Fig. 36). Accumulations of large woody debris, often transported by lahars and PDCs, can strongly influence sediment storage, channel patterns, and variations in sediment composition and geomorphic

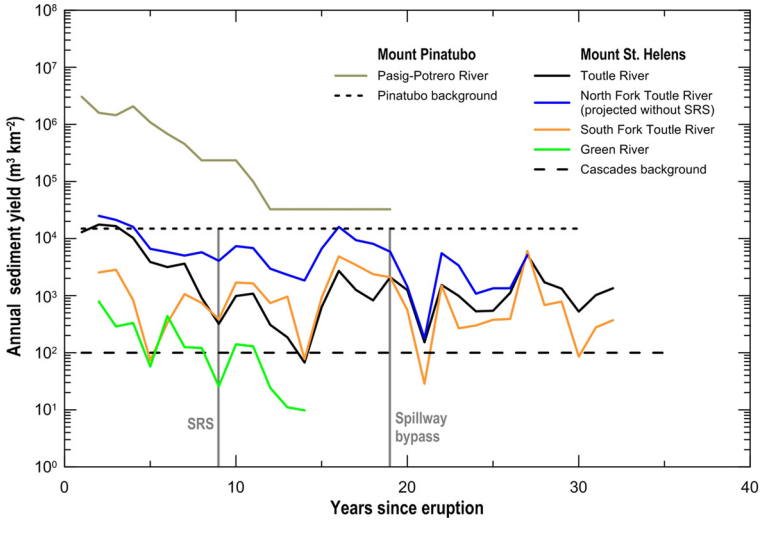

Fig. 34. Sediment yields from volcanically disturbed landscapes at Mount St Helens (USA) and Mount Pinatubo (Philippines) as a function of time since eruption. SRS labels the point in time when the US Army Corps of Engineers constructed a sediment-retention structure (SRS) at Mount St Helens to trap sediment on the North Fork Toutle River just upstream of its confluence with Green River. About 10 years after construction, sediment had filled behind the structure to the point that it began passing over the structure's spillway. Mount St Helens data, except for North Fork Toutle River, are measured suspended sediment. Data for North Fork Toutle River represent the total load (suspended sediment and bed load) that would have passed a gauging site below the SRS had it not been constructed (data from Major *et al.* 2021). Mount Pinatubo data come mainly from measurements of accumulated deposits and represent both suspended-load and bed-load sediment (Gran *et al.* 2011). Note the rapid decline in sediment yield within the first decade after each eruption. Modified from Pierson and Major (2014).

Fig. 35. Examples of channel sedimentation owing to sediment remobilization following volcanic eruptions. (**a**, **b**) Aggradation largely by lahars on Boyong River at Merapi volcano (Indonesia) three months after eruption (images from December 1994 and February 1995). The bridge deck in (a) is 7 m above the channel bed. From Lavigne *et al.* (2000). (**c**, **d**) Aggradation on the Bamban River at Mount Pinatubo (Philippines). Nearly 9 m of deposition occurred from secondary lahars during a single storm in August 1991. From Punongbayan *et al.* (1996). (**e**) Fluvial sedimentation in lower Chaitén River following eruption of Chaitén volcano (Chile). Note how aggradation caused river to avulse through town and construct a delta in Chaitén Bay. Channel fill is about 7 m thick. Photograph © P. Duhart, SERNAGEOMIN, February 2009. (**f**) Fluvial sediment fill along lower Sandy River, Oregon (USA), related to reworking of lahar and pyroclastic-density-current deposits from an eruption of Mount Hood in the late 1700s CE. This site exposes trees rapidly buried by the sediment fill. The surface on which the trees were growing is exposed near base of section. Photograph by T. Pierson, USGS. Modified from Pierson and Major (2014).

processes (Lisle 1995; Swanson *et al.* 2013; Ulloa *et al.* 2014, 2015; Umazano *et al.* 2014; Umazano and Melchor 2020).

Depositional processes. Lahars and floods become more prevalent after an eruption. The duration and dominance of lahars is a function of climate, local hydrology, durations of eruptive activity, and the distributions and characteristics of deposited volcaniclastic sediment. Following many eruptions, initial phases of hydrogeomorphic responses are dominated by an increase in sediment transport by lahars (e.g.

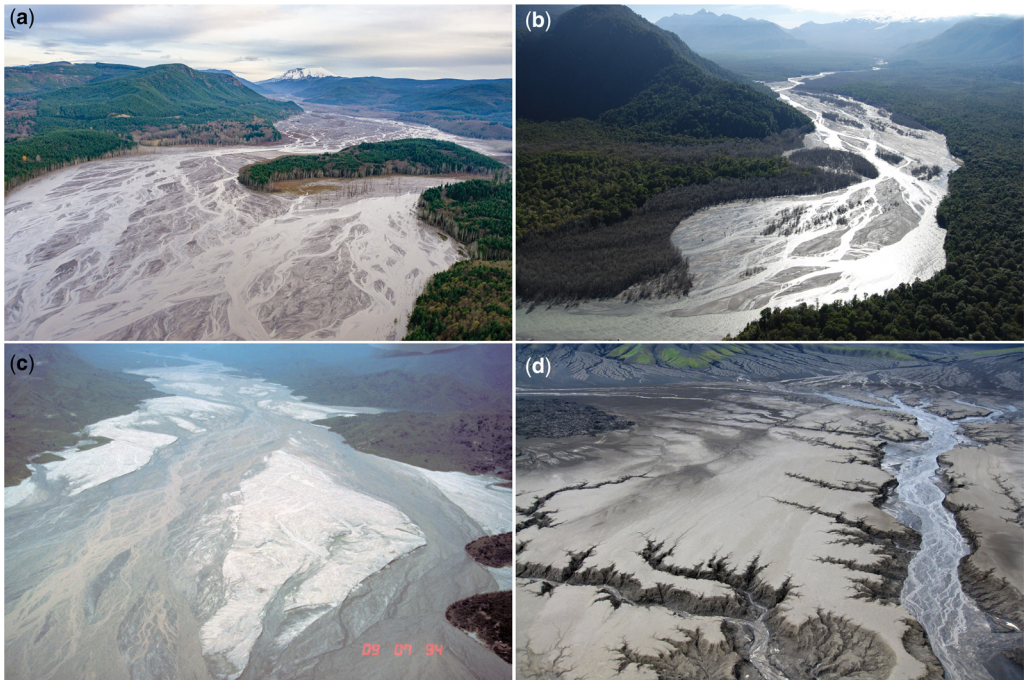

Fig. 36. Examples of braided channel patterns developed in volcanically disturbed river systems where large amounts of volcaniclastic sediment have accumulated. (**a**) Fluvially transported sediment accumulated in North Fork Toutle River, Mount St Helens (USA), upstream of sediment retention structure. Photograph by A. Mosbrucker, USGS. (**b**) Fluvial sediment accumulation in Rayas River, Chaitén volcano (Chile). Photograph by J. Major, USGS. (**c**) Braided pattern developed on O'Donnell River, Mount Pinatubo (Philippines), during reworking of secondary lahar deposits in September 1994. Photograph by C. Newhall, USGS. (**d**) Braided channel pattern developed on eroded tephra-fall deposits within Okmok caldera (USA) following 2008 eruption. Photograph by J. Schaefer, USGS/ADGGS, August 2013.

Waldron 1967; Smith 1987; Rodolfo and Arguden 1991; Umbal 1997; Lavigne *et al.* 2000; Perrotta *et al.* 2006; Barclay *et al.* 2007; Manville *et al.* 2009*a*). Following other eruptions, posteruption lahars are rare and sediment transport is dominated largely or exclusively by fluvial processes (e.g. Janda *et al.* 1984; Major 2004; Pierson *et al.* 2011, 2013). The initial posteruption phase of transport by lahars commonly evolves toward dominance by fluvial transport. Indeed, observations following modern eruptions and investigations of ancient stratigraphic sequences reveal abrupt to gradual transitions from mass-flow to fluvial-transport processes (e.g. Smith 1987; Gran and Montgomery 2005; Perrotta *et al.* 2006; Manville *et al.* 2009*a*; Pierson *et al.* 2013; Major *et al.* 2016).

Deposit characteristics. Posteruption volcaniclastic sequences exhibit a variety of deposit textures and sedimentary structures. Lahar deposits exhibit the textural characteristics typical of type-1 and type-2 lahar flows, whereas fluvial, fluvial-lacustrine, and fluvial-deltaic deposits exhibit a broad range of characteristics and sequencing from sand-rich to gravel-rich, crudely stratified to cross-bedded, well- to moderately sorted, and with variable degrees of clast imbrication and evidence of bedforms (e.g. Davies *et al.* 1977; Kuenzi *et al.* 1979; Vessell and Davies 1981; Smith 1987; White and Riggs 2001; Friele *et al.* 2005; Kataoka *et al.* 2009; Manville *et al.* 2009*b*; Sohn *et al.* 2013). Pumice clasts within fluvial deposits are typically rounded. In distal settings, tens to hundreds of kilometres from volcanic sources, posteruptive sediment deposits can be many metres thick (e.g. Kataoka *et al.* 2009; Pierson *et al.* 2011; Pierson and Major 2014). In contrast, primary deposits at these distances commonly range from a few millimetres or centimetres (fall deposits) to a few metres thick (lahars). Within tens of kilometres, debris-avalanche deposits may be many metres to tens of metres thick; in rare instances they may be similarly thick at greater distances (e.g. Stoopes and Sheridan 1992). At distances of thousands of kilometres, only trace amounts of cryptotephra may be preserved (e.g. Jensen *et al.* 2021).

Magnitudes of posteruption aggradation can vary widely. The magnitude of aggradation is affected not only by sediment supply, but also by local channel morphology. As noted by Pierson and Major (2014), peak aggradation levels have ranged from a few metres to nearly 40 m in channel reaches up to 100 km from source, with aggradation on the order of 5–10 m common. Except where massive sediment inputs are involved, aggradation levels that exceed 20 m are typically limited to confined valleys (e.g. Pierson *et al.* 2011). Beyond about 50 km from source, channel aggradation is caused mainly by fluvial deposition; at lesser distances both fluvial and lahar processes contribute.

In the geological record, vertical and lateral sequences of volcaniclastic deposits commonly exhibit a transition from primary to secondary deposits, illustrating the initial sediment input from eruptions followed by consequent deposit reworking (Fig. 37). To capture the importance of volcanism-induced sedimentation in the geological record, Smith (1991) proposed that facies sequences in volcanic settings can be divided into two fundamental conditions: syneruptive periods and intereruptive periods. Syneruptive periods represent episodes that produce large volumes of volcaniclastic sediment. This sediment production is driven by frequent volcanism and, in response, by the occurrence of lahars and floods that result from alterations to hydrogeomorphic regimes. These geologically brief but intense periods of sediment production are characterized by a general lack of lithologic diversity, deposits rich in sand, and large lateral extents of lahar and flood deposits. In contrast, intereruptive periods represent longer times when volcanism has had little detectable impact on the landscape or on the character of fluvial systems. During intereruptive periods, sediment delivery is greatly diminished, normal streamflow processes (seasonal floods and infrequent large floods) dominate, deposits exhibit greater lithological diversity as contributions from multiple parts of the landscape are averaged over time, and they are comparatively gravel rich as predominantly bed-load-transported sediment is preserved. Intereruptive deposits are commonly thinner and more spatially restricted than syneruptive deposits because they are often confined to valleys incised into syneruptive deposits.

Discussion

Volcanism affects sedimentation on a variety of scales in both space and time. Volcaniclastic sediment can mantle, modify, or create new topography at the landscape scale and alter the ‘normal’ hydrogeomorphic functioning of the landscape for years, decades, and sometimes millennia. Indeed, in some settings, volcanism may be sufficiently frequent to drive a landscape into a perpetual state of disequilibrium with regard to hydrogeomorphic functioning (repeated cycles of perturbation and response) for hundreds to thousands of years. As a result, volcanism can have an outsized impact on sedimentation in continental settings for extended periods of time. For example, Friele *et al.* (2005) showed that a

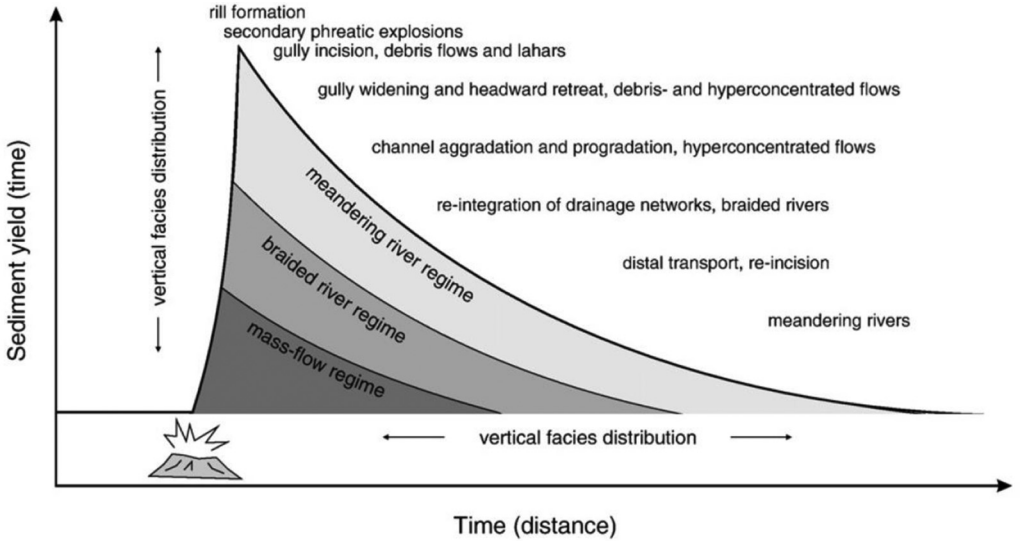

Fig. 37. Styles and environments of subaerial volcaniclastic resedimentation following large explosive eruptions (reprinted from Manville *et al.* 2009*a*, with permission from Elsevier).

disproportionate amount of sediment within the Lillooet River basin (Canada) was derived from Mount Meager volcano, a massif that constitutes only 2% of the area of the drainage basin. Manville and Wilson (2004) showed that the sedimentary response to the 530 km^3 (DRE) 26.5 ka Oruanui eruption of Taupo volcano produced a massive downstream response, including sufficient aggradation along 180 km of a major river system to trigger avulsion into a different watershed. The scale of response was driven by the character of the eruption, but the duration of response, which lasted some 10–12 000 years, was influenced and prolonged by suppression of revegetation during harsh periglacial climate conditions that accompanied the Last Glacial Maximum. Smith (1991) showed that volcaniclastic sediments in river systems draining volcanic arcs dominate stratigraphic sequences during periods of active volcanism and can form distinctive facies sequences and geometries that may be used to lend insights into the relative importance of volcanism and tectonics on arc-basin sedimentation. Recognition of volcanism-induced sedimentation in the stratigraphic record and the relative influences of volcanism, tectonism, and climate on facies sequences and geometries are key challenges for sedimentary geologists and volcanologists (e.g. Fisher and Smith 1991).

At a local scale, volcaniclastic sedimentation not only affects the landscape, but also poses a variety of hazards to society. Ensembles of volcanic processes strongly influence the nature of volcaniclastic deposition and its societal and environmental impacts. Volcanoes can shed vast amounts of clastic debris that can fill and smooth topography across reaches extending a few kilometres to many tens of kilometres. Volcaniclastic fills can be highly complex, with deposits from numerous processes intercalated, eroded, reworked, and redeposited (Fig. 38). Proximal stores of deposits tend to be thick, relatively coarse grained, and composed of variable compositions and textures. They provide a rich archive of the eruptive histories and hazards of a volcano, but they can be challenging to accurately decipher. Some deposits may be buried and not exposed whereas others may represent isolated fragments of their initial extent. With increasing distance from a

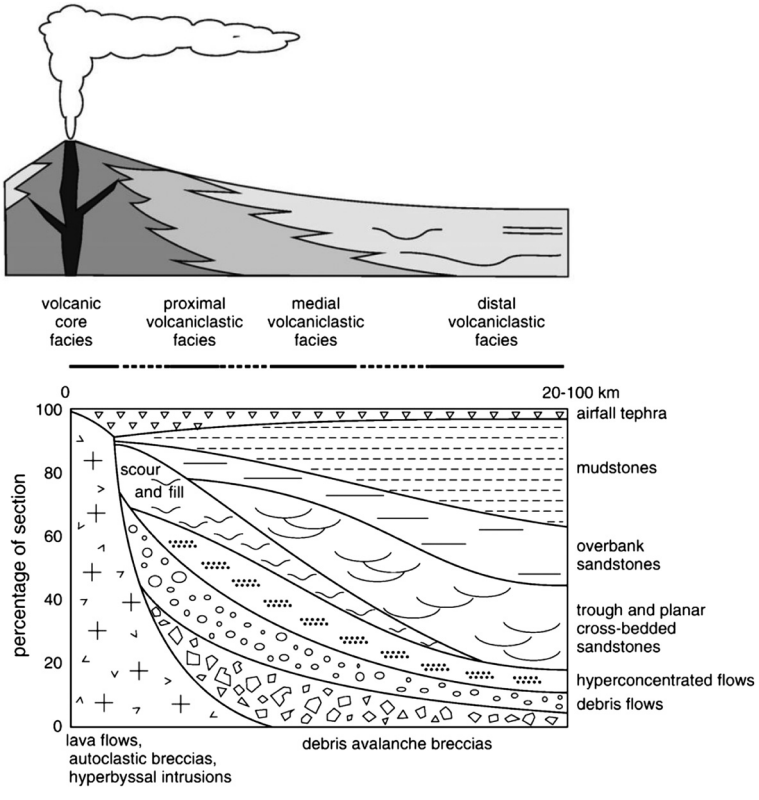

Fig. 38. Schematic distribution of sedimentary facies associated with explosive volcanism in subaerial settings (reprinted from Manville *et al.* 2009*a*, with permission from Elsevier).

volcano, volcaniclastic deposits commonly are composed of thin, fine-grained tephra falls or thick sequences of lahar and fluvially reworked sediment. Deposits along river valleys may exhibit cycles of deposition and erosion, and deposits from certain volcanic processes, such as lahars, may be easier to decipher because they are less susceptible to being trapped within the jumble of proximal processes and deposits. However, the distal geological record is incomplete and is biased toward larger events capable of inundating flood plains and terraces. Distal environments are also the store of abundant remobilized sediment accumulation, and are thus further biased toward preservation of fluvial, fluvial-lacustrine, and fluvial-deltaic sediment. Furthermore, specific information regarding the nature and character of proximal primary deposits may be obscured in distal deposits. Nevertheless, some characteristics of distal deposits, such as inclusion of pumice pebbles and cobbles, may provide insights into generalized primary processes such as occurrence of PDCs (e.g. Kataoka 2005). Distal deposits, although providing a lens through which to view partial histories of some of the more significant eruptions and eruptive impacts, are clearly inadequate for understanding the full complexity and hazards posed by a volcano. In some instances, a distal deposit preserved in the geological record may be non-representative of the hazard posed. For example, during the 2009 eruption of Redoubt volcano explosions early in the eruption sequence triggered a large, ice-rich lahar that travelled more than 40 km, had local flow depths of 6–8 m, left deposits as much as 5 m thick, and threatened a critical oil-storage and transfer facility (Waythomas *et al.* 2013). However, once the ice melted, the record of that event was an inconspicuous silty sand no more than a few centimetres thick – a deposit that might be easily overlooked or misunderstood (Waythomas 2014). Although that deposit reflects the sediment load transported by the lahar, it is not representative of the hazard posed by the lahar or by eruptions from this ice-clad volcano. Similarly, PDC deposits from directed explosions and surges may not adequately reveal the hazards posed by those processes. Correct interpretation of volcaniclastic deposits and recognition of volcanic processes is imperative for understanding both eruptive histories and the hazards posed by volcanoes.

Advances in volcaniclastic deposit and volcanic process interpretation

Interpretations of volcaniclastic deposits and the processes that produce them have advanced considerably in the past few decades. Since the eruption of Mount St Helens in 1980, volcanic debris avalanches have become recognized as a common, and oft-repeated, process at volcanoes worldwide. Their morphological and sedimentological characteristics are now well defined, their causative mechanisms much better understood, assessments of their frequency improved, and modelling of their flow behaviour is advancing (e.g. Roverato *et al.* 2021). The 1980 Mount St Helens eruption also clearly elucidated the catastrophic nature of directed volcanic blasts, an association with volcanic debris avalanches, and the unique nature of their deposits (Lipman and Mullineaux 1981; Belousov *et al.* 2007). Study of subsequent eruptions of Soufrière Hills volcano and reinvestigations of deposits from the 1956 eruption of Bezymianny volcano, the 1951 eruption of Lamington volcano, and the 1964 eruption of Shiveluch volcano (Russia) have further refined the sedimentological signature of directed-blast deposits (Bogoyavlenskaya *et al.* 1985; Sparks *et al.* 2002; Belousov *et al.* 2007, 2020). Continued advances in numerical modelling have convincingly demonstrated that although such spatially directed PDCs may be propelled initially by rapid expansion of volatiles and fragmentation of magma, they quickly collapse into high-energy gravity-driven currents (e.g. Esposti Ongaro 2012). Even small-scale directed explosions, such as occurred at Chaitén volcano in 2008, produce deposits with characteristic directed-explosion signatures. The 1980 Mount St Helens eruption along with the 1985 eruption of Nevado del Ruiz volcano and 1991 eruption of Mount Pinatubo sharpened understanding of the devastating nature of lahars, highlighted their causative mechanisms at snow-clad volcanoes, illustrated associations with debris avalanches, re-emphasized associations with rainfall, greatly improved our understanding of their propensity to evolve in space and time along their flow paths, and reinforced that even communities far from volcanoes can be vulnerable to devasting volcanic impacts (e.g. Janda *et al.* 1981; Pierson *et al.* 1990; Newhall and Punongbayan 1996; Vallance and Iverson 2015). Since those eruptions, physical understanding of the mechanics of multiphase mixtures has advanced considerably and sophisticated numerical models can now predict depth, velocity, and impact forces of lahars with substantial accuracy as well as the dynamics of explosive eruptions and characteristics of PDCs (e.g. George and Iverson 2014; Iverson and George 2014; Neri *et al.* 2022). The 1982 eruption of El Chichón volcano, the 1991 eruptions of Mount Pinatubo and Unzen volcanoes, and the 1995 and later eruptions of Soufrière Hills volcano further highlighted the impacts and hazards of PDCs – from column collapse, caldera collapse, and dome collapse (e.g. Sigurdsson *et al.* 1984; Scott *et al.* 1996; Calder *et al.* 1999; Miyabuchi 1999; Sparks *et al.* 2002; Carn *et al.* 2004). Modern

technological observations of those eruptions and others – both optically and instrumentally – have helped to better link the characteristics of deposits with the nature of the volcanic eruptions. Eruptions of Soufrière Hills volcano, Merapi volcano (Indonesia), Colima volcano (Mexico), and Santiaguito/Santa Maria volcano (Guatemala) have highlighted the hazards and deposit characteristics of PDCs (block-and-ash flows) associated with protracted growth and collapse of lava domes as well as the propensity for the occurrence of secondary lahars resulting from rainfall runoff (e.g. Rose *et al.* 1976; Calder *et al.* 1999; Saucedo *et al.* 2002; Lavigne 2004; Harris *et al.* 2006; Barclay *et al.* 2007; Charbonnier and Gertisser 2008; Capra *et al.* 2018). Eruptions of Galunggung volcano (Indonesia) in 1982, Redoubt volcano in 1989, Mount Pinatubo in 1991, and Eyjafjallajökull volcano (Iceland) in 2010 highlighted the long-range hazards of volcanic plumes to aviation and the impacts of volcanic aerosols on climate (Robock 2000; Guffanti *et al.* 2010; Guffanti and Tupper 2015). Studies of fall deposits from several eruptions in the past decades have highlighted aggregation of extremely fine ash within volcanic plumes and have identified causative processes and refined modelling of volcanic plumes and tephra fall. Characteristics of fall deposits are now used to make robust estimates of eruption characteristics such as mass eruption rates and plume heights. Several eruptions of the past few decades have highlighted the hydrological changes that can follow tephra fall. These hydrological changes can lead to widespread erosion and formation of secondary lahars and floods. Of particular note is that hazardous mobilization of sediment can be triggered by unremarkable rainfalls and that such mobilization can happen swiftly after rainfall begins (Pierson *et al.* 2013). Greater recognition that releases of crater and valley-marginal lakes, both during eruptions and intereruption periods, can influence volcaniclastic sedimentation has sharpened appreciation for ancillary hazards associated with volcanoes (e.g. Scott 1988*b*; White *et al.* 1997; Manville *et al.* 2007; Capra *et al.* 2010; Manville 2010; Massey *et al.* 2010). Many of the advances in deposit and process interpretation have allowed refined understanding of past historical and prehistoric eruptions and a greater understanding of the histories and hazards of many volcanoes.

The past few decades have also garnered greater appreciation for the impacts and hazards associated with posteruption remobilization of volcaniclastic sediment. Indeed, we are beginning to appreciate that after eruptions end, some of society's most difficult challenges may just begin, especially for communities distant from volcanoes. Volcanically disturbed landscapes can generate some of the world's greatest sediment releases, and even though extraordinary releases diminish rapidly, elevated releases can endure for years to decades, and in rare cases millennia. Posteruption sediment redistribution can be one of the greatest and costliest challenges society must confront in volcanic regions; indeed, after some eruptions, posteruption sediment redistribution can cause greater social and economic harm than the direct impacts of the eruptions themselves.

Preservation potential

Eruption processes, deposit textures and compositions, depositional environments, and climatic regimes affect deposit preservation. Eruptions can spawn ensembles of processes that produce volcaniclastic deposits on a variety of scales. Deposit volumes can range from as little as a few hundreds or thousands of cubic metres to as much as a few thousands of cubic kilometres during exceptionally rare super-eruptions. Areas affected by flowage deposits can range from a few to a few tens of thousands of square kilometres; fall deposits can affect greater areas. Deposit thicknesses can range from trace amounts to tens or hundreds of metres. Volcaniclastic deposits are also highly erodible. Deposits that are loosely textured and friable are more apt to be easily eroded than are deposits having denser textures or deposits that have been welded. Deposits that contain abundant lithic clasts may erode and leave armors of winnowed clasts that curtail further erosion, whereas loose, sandy, pumice-rich deposits may easily erode and ultimately preserve little of the original deposit. Deposit textures can also influence preservation. Tephra-fall deposits in proximal areas are commonly composed of coarse sediment (typically medium to coarse ash and lapilli) overlain by finer ash. This pavement of finer ash can severely alter the characteristics of rainfall and snowmelt runoff and lead to erosion of the tephra mantle (e.g. Chinen 1986; Collins and Dunne 1986; Németh and Cronin 2007; Ogawa *et al.* 2007; Pierson *et al.* 2013; Engel *et al.* 2021). However, after rills and gullies have eroded into the coarser underlying tephra fall, erosion can cease, leaving much of the original proximal tephra-fall deposit in place (e.g. Collins and Dunne 1986, 2019). These variations in deposit volume, area, thickness, and texture can greatly affect the preservation potential of volcaniclastic deposits.

Depositional environments and climate regimes also affect preservation potential. Proximal deposits from eruptions of glaciated volcanoes and from volcanoes in wet, tropical climates generally have lower preservation potential than do those in arid environments. In arid environments, wind erosion and aeolian transport can rework primary deposits, creating aeolian deposits that must be carefully distinguished

from (surge) PDC deposits (e.g. Smith and Katzman 1991). Consequently, variations in preservation potential can severely skew not only our understanding of eruptive histories of volcanoes and their eruptive processes, but also the perceptions of hazards their eruptions pose. For example, at Ruapehu volcano Gillies *et al.* (2020) showed that deposits from small- to medium-volume PDCs have low preservation potential, particularly on the steep, glaciated flanks of the volcano. This poor preservation has created an incomplete eruptive record of the volcano. From the limited preservation of these PDC deposits, Gillies *et al.* (2020) concluded that they formed from column collapse and dome collapse or explosion events. Hence, Ruapehu volcano produces a broader spectrum of PDC styles and sizes than has previously been inferred. At Mount Hood (USA), the Polallie eruptive period occurred *c.* 12–15 ka when glaciers at the volcano were more extensive. Topographic positions of proximal deposits of PDCs and lahars from that eruptive period are determined largely by the extent of glacier ice in valleys at the time. Those topographic positions range from deposits primarily on ridgetops exposed when glaciers filled valleys, to deposits plastered on valley sides after glaciers had shrunk, and to valley floors beyond the limits of the glaciers (Crandell 1980). The proximal record of this eruptive period is thus poorer than its distal record. In distal settings, deposit preservation is affected by depositional environment, such as channel v. flood plain, as well as by deposit thickness, and in modern times by societal actions such as dredging and channel mining.

The degree of deposit preservation affects the types of questions one can address. Variations in preservation of proximal deposits affect understanding of eruptive histories and hazards. Although distal accumulations of remobilized volcaniclastic sediment generally have high preservation potential owing to their thickness and lateral extent, they typically disaggregate information about specific volcanic processes upstream. Thus, they preserve records of volcanism and allow general questions regarding periods of syneruption v. intereruption to be addressed but can limit understanding of the timing of events and specific volcanic processes active during periods of eruption.

Concluding remarks

Volcaniclastic sedimentation has an outsized geomorphic and sedimentologic impact on proximal drainage basins and river channels downstream. Deposits of volcaniclastic flows and falls can mantle, modify, or create new topography, and can adversely affect communities many tens to hundreds of kilometres downstream and downwind of volcanoes. Posteruption erosion and sediment remobilization can endure for decades or longer, sometimes causing more social and economic harm than the direct impacts of eruptions themselves. In the last four decades, especially since the 1980 eruption of Mount St Helens, studies of volcanic processes that generate volcaniclastic sediment have blossomed (e.g. Manville *et al.* 2009*a*). As a result, our understanding of deposit character and their linkages to initiation mechanisms, transport, and depositional processes have increased immensely. Major subaerial volcaniclastic processes, including debris avalanches, pyroclastic density currents (PDCs), lahars, and tephra fall, can produce deposits with widely ranging sedimentologic characteristics. Yet, those deposits have diagnostic characteristics that can point toward deposit provenance. Debris-avalanche deposits show contextual and diagnostic association with transport of pieces of a volcano. PDC deposits exhibit characteristics that point toward hot, dry flowage emplacement and initiation by column collapse, directed explosions, or failure of lava domes or lava flows. Lahar deposits show evidence of transportation as saturated mass flows and their sedimentological and morphological characteristics point toward initiation mechanism (e.g. snowmelt triggered, transformation from a debris avalanche, lake-breakout triggered). Tephra-fall deposits exhibit characteristics indicative of fall not flow, some of which can be used to assess plume height, mass eruption rate, and relative wet v. dry eruptions. Posteruption analyses of deposits from several modern eruptions, progress in our understanding of the physical behaviour of multiphase mixtures, greater insights on the physical interactions within PDCs and volcanic plumes, and improvements in physical and numerical modelling have vastly enhanced our understanding of volcanic processes, interpretations of eruptive histories, and the hazards posed by volcanic eruptions. Each study of deposits from a new eruption, reanalysis of a past eruption, experimental interrogation of a volcaniclastic process, and analysis of hydrogeomorphic response to volcanic disturbance of landscapes further contributes to and refines our store of knowledge.

In this chapter, I have highlighted the characteristics of major subaerial volcaniclastic deposits and the influence of initiation mechanisms and transport processes on the character, storage, and preservation of those deposits. This work summarizes and builds on an immense body of literature and highlights major advances that have occurred in the past few decades. This chapter provides context for the interpretation of volcaniclastic deposits, highlights limitations of those interpretations, and illustrates how the nature of volcaniclastic processes and their initiation mechanisms and transport behaviour can bias their preservation in the geological record.

Acknowledgements My ability to contribute this review is based on a career of interactions with many colleagues worldwide. I am particularly indebted to field excursions and discussions with Tom Pierson, Jim Vallance, Richard Iverson, Kevin Scott, Willie Scott, Cynthia Gardner, Richard Waitt, Lee Siebert, Barry Voight, Fred Swanson, Patrick Pringle, and my late colleagues Dick Janda, Hiroshi Suwa, and Harry Glicken. I am also indebted to the many colleagues and associates who graciously granted me permission to use their photographs. Thoughtful critiques by Chris Harpel, Vern Manville, Larry Mastin, Y.K. Sohn, and Sebastian Watt improved the clarity and sharpened the presentation of this contribution.

Competing interests The authors declare that they have no known competing financial interests or personal relationships that could have appeared to influence the work reported in this paper.

Author contributions **JM**: conceptualization (lead), writing – original draft (lead), writing – review & editing (lead).

Funding Funding to produce this review was provided by the United States Geological Survey, Volcano Science Center, Cascades Volcano Observatory.

Data availability All data generated or analysed during this study are included in this published article (and its supplementary information files).

References

Abbott, P.M. and Davies, S.M. 2012. Volcanism and the Greenland ice-cores: the tephra record. *Earth-Science Reviews*, **115**, 173–191, https://doi.org/10.1016/j.earscirev.2012.09.001

Aguila, L.G., Newhall, C.G., Miller, C.D. and Listanco, E.L. 1986. Reconnaissance geology of a large debris avalanche from Iriga volcano Philippines. *Philippines Journal of Volcanology*, **3**, 54–72.

Alexander, J., Barclay, J., Sušnik, J., Loughlin, S.C., Herd, R.A., Darnell, A. and Crosweller, S. 2010. Sediment-charged flash floods on Montserrat: the influence of synchronous tephra fall and varying extent of vegetation change. *Journal of Volcanology and Geothermal Research*, **194**, 127–138, https://doi.org/10.1016/j.jvolgeores.2010.05.002

Allen, S.R. 2001. Reconstruction of a major caldera-forming eruption from pyroclastic deposit characteristics: Kos Plateau Tuff, eastern Aegean Sea. *Journal of Volcanology and Geothermal Research*, **105**, 141–162, https://doi.org/10.1016/S0377-0273(00)00222-5

Alloway, B., McComb, P., Neall, V., Vucetich, C., Gibb, J., Sherburn, S. and Stirling, M. 2005. Stratigraphy, age, and correlation of voluminous debris-avalanche events from an ancestral Egmont Volcano: implications for coastal plain construction and regional hazard assessment. *Journal of the Royal Society of New Zealand*, **35**, 229–267, https://doi.org/10.1080/03014223.2005.9517782

Ayris, P.N. and Delmelle, P. 2012. The immediate environmental effects of tephra emission. *Bulletin of Volcanology*, **74**, 1905–1936, https://doi.org/10.1007/s00445-012-0654-5

Bacon, C.R. 1983. Eruptive history of Mount Mazama and Crater Lake caldera, Cascade Range U.S.A. *Journal of Volcanology and Geothermal Research*, **18**, 57–115, https://doi.org/10.1016/0377-0273(83)90004-5

Báez, W., de Silva, S. *et al*. 2020. Pulsating flow dynamics of sustained, forced pyroclastic density currents: insights from a facies analysis of the Campo del la Piedra Pómez ignimbrite, southern Puna, Argentina. *Bulletin of Volcanology*, **82**, 53, https://doi.org/10.1007/s00445-020-01385-5

Barclay, J., Alexander, J. and Sušnik, J. 2007. Rainfall-induced lahars in the Belham Valley, Montserrat, West Indies. *Journal of the Geological Society, London*, **164**, 815–827, https://doi.org/10.1144/0016-76492006-078

Baumann, V., Bonadonna, C., Cuomo, S. and Moscariello, M. 2020. Modelling of erosion processes associated with rainfall-triggered lahars following the 2011 Cordon Caulle eruption (Chile). *Journal of Volcanology and Geothermal Research*, **390**, https://doi.org/10.1016/j.jvolgeores.2019.106727

Belousov, A.B. 1995. The Shiveluch volcanic eruption of 12 November 1964 – explosive eruption provoked by failure of the edifice. *Journal of Volcanology and Geothermal Research*, **66**, 357–365, https://doi.org/10.1016/0377-0273(94)00072-O

Belousov, A. 1996. Deposits of the 30 March 1956 directed blast at Bezymianny volcano, Kamchatka, Russia. *Bulletin of Volcanology*, **57**, 649–662, https://doi.org/10.1007/s004450050118

Belousov, A., Belasouva, M. and Voight, B. 1999. Multiple edifice failures, debris avalanches and associated eruptions in the Holocene history of Shiveluch volcano, Kamchatka, Russia. *Bulletin of Volcanology*, **61**, 324–342, https://doi.org/10.1007/s004450050300

Belousov, A., Voight, B. and Belousova, M. 2007. Directed blasts and blast-generated pyroclastic density currents: a comparison of the Bezymianny 1956, Mount St Helens 1980, and Soufrière Hills, Montserrat 1997 eruptions and deposits. *Bulletin of Volcanology*, **69**, 701–740, https://doi.org/10.1007/s00445-006-0109-y

Belousov, A., Belousova, M., Hoblitt, R. and Herman, P. 2020. The 1951 eruption of Mount Lamington, Papua New Guinea: devastating directed blast triggered by small-scale edifice failure. *Journal of Volcanology and Geothermal Research*, **401**, 106947, https://doi.org/10.1016/j.jvolgeores.2020.106947

Belousova, M.G. and Belousov, A.B. 1995. Prehistoric and 1933 debris avalanches and associated eruptions of Harimkotan Volcano (Kurile Islands). *Periodico di Mineralogia*, **64**, 99–100.

Blodgett, J.C., Poeschel, K.R. and Osterkamp, W.R. 1996. *Characteristics of debris flows of noneruptive origin on Mount Shasta, Northern California*. US Geological Survey Open-File Report **96-144**.

Blong, R., Enright, N. and Grasso, P. 2017. Preservation of thin tephra. *Journal of Applied Volcanology*, **6**, 10, https://doi.org/10.1186/s13617-017-0059-4

Bogoyavlenskaya, G.E., Braitseva, O.A., Melekestsev, I.V., Kiriyanov, V.Y. and Miller, C.D. 1985. Catastrophic eruptions of the directed-blast type at Mount St. Helens, Bezymianny, and Shiveluch volcanoes. *Journal of Geodynamics*, **3**, 189–218, https://doi.org/10.1016/0264-3707(85)90035-3

Bonadonna, C. and Costa, A. 2013. Modeling tephra sedimentation from volcanic plumes. *In*: Fagents, S.A., Gregg, T.K.P. and Lopes, R.M.C. (eds) *Modeling Volcanic Processes – The Physics and Mathematics of Volcanism*. Cambridge University Press, Cambridge, 173–202.

Bonadonna, C., Costa, A., Folch, A. and Koyaguchi, T. 2015. Tephra dispersal and sedimentation. *In*: Sigurdsson, H., Houghton, B., Rymer, H., Stix, J. and McNutt, S. (eds) *The Encyclopedia of Volcanoes*. Academic Press, 587–597.

Boudon, G., Semet, M.P. and Vincent, P.M. 1984. Flank failure-directed blast eruption at Soufrière, Guadeloupe, French West Indies: a 3000-yr-old Mt. St. Helens? *Geology*, **12**, 350–353, https://doi.org/10.1130/0091-7613(1984)12<350:FFBEAS>2.0.CO;2

Boudon, G., Bourdier, J.-L., Gourgaud, A. and Lajoie, J. 1990. The May 1902 eruptions of Mount Pelée: high-velocity directed blasts of column-collapse nuées ardentes? *Journal of Volcanology and Geothermal Research*, **43**, 359–364, https://doi.org/10.1016/0377-0273(90)90062-K

Brand, B.D. and Clarke, A.B. 2012. An unusually energetic basaltic phreatomagmatic eruption: using deposit characteristics to constrain dilute pyroclastic density current dynamics. *Journal of Volcanology and Geothermal Research*, **243–244**, 81–90, https://doi.org/10.1016/j.jvolgeores.2012.06.011

Brand, B.D., Mackaman-Lofland, C., Pollock, N.M., Bendaña, S., Dawson, B. and Wichgers, P. 2014. Dynamics of pyroclastic density currents: conditions that promote substrate erosion and self-channelization – Mount St. Helens, Washington (USA). *Journal of Volcanology and Geothermal Research*, **276**, 189–214, https://doi.org/10.1016/j.jvolgeores.2014.01.007

Brand, B.D., Bendaña, S., Self, S. and Pollock, N. 2016. Topographic controls on pyroclastic density current dynamics: insight from 18 May 1980 deposits at Mount St. Helens, Washington USA). *Journal of Volcanology and Geothermal Research*, **321**, 1–17, https://doi.org/10.1016/j.jvolgeores.2016.04.018

Branney, M.J. and Gilbert, J.S. 1995. Ice-melt collapse pits and associated features in the 1991 lahar deposits of Volcán Hudson, Chile: criteria to distinguish eruption-induced glacier melt. *Bulletin of Volcanology*, **57**, 293–302, https://doi.org/10.1007/BF00301289

Branney, M.J. and Kokelaar, P. 1992. A reappraisal of ignimbrite emplacement: progressive aggradation and changes from particulate to non-particulate flow during emplacement of high-grade ignimbrite. *Bulletin of Volcanology*, **54**, 504–520, https://doi.org/10.1007/BF00301396

Branney, M.J. and Kokelaar, P. 2002. *Pyroclastic Density Currents and the Sedimentation of Ignimbrites*. Geological Society, London, Memoirs, **27**, https://doi.org/10.1144/GSL.MEM.2003.027.01.10

Brazier, S., Sparks, R.S.J., Carey, S.N., Sigurdsson, H. and Westgate, J.A. 1983. Bimodal grain size distribution and secondary thickening in air-fall ash layers. *Nature*, **301**, 115–119, https://doi.org/10.1038/301115a0

Brown, R.J. and Andrews, G.D.M. 2015. Deposits of pyroclastic density currents. *In*: Sigurdsson, H., Houghton, B., Rymer, H., Stix, J. and McNutt, S. (eds) *The Encyclopedia of Volcanoes*. Academic Press, 631–648.

Burgisser, A. and Bergantz, G.W. 2002. Reconciling pyroclastic flow and surge: the multiphase physics of pyroclastic density currents. *Earth and Planetary Science Letters*, **202**, 405–418, https://doi.org/10.1016/S0012-821X(02)00789-6

Bursik, M.I., Sparks, R.S.J., Gilbert, J.S. and Carey, S.N. 1992. Sedimentation of tephra by volcanic plumes: I. Theory and its comparison with a study of the Fogo A Plinian deposit, Sao Miguel (Azores). *Bulletin of Volcanology*, **54**, 329–344, https://doi.org/10.1007/BF00301486

Calder, E.S., Cole, P.D. *et al*. 1999. Mobility of pyroclastic flows and surges at the Soufriere Hills Volcano, Montserrat. *Geophysical Research Letters*, **26**, 537–540, https://doi.org/10.1029/1999GL900051

Calvari, S., Tanner, L.H. and Groppelli, G. 1998. Debris-avalanche deposits of the Milo Lahar sequence and the opening of the Valle del Bove on Etna volcano (Italy). *Journal of Volcanology and Geothermal Research*, **87**, 193–209, https://doi.org/10.1016/S0377-0273(98)00089-4

Cando-Jácome, M. and Martínez-Graña, A. 2019. Determination of primary and secondary lahar flow paths of the Fuego Volcano (Guatemala) using morphometric parameters. *Remote Sensing*, **11**, 727, https://doi.org/10.3390/rs11060727

Cantagrel, J.M., Arnaud, N.O., Ancochea, E., Fúster, J. M. and Huertas, M. J. 1999. Repeated debris avalanches on Tenerife and genesis of Las Cañadas caldera wall (Canary Islands). *Geology*, **27**, 739–742, https://doi.org/10.1130/0091-7613(1999)027<0739:RDAOTA>2.3.CO;2

Capra, L. 2007. Volcanic natural dams: identification, stability, and secondary effects. *Natural Hazards*, **43**, 45–61, https://doi.org/10.1007/s11069-006-9101-2

Capra, L. 2011. Volcanic natural dams associated with sector collapses: textural and sedimentological constraints on their stability. *In*: Evans, S.G., Hermanns, R.L. *et al*. (eds) *Natural and Artificial Rockslide Dams*. Springer-Verlag, Berlin, Lecture Notes in Earth Sciences, **133**, 279–294.

Capra, L. and Macías, J.L. 2000. Pleistocene cohesive debris flows at Nevado de Toluca Volcano, central Mexico. *Journal of Volcanology and Geothermal Research*, **102**, 149–168, https://doi.org/10.1016/S0377-0273(00)00186-4

Capra, L. and Macías, J.L. 2002. The cohesive Naranjo debris-flow deposit (10 km^3): a dam breakout flow derived from the Pleistocene debris-avalanche deposit of Nevado de Colima Volcano (México). *Journal of Volcanology and Geothermal Research*, **117**, 213–235, https://doi.org/10.1016/S0377-0273(02)00245-7

Capra, L., Macías, J.L., Scott, K.M., Abrams, M. and Garduño-Monroy, V.H. 2002. Debris avalanches and debris flows transformed from collapses in the Trans-Mexican Volcanic Belt, Mexico – behavior, and implications for hazard assessment. *Journal of Volcanology and Geothermal Research*, **113**, 81–110, https://doi.org/10.1016/S0377-0273(01)00252-9

Capra, L., Borselli, L. *et al*. 2010. Rainfall-triggered lahars at Volcán de Colima, Mexico: surface hydro-repellency as initiation process. *Journal of Volcanology and Geothermal Research*, **189**, 105–117, https://doi.org/10.1016/j.jvolgeores.2009.10.014

Capra, L., Coviello, V., Borselli, L., Márquez-Ramírez, V.-H. and Arámbula-Mendoza, R. 2018. Hydrological control of large hurricane-induced lahars: evidence from rainfall-runoff modeling, seismic and video monitoring. *Natural Hazards and Earth Systems Science*, **18**, 781–794, https://doi.org/10.5194/nhess-18-781-2018

Carey, S. and Bursik, M. 2015. Volcanic plumes. *In*: Sigurdsson, H., Houghton, B., Rymer, H., Stix, J. and McNutt, S. (eds) *The Encyclopedia of Volcanoes*. Academic Press, 571–585.

Carey, S.N. and Sigurdsson, H. 1982. Influence of particle aggregation on deposition of distal tephra from the May 18, 1980, eruption of Mount St. Helens volcano. *Journal of Geophysical Research*, **87**, 7061–7072, https://doi.org/10.1029/JB087iB08p07061

Carey, S. and Sparks, R.S.J. 1986. Quantitative models of the fallout and dispersal of tephra from volcanic eruption columns. *Bulletin of Volcanology*, **48**, 109–125, https://doi.org/10.1007/BF01046546

Carlyle-Moses, D.E. and Gash, J.H.C. 2011. Rainfall interception loss by forest canopies. *In*: Levia, D.F., Carlyle-Moses, D.E. and Tanaka, T. (eds) *Forest Hydrology and Biogeochemistry: Syntheses of Past Research and Future Directions*. Ecological Studies, **216**. Springer, Dordrecht, 407–423.

Carn, S.A., Watts, R.B., Thompson, G. and Norton, G.E. 2004. Anatomy of a lava dome collapse: the 20 March 2000 event at Soufrière Hills Volcano, Montserrat. *Journal of Volcanology and Geothermal Research*, **131**, 241–264, https://doi.org/10.1016/S0377-0273(03)00364-0

Carrasco-Núñez, G. and Rose, W.I. 1995. Eruption of a major Holocene pyroclastic flow at Citlaltépetl volcano (Pico de Orizaba), México, 8.5–9.0 ka. *Journal of Volcanology and Geothermal Research*, **69**, 197–215, https://doi.org/10.1016/0377-0273(95)00023-2

Carrasco-Núñez, G., Vallance, J.W. and Rose, W.I. 1993. A voluminous avalanche-induced lahar from Citlaltépetl volcano, Mexico: implications for hazard assessment. *Journal of Volcanology and Geothermal Research*, **59**, 35–46, https://doi.org/10.1016/0377-0273(93)90076-4

Cas, R.A.F. and Wright, J.V. 1987. *Volcanic Successions – Modern and Ancient*. Chapman and Hall, London.

Cas, R.A.F., Wright, H.M.N., Folkes, C.B., Lesti, C., Porreca, M., Giordano, G. and Viramonte, J.G. 2011. The flow dynamics of an extremely large volume pyroclastic flow, the 2.08-Ma Cerro Galán Ignimbrite, NW Argentina, and comparison with other flow types. *Bulletin of Volcanology*, **73**, 1583–1609, https://doi.org/10.1007/s00445-011-0564-y

Cecchi, E., van Wyk de Vries, B. and Lavest, J.-M. 2005. Flank spreading and collapse of weak-cored volcanoes. *Bulletin of Volcanology*, **67**, 72–91, https://doi.org/10.1007/s00445-004-0369-3

Chan, K.J. 2008. *Late Quaternary volcanically-influenced sedimentation in the Cowlitz River, Washington: implications for hazard mitigation*. MS Thesis, Washington State University, Pullman, Washington.

Charbonnier, S.J. and Gertisser, R. 2008. Field observations and surface characteristics of pristine block-and-ash flow deposits from the 2006 eruption of Merapi Volcano, Java, Indonesia. *Journal of Volcanology and Geothermal Research*, **177**, 971–982, https://doi.org/10.1016/j.jvolgeores.2008.07.008

Chesner, C.A. 2012. The Toba Caldera complex. *Quaternary International*, **258**, 5–18, https://doi.org/10.1016/j.quaint.2011.09.025

Chinen, T. 1986. Surface erosion associated with tephra deposition on Mt. Usu and other volcanoes. *Environmental Sciences Hokkaido*, **9**, 137–149.

Choux, C.M. and Druitt, T.H. 2002. Analogue study of particle segregation in pyroclastic density currents, with implications for the emplacement mechanisms of large ignimbrites. *Sedimentology*, **49**, 907–928, https://doi.org/10.1046/j.1365-3091.2002.00481.x

Christiansen, R.L. 2001. *The Quaternary and Pliocene Yellowstone Plateau Volcanic Field of Wyoming, Idaho, and Montana*. US Geological Survey Professional Paper **729-G**.

Cinque, A. and Robustelli, G. 2009. Alluvial and coastal hazards caused by long-range effects of Plinian eruptions: the case of the Lattari Mts. after the AD 79 eruption of Vesuvius. *Geological Society, London, Special Publications*, **322**, 155–171, https://doi.org/10.1144/SP322.7

Clark, R.H. 1977. Volcanic disasters in the Japanese Main Islands and New Zealand. *Journal of the Faculty of Science, Hokaido University, Series 4*, **17**, 541–552.

Clarke, A.B., Voight, B., Neri, A. and Macedonio, G. 2002. Transient dynamics of vulcanian explosions and column collapse. *Nature*, **415**, 897–901, https://doi.org/10.1038/415897a

Clavero, J.E., Sparks, R.S.J., Huppert, H.E. and Dade, W.B. 2002. Geological constraints on the emplacement mechanism of the Parinacota debris avalanche, northern Chile. *Bulletin of Volcanology*, **64**, 40–54, https://doi.org/10.1007/s00445-001-0183-0

Clynne, M.A., Calvert, A.T., Wolfe, E.W., Evarts, R.C., Fleck, R.J. and Lanphere, M.A. 2008. The Pleistocene eruptive history of Mount St. Helens, Washington, from 300 000 to 12 800 years before present. *In*: Sherrod, D.R., Scott, W.E. and Stauffer, P.H. (eds) *A Volcano Rekindled: The Renewed Eruption of Mount St. Helens, 2004–2006*. U.S Geological Survey Professional Paper, **1750**, 593–627.

Cole, P.D., Fernandez, E., Duarte, E. and Duncan, A.M. 2005. Explosive activity and generation mechanisms of pyroclastic flows at Arenal volcano, Costa Rica between 1987 and 2001. *Bulletin of Volcanology*, **67**, 695–716, https://doi.org/10.1007/s00445-004-0402-6

Collins, B.D. and Dunne, T. 1986. Erosion of tephra from the 1980 eruption of Mount St. Helens. *Geological Society of America Bulletin*, **97**, 896–905, https://doi.org/10.1130/0016-7606(1986)97<896:EOTFTE>2.0.CO;2

Collins, B.D. and Dunne, T. 2019. Thirty years of tephra erosion following the 1980 eruption of Mount St. Helens. *Earth Surface Processes and Landforms*, **44**, 2780–2793, https://doi.org/10.1002/esp.4707

Collot, J.-Y., Lewis, K., Lamarche, G. and Lallemand, S. 2001. The gigantic Ruatoria debris avalanche on the northern Hikurangi margin, New Zealand: result of

oblique seamount subduction. *Journal of Geophysical Research*, **106**, 19,271–19,297, https://doi.org/10.1029/2001JB900004

Coombs, M.L., Neal, C.A., Wessels, R.L. and McGimsey, R.G. 2006. Geothermal disruption of summit glaciers at Mount Spurr volcano, 2004–6: an unusual manifestation of volcanic unrest. *US Geological Professional Paper*, **1732-B**.

Cortés, A., Komorowski, J-C., Macías, J.L., Capra, L. and Layer, P.W. 2019. Late Pleistocene–Holocene debris avalanche deposits from Volcán de Colima, Mexico. *In*: Varley, N., Connor, C. and Komorowski, J.-C. (eds) *Volcán de Colima. Active Volcanoes of the World*. Springer, Berlin, 55–79.

Crandell, D.R. 1971. Postglacial lahars at Mount Rainier volcano, Washington. *US Geological Survey Professional Paper*, **677**.

Crandell, D.R. 1980. Recent eruptive history of Mount Hood, Oregon, and potential hazards from future eruptions. *US Geological Survey Bulletin*, **1492**.

Crandell, D.R. 1987. Deposits of pre-1980 pyroclastic flows and lahars from Mount St. Helens Volcano, Washington. *US Geological Survey Professional Paper*, **1444**.

Crandell, D.R. 1989. Gigantic debris avalanche of Pleistocene age from ancestral Mount Shasta Volcano, California, and debris-avalanche hazard zonation. *US Geological Survey Bulletin*, **1861**.

Crandell, D.R., Miller, C.D., Glicken, H.X., Christiansen, R.L. and Newhall, C.G. 1984. Catastrophic debris avalanche from ancestral Mount Shasta volcano, California. *Geology*, **12**, 143–146, https://doi.org/10.1130/0091-7613(1984)12<143:CDAFAM>2.0.CO;2

Crittenden, K.S. and Rodolfo, K.S. 2002. Bacolor town and Pinatubo volcano, Philippines: coping with recurrent lahar disaster. *In*: Torence, R. and Grattan, J. (eds) *Natural Disasters and Cultural Change*. Routledge, London, 43–65.

Cronin, S.J., Neall, V.E., Lecointre, J.A. and Palmer, A.S. 1996. Unusual 'snow slury' lahars from Ruapehu volcano, New Zealand, September 1995. *Geology*, **24**, 1107–1110, https://doi.org/10.1130/0091-7613(1996)024<1107:USSLFR>2.3.CO;2

Cronin, S.J., Hodgson, K.A., Neall, V.E., Palmer, A.S. and Lecointre, J.A. 1997*a*. 1995 Ruapehu lahars in relation to the late Holocene of Whangaehu River, New Zealand. *New Zealand Journal of Geology and Geophysics*, **40**, 507–520, https://doi.org/10.1080/00288306.1997.9514780

Cronin, S.J., Neall, V.E., Lecointre, J.A. and Palmer, A.S. 1997*b*. Changes in Whangaehu river lahar characteristics during the 1995 eruption sequence, Ruapehu volcano, New Zealand. *Journal of Volcanology and Geothermal Research*, **76**, 47–61, https://doi.org/10.1016/S0377-0273(96)00064-9

Cronin, S.J., Neall, V.E., Lecointre, J.A. and Palmer, A.S. 1999. Dynamic interactions between lahars and stream flow: a case study from Ruapehu volcano, New Zealand. *Geological Society of America Bulletin*, **111**, 28–38, https://doi.org/10.1130/0016-7606(1999)111<0028:DIBLAS>2.3.CO;2

Cutler, K.S., Watt, S.F.L. *et al*. 2022. Downward-propagating eruption following vent unloading implies no direct magmatic trigger for the 2018 lateral collapse of Anak Krakatau. *Earth and Planetary Science Letters*, **578**, 117332, https://doi.org/10.1016/j.epsl.2021.117332

Cutler, N.A., Streeter, R.T., Marple, J., Shotter, L.R., Yeoh, J.S. and Dugmore, A.J. 2018. Tephra transformations: variable preservation of tephra layers from two well-studied eruptions. *Bulletin of Volcanology*, **80**, 77, https://doi.org/10.1007/s00445-018-1251-z

Daag, A. and van Westen, C.J. 1996. Cartographic modelling of erosion in pyroclastic flow deposits of Mount Pinatubo, Philippines. *ITC Journal*, **2**, 110–124.

Dale, V.H., Delgado-Acevedo, J. and MacMahon, J. 2005. Effects of modern volcanic impacts on vegetation. *In*: Marti, J. and Ernst, G.G.J. (eds) *Volcanoes and the Environment*. Cambridge University Press, 227–249.

Darmawan, H., Yuliantoro, P., Suryanto, W., Rakhman, A. and Budi Santoso, A. 2020. Deformation and instability at Merapi dome identified by high resolution camera. *Earth and Environmental Science*, **500**, 012008, https://doi.org/10.1088/1755-1315/500/1/012008

Davies, D.K., Vessell, R.K., Miles, R.C., Foley, M.G. and Bonis, S.B. 1977. Fluvial transport and downstream sediment modifications in an active volcanic region. *In*: Miall, A.D. (ed.) *Fluvial Sedimentation*. Canadian Society of Petroleum Geologists Memoir 5. Calgary, Canada, 61–84.

Day, S.J. 1996. Hydrothermal pore fluid pressure and the stability of porous, permeable volcanoes. *Geological Society, London, Special Publications*, **110**, 77–93, https://doi.org/10.1144/GSL.SP.1996.110.01.06

Day, S., Llanes, P., Silver, E., Hoffman, G., Ward, S. and Driscoll, N. 2015. Submarine landslide deposits of the historical lateral collapse of Ritter Island, Papua New Guinea. *Marine and Petroleum Geology*, **67**, 419–438, https://doi.org/10.1016/j.marpetgeo.2015.05.017

de Bélizal, E., Lavigne, F. *et al*. 2013. Rain-triggered lahars following the 2010 eruption of Merapi volcano, Indonesia: a major risk. *Journal of Volcanology and Geothermal Research*, **261**, 330–347, https://doi.org/10.1016/j.jvolgeores.2013.01.010

Detienne, M., Delmelle, P., Guevara, A., Samaniego, P., Opfergelt, S. and Mothes, P.A. 2017. Contrasting origin of two clay-rich debris flows at Cayambe Volcanic Complex, Ecuador. *Bulletin of Volcanology*, **79**, 27, https://doi.org/10.1007/s00445-017-1111-2

Dibyosaputro, S., Dipayana, G.A., Nugraha, H., Pratiwi, K. and Valeda, H.P. 2015. Lahar at Kali Konto after the 2014 eruption of Kelud Volcano, East Java: impacts and risk. *Forum Geografi*, **29**, 59–72, https://doi.org/10.23917/forgeo.v29i1.793

Di Capua, A., De Rosa, R., Kereszturi, G., Rosi, M. and Watt, S.F.L. 2022. Volcaniclastic deposits and sequences: a unified terminology for application in modern and ancient environments. *Geological Society, London, Special Publications*, **520**, https://doi.org/10.1144/SP520-2021-201

Dinehart, R.L. 1998. Sediment transport at gaging stations near Mount St. Helens, Washington, 1980–90. Data collection and analysis. *US Geological Survey Professional Paper*, **1573**.

Dorava, J.M. and Meyer, D.F. 1994. Hydrologic hazards in the lower Drift River basin associated with the 1989–1990 eruptions of Redoubt Volcano, Alaska. *Journal of*

Volcanology and Geothermal Research, **62**, 387–407, https://doi.org/10.1016/0377-0273(94)90044-2

Douillet, G.A., Taisne, B., Tsang-Hin-Sun, È., Müller, S.K., Kueppers, U. and Dingwell, D.B. 2015. Syn-eruptive, soft-sediment deformation of deposits from dilute pyroclastic density current: triggers from granular shear, dynamic pore pressure, ballistic impacts and shock waves. *Solid Earth*, **6**, 553–572, https://doi.org/10.5194/se-6-553-2015

Doyle, E.E., Cronin, S.J. and Thouret, J.-C. 2011. Defining conditions for bulking and debulking in lahars. *Geological Society of America Bulletin*, **123**, 1234–1246, https://doi.org/10.1130/B30227.1

Druitt, T.H. 1998. Pyroclastic density currents. *Geological Society, London, Special Publications*, **145**, 145–182, https://doi.org/10.1144/GSL.SP.1996.145.01.08

Druitt, T.H. and Bacon, C.R. 1986. Lithic breccia and ignimbrite erupted during the collapse of Crater Lake caldera, Oregon. *Journal of Volcanology and Geothermal Research*, **29**, 1–32, https://doi.org/10.1016/0377-0273(86)90038-7

Dufek, J., Manga, M. and Patel, A. 2012. Granular disruption during explosive volcanic eruptions. *Nature Geoscience*, **5**, 561–564, https://doi.org/10.1038/ngeo1524

Dufek, J., Esposti Ongaro, T. and Roche, O. 2015. Pyroclastic density currents: processes and models. *In*: Sigurdsson, H., Houghton, B., Rymer, H., Stix, J. and McNutt, S. (eds) *The Encyclopedia of Volcanoes*. Academic Press, 617–629.

Dufresne, A., Siebert, L. and Bernard, B. 2021*a*. Distribution and geometric parameters of volcanic debris avalanche deposits. *In*: Roverato, M., Dufresne, A. and Procter, J. (eds) *Volcanic Debris Avalanches: from Collapse to Hazards*. Springer Nature, Switzerland, 75–90.

Dufresne, A., Zernack, A., Bernard, K., Thouret, J.-C. and Roverato, M. 2021*b*. Sedimentology of volcanic debris avalanche deposits. *In*: Roverato, M., Dufresne, A. and Procter, J. (eds) *Volcanic Debris Avalanches: from Collapse to Hazards*. Springer Nature, Switzerland, 175–210.

Elsworth, D. and Voight, B. 1996. Evaluation of volcano flank instability triggered by dyke intrusion. *Geological Society, London, Special Publications*, **110**, 45–53, https://doi.org/10.1144/GSL.SP.1996.110.01.03

Engel, M., Dotterweich, M. *et al*. 2021. Syn- and post-eruptive gully formation near the Laacher See volcano. *Earth Surface Processes and Landforms*, **46**, 1783–1796, https://doi.org/10.1002/esp.5119

Engwell, S.L., Sparks, R.S.J. and Aspinall, W.P. 2013. Quantifying uncertainties in the measurement of tephra fall thickness. *Journal of Applied Volcanology*, **2**, https://doi.org/10.1186/2191-5040-2-5

Eppler, D.B. 1987. The May 1915 eruptions of Lassen Peak, II: May 22 volcanic blast effects, sedimentology and stratigraphy of deposits, and characteristics of the blast cloud. *Journal of Volcanology and Geothermal Research*, **31**, 65–85, https://doi.org/10.1016/0377-0273(87)90006-0

Esposti Ongaro, T., Clarke, A.B., Voight, B., Neri, A. and Widiwijayanti, C. 2012. Multiphase flow dynamics of pyroclastic density currents during the May 18, 1980 lateral blast of Mount St. Helens. *Journal of Geophysical Research*, **117**, B06208, https://doi.org/10.1029/2011JB009081

Eychenne, J., Le Pennec, J.-L., Troncoso, L., Gouhier, M. and Nedelec, J.-M. 2012. Causes and consequences of bimodal grain-size distribution of tephra fall deposited during the August 2006 Tungurahua eruption (Ecuador). *Bulletin of Volcanology*, **74**, 187–205, https://doi.org/10.1007/s00445-011-0517-5

Fairchild, L.H. 1987. The importance of lahar initiation processes. *In*: Costa, J.E. and Wieczorek, G.F. (eds) *Debris Flows/Avalanches: Process, Recognition, and Mitigation*. Geological Society of America Reviews in Engineering Geology, **7**, 51–61.

Fairchild, L.H. and Wigmosta, M. 1983. Dynamic and volumetric characteristics of the 18 May 1980 lahars on the Toutle River, Washington. *Proceedings of the Symposium on Erosion Control in Volcanic Areas, Technical Memorandum*, 1908, 131–153. Public Works Research Institute, Tsukuba, Japan.

Favalli, M., Pareschi, M.T. and Zanchetta, G. 2006. Simulation of syn-eruptive floods in the circumvesuvian plain (southern Italy). *Bulletin of Volcanology*, **68**, 349–362, https://doi.org/10.1007/s00445-005-0011-z

Fierstein, J. and Nathenson, M. 1992. Another look at the calculation of fallout tephra volume. *Bulletin of Volcanology*, **54**, 156–167, https://doi.org/10.1007/BF00278005

Fisher, R.V. 1979. Models for pyroclastic surges and pyroclastic flows. *Journal of Volcanology and Geothermal Research*, **6**, 305–318, https://doi.org/10.1016/0377-0273(79)90008-8

Fisher, R.V. 1983. Flow transformations in sediment gravity flows. *Geology*, **11**, 273–274, https://doi.org/10.1130/0091-7613(1983)11<273:FTISGF>2.0.CO;2

Fisher, R.V. 1990. Transport and deposition of a pyroclastic surge across an area of high relief: the 18 May 1980 eruption of Mount St. Helens, Washington. *Geological Society of America Bulletin*, **102**, 1038–1054, https://doi.org/10.1130/0016-7606(1990)102<1038:TADOAP>2.3.CO;2

Fisher, R.V. 1995. Decoupling of pyroclastic currents: hazards assessments. *Journal of Volcanology and Geothermal Research*, **66**, 257–263, https://doi.org/10.1016/0377-0273(94)00075-R

Fisher, R.V. and Heiken, G. 1982. Mt. Pelée, Martinique: May 8 and 20, 1902, pyroclastic flows and surges. *Journal of Volcanology and Geothermal Research*, **13**, 339–371, https://doi.org/10.1016/0377-0273(82)90056-7

Fisher, R.V. and Heiken, G. 1990. Discussion of four papers in the Mount Pelée Special Issue (J. Volanol. Geotherm. Res., 38/1989: 1–213). *Journal of Volcanology and Geothermal Research*, **43**, 353–358, https://doi.org/10.1016/0377-0273(90)90061-J

Fisher, R.V. and Schmincke, H.-U. 1984. *Pyroclastic Rocks*. Springer-Verlag, Berlin.

Fisher, R.V. and Smith, G.A. (eds) 1991. *Sedimentation in Volcanic Settings*. SEPM Special Publication, 45.

Fisher, R.V., Glicken, H.X. and Hoblitt, R.P. 1987. May 18, 1980, Mount St. Helens deposits in South Coldwater Creek, Washington. *Journal of Geophysical Research*, **92**, 10,267–10,283, https://doi.org/10.1029/JB092iB10p10267

Fisher, R.V., Orsi, G., Ort, M. and Heiken, G. 1993. Mobility of a large-volume pyroclastic flow – emplacement of the Campanian ignimbrite, Italy. *Journal of Volcanology and Geothermal Research*, **56**, 205–220, https://doi.org/10.1016/0377-0273(93)90017-L

Folk, R.L. and Ward, W.C. 1957. Brazos River bar: a study in the significance of grain size parameters. *Journal of Sedimentary Petrology*, **27**, 3–26, https://doi.org/10.1306/74D70646-2B21-11D7-8648000102C1865D

Francis, P.W., Gardeweg, M., Ramirez, C.F. and Rothery, D.A. 1985. Catastrophic debris avalanche deposit of Socompa volcano, northern Chile. *Geology*, **13**, 600–603, https://doi.org/10.1130/0091-7613(1985)13<600:CDADOS>2.0.CO;2

Friele, P.A., Clague, J.J., Simpson, K. and Stasiuk, M. 2005. Impact of a Quaternary volcano on Holocene sedimentation in Lillooet River valley, British Columbia. *Sedimentary Geology*, **176**, 305–322, https://doi.org/10.1016/j.sedgeo.2005.01.011

Gallino, G.L. and Pierson, T.C. 1985. Polallie Creed debris flow and subsequent dam-break flood of 1980, East Fork Hood River Basin, Oregon. *US Geological Survey Water-Supply Paper*, **2273**.

Gardner, C.A., Neal, C.A., Waitt, R.B. and Janda, R.J. 1994. Proximal pyroclastic deposits from the 1989–1990 eruption of Redoubt Volcano, Alaska – Stratigraphy, distribution, and physical characteristics. *Journal of Volcanology and Geothermal Research*, **62**, 213–250, https://doi.org/10.1016/0377-0273(94)90035-3

George, D.L. and Iverson, R.M. 2014. A depth-averaged debris-flow model that includes the effects of evolving dilatancy. II. Numerical predictions and experimental tests. *Proceedings of the Royal Society A*, **470**, 20130820, https://doi.org/10.1098/rspa.2013.0820

George, D.L., Iverson, R.M. and Cannon, C.M. 2019. Seamless numerical simulation of a hazard cascade in which a landslide triggers a dam-breach flood and consequent debris flow. *In*: Kean, J., Coe, J.A., Santi, P.M. and Guillen, B.K. (eds) *Debris-flow Hazards Mitigation: Mechanics, Monitoring, Modeling, and Assessment*. Proceedings of 7th International Conference on Debris-Flow Hazards Mitigation, Golden, Colorado, 10–13 June 2019, 287–293, https://doi.org/10.25676/11124/173208

Geshi, N. and Itoh, J. 2018. Pyroclastic density currents associated with the 2015 phreatomagmatic eruption of the Kuchinoerabujima volcano. *Earth, Planets and Space*, **70**, 119, https://doi.org/10.1186/s40623-018-0881-x

Giachetti, T., Paris, R., Kelfoun, K. and Pérez-Torrado, F.J. 2011. Numerical modelling of the tsunami triggered by the Güìmar debris avalanche, Tenerife (Canary Islands): comparison with field-based data. *Marine Geology*, **284**, 189–202, https://doi.org/10.1016/j.margeo.2011.03.018

Gillies, J.K., Kennedy, B.M., Gravley, D.M., Leonard, G.S. and Cowlyn, J. 2020. Identifying pyroclastic density currents from partial outcrop exposure on Mt. Ruapehu, New Zealand. *Frontiers in Earth Sciences*, **8**, 542932, https://doi.org/10.3389/feart.2020.542932

Glicken, H. 1996. *Rockslide-debris avalanche of the May 18, 1980, Mount St. Helens volcano, Washington*. US Geological Survey Open-File Report **96-677**.

Gorshkov, G.S. 1959. Gigantic eruption of the volcano Bezymianny. *Bulletin Volcanologique*, **20**, 77–109, https://doi.org/10.1007/BF02596572

Gorshkov, G.S. 1963. Directed volcanic blasts. *Bulletin of Volcanology*, **26**, 83–88, https://doi.org/10.1007/BF02597277

Gorshkov, G.S. and Dubik, Y.M. 1970. Gigantic directed blast at Shiveluch volcano (Kamchatka). *Bulletin Volcanologique*, **34**, 261–288, https://doi.org/10.1007/BF02597790

Gran, K.B. 2012. Strong seasonality in sand loading and resulting feedbacks on sediment transport, bed texture, and channel planform at Mount Pinatubo, Philippines. *Earth Surface Processes and Landforms*, **37**, 1012–1022, https://doi.org/10.1002/esp.3241

Gran, K.B. and Montgomery, D.R. 2005. Spatial and temporal patterns in fluvial recovery following volcanic eruptions – channel response to basin-wide sediment loading at Mount Pinatubo, Philippines. *Geological Society of America Bulletin*, **117**, 195–211, https://doi.org/10.1130/B25528.1

Gran, K.B., Montgomery, D.R. and Halbur, J.C. 2011. Long-term elevated post-eruption sedimentation at Mount Pinatubo, Philippines. *Geology*, **39**, 367–370, https://doi.org/10.1130/G31682.1

Grilli, S.T., Tappin, D.R. *et al*. 2019. Modelling of the tsunami from the December 22, 2018 lateral collapse of Anak Krakatau volcano in the Sunda Straits, Indonesia. *Scientific Reports*, **9**, 11946, https://doi.org/10.1038/s41598-019-48327-6

Gudmundsson, M.T. 2015. Hazards from lahars and jökulhlaups. *In*: Sigurdsson, H., Houghton, B., Rymer, H., Stix, J. and McNutt, S. (eds) *The Encyclopedia of Volcanoes*. Academic Press, 971–984.

Gueugneau, V., Kelfoun, K., Charbonnier, S., Germa, A. and Carazzo, G. 2020. Dynamics and impacts of the May 8th, 1902 pyroclastic current at Mount Pelée (Martinique): new insights from numerical modeling. *Frontiers in Earth Science*, **8**, 279, https://doi.org/10.3389/feart.2020.00279

Guffanti, M. and Tupper, A. 2015. Volcanic ash hazards and aviation risks. *In*: Schroder, J.F. and Papale, P. (eds) *Volcanic Hazards, Risks and Disasters*. Elsevier, Amsterdam, 87–108.

Guffanti, M., Casadevall, T.J. and Budding, K. 2010. Encounters of aircraft with volcanic ash clouds – a compilation of known incidents, 1953–2009. *US Geological Survey Data Series*, **545**, http://pubs.er.usgs.gov/ds/545

Hall, M. and Mothes, P. 2008. The rhyolitic–andesitic eruptive history of Cotopaxi volcano, Ecuador. *Bulletin of Volcanology*, **70**, 675–702, https://doi.org/10.1007/s00445-007-0161-2

Hall, M.L., Steele, A.L., Mothes, P.A. and Ruiz, M.C. 2013. Pyroclastic density currents (PDC) of the 16–17 August 2006 eruptions of Tungurahua volcano, Ecuador: geophysical registry and characteristics. *Journal of Volcanology and Geothermal Research*, **265**, 78–93, https://doi.org/10.1016/j.jvolgeores.2013.08.011

Hardardóttir, J., Geirsdóttir, A. and Thordarson, T. 2001. Tephra layers in a sediment core from Lake Hestvatn, southern Iceland: implications for evaluating sedimentation processes and environmental impacts on a lacustrine system caused by tephra fall deposits in the

surrounding watershed. *International Association of Sedimentologists Special Publication*, **30**, 225–246.

Harnett, C.E., Thomas, M.E., Calder, E.S., Ebmeier, S.K., Telford, A., Murphy, W. and Neuberg, J. 2019. Presentation and analysis of a worldwide database for lava dome collapse events: the Global Archive of Dome Instabilities (GLADIS). *Bulletin of Volcanology*, **81**, 16, https://doi.org/10.1007/s00445-019-1276-y

Harris, A.J.L., Flynn, L.P., Matías, O. and Rose, W.I. 2002. The thermal stealth flows of Santiaguito dome, Guatemala: implicatons for the cooling and emplacement of dacite block-lava flows. *Geological Society of America Bulletin*, **114**, 533–546, https://doi.org/10.1130/0016-7606(2002)114<0533:TTSFOS>2.0.CO;2

Harris, A.J.L., Vallance, J.W. *et al*. 2006. Downstream aggradation owing to lava dome extrusion and rainfall runoff at Volcán Santiaguito, Guatemala. *Geological Society of America Special Paper*, **412**, 85–104.

Hausback, B.P. and Swanson, D.A. 1990. Record of prehistoric debris avalanches on the north flank of Mount St. Helens volcano, Washington. *Geoscience Canada*, **17**, 142–145.

Hayes, J.L., Calderón B, R. *et al*. 2019. Timber-framed building damage from tephra fall and lahar: 2015 Calbuco eruption, Chile. *Journal of Volcanology and Geothermal Research*, **374**, 142–159, https://doi.org/10.1016/j.jvolgeores.2019.02.017

Hildreth, W. and Fierstein, J. 2012. The Novarupta-Katmai eruption of 1912 – Largest eruption of the twentieth century: centennial perspectives. *US Geological Survey Professional Paper*, **1791**.

Hildreth, W. and Mahood, G.A. 1986. Ring-fracture eruption of the Bishop Tuff. *Geological Society of America Bulletin*, **97**, 396–403, https://doi.org/10.1130/0016-7606(1986)97<396:REOTBT>2.0.CO;2

Hoblitt, R.P. 1986. Observations of the eruptions of July 22 and August 7, 1980, at Mount St. Helens, Washington. *US Geological Survey Professional Paper*, **1335**.

Hoblitt, R.P. 2000. Was the 18 May 1980 lateral blast at Mt St Helens the product of two explosions? *Philosophical Transactions of the Royal Society of London*, **A358**, 1639–1661, https://doi.org/10.1098/rsta.2000.0608

Hoblitt, R.P., Miller, C.D. and Vallance, J.W. 1981. Origin and stratigraphy of the deposit produced by the May 18 directed blast. *US Geological Survey Professional Paper*, **1250**, 401–419.

Hoblitt, R.P., Wolfe, E.W., Scott, W.E., Couchman, M.R., Pallister, J.P. and Javier, D. 1996. The preclimactic eruptions of Mount Pinatubo, June 1991. *In*: Newhall, C.G. and Punongbayan, R.S. (eds) *Fire and Mud: Eruptions and Lahars of Mount Pinatubo, Philippines*. University of Washington Press, Seattle, 457–511.

Hodgson, K.A. and Manville, V.R. 1999. Sedimentology and flow behavior of a rain-triggered lahar, Mangatoetoenui Stream, Ruapehu volcano, New Zealand. *Geological Society of America Bulletin*, **111**, 743–754, https://doi.org/10.1130/0016-7606(1999)111<0743:SAFBOA>2.3.CO;2

Houghton, B and Carey, R.J. 2015. Pyroclastic fall deposits. *In*: Sigurdsson, H., Houghton, B., Rymer, H., Stix, J. and McNutt, S. (eds) *The Encyclopedia of Volcanoes*. Academic Press, 599–616.

Inbar, M., Enriquez, A.R. and Graniel, J.H.G. 2001. Morphological changes and erosion processes following the 1982 eruption of El Chichón volcano, Chiapas, Mexico. *Géomorphologie Relief Processus Environnement*, **3**, 175–184, https://doi.org/10.3406/morfo.2001.1100

Inman, D.L. 1952. Measures for describing the size distribution of sediments. *Journal of Sedimentary Petrology*, **22**, 125–145.

Iverson, R.M. and George, D.L. 2014. A depth-averaged debris-flow model that includes the effects of evolving dilatancy. I. Physical basis. *Proceedings of the Royal Society A*, **470**, 20130819, https://doi.org/10.1098/rspa.2013.0819

Janda, R.J., Scott, K.M., Nolan, K.M. and Martinson, H.A. 1981. Lahar movement, effects and deposits. *US Geological Survey Professional Paper*, **1250**, 461–478.

Janda, R.J., Meyer, D.F. and Childers, D. 1984. Sedimentation and geomorphic changes during and following the 1980–1983 eruptions of Mount St. Helens, Washington. *Shin Sabo*, **37**(2), 10–21 and **37**(3), 5–19.

Jensen, B.J.L., Davies, L.J. *et al*. 2021. A latest Pleistocene and Holocene composite tephrostratigraphic framework for northeastern North America. *Quaternary Science Reviews*, **272**, https://doi.org/10.1016/j.quascirev.2021.107242

Jensen, E.H., Helgason, J.K., Einarsson, S., Sverrisdottir, G., Höskuldsson, A. and Oddsson, B. 2013. Lahar, floods and debris flows resulting from the 2010 eruption of Eyjafjallajökull: observations, mapping and modelling. *In*: Margottini, C., Canuti, P. and Sassa, K. (eds) *Landslide Science and Practice*, **3**, 435–440.

Johnson, A.M. 1970. *Physical Processes in Geology*. Freeman Cooper.

Johnson, C.G., Kokelaar, B.P., Iverson, R.M., Logan, M., LaHusen, R.G. and Gray, J.M.N.T. 2012. Grain-size segregation and levee formation in geophysical mass flows. *Journal of Geophysical Research – Earth Surface*, **117**, F01032, https://doi.org/10.1029/2011JF 002185

Johnson, P.J., Valentine, G.A. *et al*. 2018. Groundwater drainage from fissures as a source for lahars. *Bulletin of Volcanology*, **80**, 39, https://doi.org/10.1007/s00445-018-1214-4

Johnson, R.W. 1987. Large-scale volcano cone collapse: the 1888 slope failure of Ritter volcano and other examples from Papua New Guinea. *Bulletin of Volcanology*, **49**, 669–679, https://doi.org/10.1007/BF01080358

Jones, R., Manville, V. and Andrade, D. 2015. Probabilistic analysis of rainfall-triggered lahar initiation at Tungurahua volcano. *Bulletin of Volcanology*, **77**, 68, https://doi.org/10.1007/s00445-015-0946-7

Jones, R., Thomas, R.E., Peakall, J. and Manville, V. 2017. Rainfall-runoff properties of tephra: simulated effects of grain-size and antecedent rainfall. *Geomorphology*, **282**, 39–51, https://doi.org/10.1016/j.geomorph.2016.12.023

Kadomura, H., Imagawa, T. and Yamamoto, H. 1983. Eruption-induced rapid erosion and mass movements on Usu Volcano, Hokkaido. *Zeitschrift für Geomorphologie Supplementary*, **46**, 123–142.

Kandlbauer, J. and Sparks, R.S.J. 2014. New estimates of the 1815 Tambora eruption volume. *Journal of Volcanology and Geothermal Research*, **286**, 93–100, https://doi.org/10.1016/j.jvolgeores.2014.08.020

Kaneko, T., Maeno, F. and Nakada, S. 2016. 2014 Mount Ontake eruption: characteristics of the phreatic eruption

as inferred from aerial obserations. *Earth, Planets and Space*, **68**, 72, https://doi.org/10.1186/s40623-016-0452-y

Kataoka, K. 2005. Distal fluvio-lacustrine volcaniclastic resedimentation in response to an explosive silicic eruption: the Pliocene Mushono tephra bed, central Japan. *Geological Society of America Bulletin*, **117**, 3–17, https://doi.org/10.1130/B25379.1

Kataoka, K.S., Manville, V., Nakajo, T. and Urabe, A. 2009. Impacts of explosive volcanism on distal alluvial sedimentation: examples from the Pliocene–Holocene volcaniclastic successions of Japan. *Sedimentary Geology*, **220**, 306–317, https://doi.org/10.1016/j.sedgeo.2009.04.016

Kataoka, K.S., Matsumoto, T. *et al*. 2018. Lahar characteristics as a function of triggering mechanism at a seasonally snow-clad volcano: contrasting lahars following the 2014 phreatic eruption of Ontake Volcano, Japan. *Earth, Planets and Space*, **70**, 113, https://doi.org/10.1186/s40623-018-0873-x

Katayama, N. 1974. Old records of natural phenomena concerning the Shimabara catastrophe. *Scientific Reports of the Shimabara Volcano Observatory, Faculty of Science Kyushu University*, **9**, 1–45.

Katsui, K. and Yamamoto, M. 1981. The 1741–1742 activity of Oshima-Ōshima Volcano, north Japan. *Journal of the Faculty of Science*, **19**, 527–536, Hokkaido University, Series 4.

Kelfoun, K., Druitt, T., van Wyk de Vries, B. and Guilbaud, M.-N. 2008. Topographic reflection of the Socompa debris avalanche, Chile. *Bulletin of Volcanology*, **70**, 1169–1187, https://doi.org/10.1007/s00445-008-0201-6

Komorowski, J.-C., Glicken, H.X. and Sheridan, M.F. 1991. Secondary electron imagery of microcracks and hackly fracture surfaces in sand-size clasts from the 1980 Mount St. Helens debris-avalanche deposit: implications for particle-particle interactions. *Geology*, **19**, 261–264, https://doi.org/10.1130/0091-7613(1991)019<0261:SEIOMA>2.3.CO;2

Komorowski, J.-C., Jenkins, S. *et al*. 2013. Paroxysmal dome explosion during the Merapi 2010 eruption: processes and facies relationships of associated high-energy pyroclastic density currents. *Journal of Volcanology and Geothermal Research*, **261**, 260–294, https://doi.org/10.1016/j.jvolgeores.2013.01.007

Korup, O., Seidemann, J. and Mohr, C.H. 2019. Increased landslide activity on forested hillslopes following two recent volcanic eruptions in Chile. *Nature Geoscience*, **12**, 284–289, https://doi.org/10.1038/s41561-019-0315-9

Kuehn, S.C. and Negrini, R.M. 2010. A 250 k.y. record of Cascade arc pyroclastic volcanism from late Pleistocene lacustrine sediments near Summer Lake, Oregon, USA. *Geosphere*, **6**, 397–429, https://doi.org/10.1130/GES00515.1

Kuenzi, W.D., Horst, O.H., and McGehee, R.V. 1979. Effect of volcanic activity on fluvial-deltaic sedimentation in a modern arc-trench gap, southwestern Guatemala. *Geological Society of America Bulletin*, **90**, 827–838, https://doi.org/10.1130/0016-7606(1979)90<827:EOVAOF>2.0.CO;2

LaCroix, A. 1904. *La Montagne Pelée et ses Éruptions*. Masson et Cie, Paris.

Lagmay, A.M.F., van Wyk de Vries, B., Kerle, N. and Pyle, D.M. 2000. Volcano instability induced by strike-slip faulting. *Bulletin of Volcanology*, **62**, 331–346, https://doi.org/10.1007/s004450000103

Lavigne, F. 2004. Rate of sediment yield following small-scale volcanic eruptions: a quantitative assessment at the Merapi and Semeru stratovolcanoes, Java, Indonesia. *Earth Surface Processes and Landforms*, **29**, 1045–1058, https://doi.org/10.1002/esp.1092

Lavigne, F. and Suwa, H. 2004. Contrasts between debris flows, hyperconcentrated flows and stream flows at a channel of Mount Semeru, East Java, Indonesia. *Geomorphology*, **61**, 41–58, https://doi.org/10.1016/j.geomorph.2003.11.005

Lavigne, F., Thouret, J.C., Voight, B., Suwa, H. and Sumaryono, A. 2000. Lahars at Merapi volcano, Central Java: an overview. *Journal of Volcanology and Geothermal Research*, **100**, 423–456, https://doi.org/10.1016/S0377-0273(00)00150-5

Leavesley, G.H., Lusby, G.C. and Lichty, R.W. 1989. Infiltration and erosion characteristics of selected tephra deposits from the 1980 eruption of Mount St. Helens, Washington, USA. *Hydrological Sciences Journal*, **34**, 339–353, https://doi.org/10.1080/02626668909491338

Lehre, A.K., Collins, B.D. and Dunne, T. 1983. Post-eruption sediment budget for the North Fork Toutle River drainage, June 1980–June 1981. *Zeitschrift für Geomorphologie, Supplementary*, **46**, 143–163.

Lipman, P.W. and Mullineaux, D.R. (eds) 1981. *The 1980 Eruptions of Mount St. Helens, Washington*. US Geological Survey Professional Paper, **1250**.

Lisle, T. 1995. Effects of coarse woody debris and its removal on a channel affected by the 1980 eruption of Mount St. Helens, Washington. *Water Resoures Research*, **31**, 1797–1808, https://doi.org/10.1029/95WR00734

Lisle, T.E., Cui, Y., Parker, G., Pizzuto, J.E. and Dodd, A.M. 2001. The dominance of dispersion in the evolution of bed material waves in gravel-bed rivers. *Earth Surface Processes and Landforms*, **26**, 1409–1420, https://doi.org/10.1002/esp.300

Lube, G., Breard, E.C.P., Esposti-Ongaro, T., Dufek, J. and Brand, B. 2020. Multiphase flow behaviour and hazard prediction of pyroclastic density currents. *Nature Reviews Earth & Environment*, **1**, 348–365, https://doi.org/10.1038/s43017-020-0064-8

MacPhail, D.D. 1973. The geomorphology of the Rio Teno lahar, Central Chile. *Geographical Review*, **63**, 517–532, https://doi.org/10.2307/213919

Maeno, F. and Taniguchi, H. 2007. Spatiotemporal evolution of a marine caldera-forming eruption, generating a low-aspect ratio pyroclastic flow, 7.3 ka, Kikai caldera, Japan: implication from near-vent eruptive deposits. *Journal of Volcanology and Geothermal Research*, **167**, 212–238, https://doi.org/10.1016/j.jvolgeores.2007.05.003

Maeno, F., Nakada, S. *et al*. 2016. Reconstruction of a phreatic eruption on 27 September 2014 at Ontake volcano, central Japan, based on proximal density current and fallout deposits. *Earth, Planets and Space*, **68**, 82, https://doi.org/10.1186/s40623-016-0449-6

Major, J.J. 1997. Depositional processes in large-scale debris-flow experiments. *Journal of Geology*, **105**, 345–366, https://doi.org/10.1086/515930

Major, J.J. 2004. Posteruption suspended sediment transport at Mount St. Helens: decadal-scale relationships with landscape adjustments and river discharges. *Journal of Geophysical Research – Earth Surface*, **109**, F01002, https://doi.org/10.1029/2002JF000010

Major, J.J. 2020. Mount St. Helens at 40. *Science (New York, NY)*, **368**, 704–705, https://doi.org/10.1126/science.abb4120

Major, J.J. and Lara, L.E. 2013. Overview of Chaitén Volcano, Chile and its 2008–2009 eruption. *Andean Geology*, **42**, 196–215, https://doi.org/10.5027/andgeoV40n2-a01

Major, J.J. and Mark, L.E. 2006. Peak flow responses to landscape disturbances caused by the cataclysmic 1980 eruption of Mount St. Helens, Washington. *Geological Society of America Bulletin*, **118**, 938–958, https://doi.org/10.1130/B25914.1

Major, J.J. and Newhall, C.G. 1989. Snow and ice perturbation during historical volcanic eruptions and the formation of lahars and floods. *Bulletin of Volcanology*, **52**, 1–27, https://doi.org/10.1007/BF00641384

Major, J.J. and Scott, K.M. 1988. Volcaniclastic sedimentation in the Lewis River valley, Mount St. Helens, Washington-processes, extent and hazards. *US Geological Survey Bulletin*, **1383-D**.

Major, J.J. and Yamakoshi, T. 2005. Decadal-scale change of infiltration characteristics of a tephra-mantled hillslope at Mount St. Helens, Washington. *Hydrological Processes*, **19**, 3621–3630, https://doi.org/10.1002/hyp.5863

Major, J.J., Pierson, T.C., Dinehart, R.L. and Costa, J.E. 2000. Sediment yield following severe volcanic disturbance – a two-decade perspective from Mount St. Helens. *Geology*, **28**, 819–822, https://doi.org/10.1130/0091-7613(2000)28<819:SYFSVD>2.0.CO;2

Major, J.J., Schilling, S.P., Pullinger, C.R. and Escobar, C.D. 2004. Debris-flow hazards at San Salvador, San Vicente and San Miguel volcanoes, El Salvador. *Geological Society of America Special Paper*, **375**, 89–108.

Major, J.J., Pierson, T.C., Hoblitt, R.P. and Moreno, H. 2013. Pyroclastic density currents associated with the 2008–2009 eruption of Chaitén volcano (Chile): forest disturbances, deposits and dynamics. *Andean Geology*, **40**, 324–358, https://doi.org/10.5027/andgeoV40n2-a09.

Major, J.J., Bertin, D., Pierson, T.C., Amigo, Á., Iroumé, A., Ulloa, H. and Castro, J. 2016. Extraordinary sediment delivery and rapid geomorphic response following the 2008–2009 eruption of Chaitén Volcano, Chile. *Water Resources Research*, **52**, 5075–5094, https://doi.org/10.1002/2015WR018250

Major, J.J., Mosbrucker, A.R. and Spicer, K.R. 2018. Sediment erosion and delivery from Toutle River basin after the 1980 eruption of Mount St. Helens – a 30-year perspective. *In*: Crisafulli, C.M. and Dale, V.H. (eds) *Ecological Responses at Mount St. Helens: Revisited 35 years After the 1980 Eruption*. Springer, New York, 19–44.

Major, J.J., Zheng, S., Mosbrucker, A.R., Spicer, K.R., Christianson, T. and Thorne, C.R. 2019. Multidecadal geomorphic evolution of a profoundly disturbed gravel bed river system – a complex, nonlinear response and its impact on sediment delivery. *Journal of Geophysical Research – Earth Surface*, **124**, 1281–1309, https://doi.org/10.1029/2018JF004843

Major, J.J., Crisafulli, C.M. and Swanson, F.J. 2020. Lessons from a post-eruption landscape. *Eos – Earth and Space Science News*, **101**, 34–40, https://doi.org/10.1029/2020EO143198

Major, J.J., Spicer, K.R. and Mosbrucker, A.R. 2021. Effective hydrological events in an evolving mid-latitude mountain river system following cataclysmic disturbance – a saga of multiple influences. *Water Resources Research*, **57**, e2019WR026851, https://doi.org/10.1029/2019WR026851

Manville, V. 2010. An overview of break-out floods from intracaldera lakes. *Global and Planetary Change*, **70**, 14–23, https://doi.org/10.1016/j.gloplacha.2009.11.004

Manville, V. and Wilson, C.J.N. 2004. The 26.5 ka Oruanui eruption, New Zealand: a review of the roles of volcanism and climate in the post-eruptive sedimentary response. *New Zealand Journal of Geology and Geophysics*, **47**, 525–547, https://doi.org/10.1080/00288306.2004.9515074

Manville, V., Hodgson, K.A. and Nairn, I.A. 2007. A review of break-out floods from volcanogenic lakes in New Zealand. *New Zealand Journal of Geology and Geophysics*, **50**, 131–150, https://doi.org/10.1080/00288300709509826

Manville, V., Németh, K. and Kano, K. 2009*a*. Source to sink: a review of three decades of progress in the understanding of volcaniclastic processes, deposits and hazards. *Sedimentary Geology*, **220**, 136–161, https://doi.org/10.1016/j.sedgeo.2009.04.022

Manville, V., Segschneider, B., Newton, E., White, J.D.L., Houghton, B.F. and Wilson, C.J.N. 2009*b*. Environmental impact of the 1.8 ka Taupo eruption, New Zealand: landscape responses to a large-scale explosive rhyolite eruption. *Sedimentary Geology*, **220**, 318–336, https://doi.org/10.1016/j.sedgeo.2009.04.017

Marti, A., Folch, A., Costa, A. and Engwell, S. 2016. Reconstructing the Plinian and co-ignimbrite sources of large volcanic eruptions: a novel approach for the Campanian Ignimbrite. *Scientific Reports*, **6**, 21220, https://doi.org/10.1038/srep21220

Massey, C.I., Manville, V., Hancox, G.H., Keys, H.J., Lawrence, C. and McSaveney, M. 2010. Out-burst flood (lahar) triggered by retrogressive landsliding, 18 March 2007 at Mt Ruapehu, New Zealand – a successful early warning. *Landslides*, **7**, 303–315, https://doi.org/10.1007/s10346-009-0180-5

McGuire, W.J. 1996. Volcano instability: a review of contemporary themes. *Geological Society, London, Special Publications*, **110**, 1–23, https://doi.org/10.1144/GSL.SP.1996.110.01.01

Meadows, T. 2014. *Forecasting long-term sediment yield from the upper North Fork Toutle River, Mount St. Helens, USA*. PhD thesis, University of Nottingham http://eprints.nottingham.ac.uk/27800/1/Thesis_FINAL_TM.pdf

Mellors, R.A., Waitt, R.B. and Swanson, D.A. 1988. Generation of pyroclastic flows and surges by hot-rock avalanches from the dome of Mount St. Helens volcano, USA. *Bulletin of Volcanology*, **50**, 14–25, https://doi.org/10.1007/BF01047505

Meyer, D.F. and Martinson, H.A. 1989. Rates and processes of channel development and recovery following

the 1980 eruption of Mount St. Helens, Washington. *Hydrological Sciences Journal*, **34**, 115–127, https://doi.org/10.1080/02626668909491318

Meyer, W., Sabol, M. and Schuster, R. 1986. Landslide dammed lakes at Mount St. Helens, Washington. *In*: Schuster, R.L. (ed.) *Landslide Dams – Processes, Risks and Mitigation*. American Society of Civil Engineers Geotechnical Special Publication, **3**, 21–41.

Miyabuchi, Y. 1999. Deposits associated with the 1990–1995 eruption of Unzen volcano, Japan. *Journal of Volcanology and Geothermal Research*, **89**, 139–158, https://doi.org/10.1016/S0377-0273(98)00129-2

Miyabuchi, Y., Maeno, F. and Nakada, S. 2015. The October 16, 2013 rainfall-induced landslides and associated lahars at Izu Oshima Volcano, Japan. *Journal of Volcanology and Geothermal Research*, **302**, 242–256, https://doi.org/10.1016/j.jvolgeores.2015.07.012

Miyabuchi, Y., Iizuka, Y., Hara, C., Yokoo, A. and Ohkura, T. 2018. The September 14, 2015 phreatomagmatic eruption of Nakadake first crater, Aso Volcano, Japan: eruption sequence inferred from ballistic pyroclastic density current and fallout deposits. *Journal of Volcanology and Geothermal Research*, **351**, 41–56, https://doi.org/10.1016/j.jvolgeores.2017.12.009

Moore, J.G. and Melson, W.G. 1969. Nuées ardentes of the 1968 eruption of Mayon Volcano, Philippines. *Bulletin Volcanologique*, **33**, 600–620, https://doi.org/10.1007/BF02596528

Moore, J.G. and Moore, G.W. 1984. Deposit from a giant wave on the island of Lanai, Hawaii. *Science (New York, NY)*, **226**, 1312–1315, https://doi.org/10.1126/science.226.4680.1312

Moreno, P.I., Alloway, B.V., Villarosa, G., Outes, V., Henríquez, W.I., De Pol-Holz, R. and Pearce, N.J.G. 2015. A past-millennium maximum in postglacial activity from Volcán Chaitén, southern Chile. *Geology*, **43**, 47–50, https://doi.org/10.1130/G36248.1

Mosbrucker, A.R., Spicer, K.R. and Major, J.J. 2019. North Fork Toutle River debris flows initiated by atmospheric rivers: November 2006. *SEDHYD Federal Interagency Sediment and Hydrology Conference*, 24–28 June, Reno, Nevada, https://www.sedhyd.org/2019/openconf/modules/request.php?module=oc_program&action=view.php&id=202&file=1/202.pdf

Mothes, P.A., Hall, M.L. and Janda, R.J. 1998. The enormous Chillos Valley Lahar: an ash-flow-generated debris flow from Cotopaxi Volcano, Ecuador. *Bulletin of Volcanology*, **59**, 233–244, https://doi.org/10.1007/s004450050188

Mullineaux, D.R. 1986. Summary of pre-1980 tephra-fall deposits erupted form Mount St. Helens, Washington State, USA. *Bulletin of Volcanology*, **48**, 17–26, https://doi.org/10.1007/BF01073510

Murai, I. 1960. On the mud-flows of the 1926 eruption of Volcano Tokachi-daké, Central Hokkaido, Japan. *University of Tokyo Bulletin of the Earthquake Research Institute*, **38**, 55–70.

Nairn, L.A. and Self, S. 1978. Explosive eruptions and pyroclastic avalanches from Ngauruhoe in February 1975. *Journal of Volcanology and Geothermal Research*, **3**, 39–60, https://doi.org/10.1016/0377-0273(78)90003-3

Naranjo, J.L., Sigurdsson, H., Carey, S.N. and Fritz, W. 1986. Eruption of the Nevado del Ruiz Volcano, Colombia, on 13 November 1985: tephra fall and lahars. *Science (New York, NY)*, **233**, 961–963, https://doi.org/10.1126/science.233.4767.961

Narcisi, B. and Petit, J.R. 2021. Englacial tephras of East Antarctica. *Geological Society, London, Memoirs*, **55**, 649–664, https://doi.org/10.1144/M55-2018-86

Németh, K. and Cronin, S.J. 2007. Syn- and post-eruptive erosion, gully formation and morphological evolution of a tephra ring in tropical climate erupted in 1913 in West Ambrym, Vanuatu. *Geomorphology*, **86**, 115–130, https://doi.org/10.1016/j.geomorph.2006.08.016

Neri, A., Di Muro, A. and Rosi, M. 2002. Mass partitioning during collapsing and transitional columns by using numerical simulations. *Journal of Volcanology and Geothermal Research*, **115**, 1–18, https://doi.org/10.1016/S0377-0273(01)00304-3

Neri, A., Esposti Ongaro, T., Menconi, G., De'Michieli Vitturi, M., Cavazzoni, C., Erbacci, G. and Baxter, P.J. 2007. 4D simulation of explosive eruption dynamics at Vesuvius. *Geophysical Research Letters*, **34**, L04309, https://doi.org/10.1029/2006GL028597

Neri, A., Esposti Ongaro, T., de' Michieli Vitturi, M. and Cerminara, M. 2022. Multiphase flow modeling of explosive volcanic eruptions. *In*: Arastoopour, H., Gidaspow, D. and Lyczkowski, R.W. (eds) *Transport Phenomena in Multiphase Systems*. Springer, https://doi.org/10.1007/978-3-030-68578-2_10

Newhall, C.G. and Punongbayan, R.S. (eds) 1996. *Fire and Mud: Eruptions and Lahars of Mount Pinatubo, Philippines*. University of Washington Press, Seattle.

Ogawa, Y., Daimaru, H. and Shimizu, A. 2007. Experimental study of post-eruption overland flow and sediment load from slopes overlain by pyroclastic-flow deposits, Unzen volcano, Japan. *Géomorphologie: Relief, Processus, Environnement*, **13**, 237–246, https://doi.org/10.4000/geomorphologie.3962

Pagneaux, E., Gudmundsson, M.T., Karlsdóttir, S. and Roberts, M.J. (eds) 2015. *Volcanogenic Floods in Iceland: An Assessment of Hazards and Risks at Öræfajökull and on the Markarfljót Outwash Plain*. Icelandic Meteorological Office, Institute of Earth Sciences – University of Iceland, National Commissioner of Icelandic Police – Department of Civil Protection and Emergency Management, Reykjavik.

Paguican, E.M.R., Lagmay, A.M.F. *et al*. 2009. Extreme rainfall-induced lahars and dike breaching, 30 November 2006, Mayon Volcano, Philippines. *Bulletin of Volcanology*, **71**, 845–857, https://doi.org/10.1007/s00445-009-0268-8

Paguican, E.M.R., van Wyk de Vries, B. and Lagmay, A.M.F. 2012. Volcano-tectonic controls and emplacement kinematics of the Iriga debris avalanches (Philippines). *Bulletin of Volcanology*, **74**, 2067–2081, https://doi.org/10.1007/s00445-012-0652-7

Paguican, E.M.R., van Wyk de Vries, B. and Lagmay, A. 2014. Hummocks: how they form and how they evolve in rockslide-debris avalanches. *Landslides*, **11**, 67–80, https://doi.org/10.1007/s10346-012-0368-y

Paladio-Melosantos, M.L.O., Solidum, R.U. *et al*. 1996. Tephra falls of the 1991 eruptions of Mount Pinatubo. *In*: Newhall, C.G. and Punongbayan, R.S. (eds) *Fire and Mud: Eruptions and Lahars of Mount Pinatubo, Philippines*. University of Washington Press, Seattle, 513–535.

Pallister, J.S., Diefenbach, A.K. *et al*. 2013. The Chaitén rhyolite lava dome: Eruption sequence, lava dome volumes, rapid effusion rates and source of the rhyolite magma. *Andean Geology*, **42**, 277–294, https://doi.org/10.5027/andgeoV40n2-a06

Pallister, J., Wessels, R. *et al*. 2019. Monitoring, forecasting collapse events, and mapping pyroclastic deposits at Sinabung volcano with satellite imagery. *Journal of Volcanology and Geothermal Research*, **382**, 149–163, https://doi.org/10.1016/j.jvolgeores.2018.05.012

Palmer, B.A. and Neall, V.E. 1989. The Murimotu Formation – 9500 year old deposits of a debris avalanche and associated lahars, Mount Ruapehu, North Island, New Zealand. *New Zealand Journal of Geology and Geophysics*, **32**, 477–486, https://doi.org/10.1080/00288306.1989.10427555

Pareschi, M.T., Boschi, E., Mazzarini, F. and Favalli, M. 2006. Large submarine landslides offshore Mt. Etna. *Geophysical Research Letters*, **33**, L13302, https://doi.org/10.1029/2006GL026064

Paris, R. 2015. Source mechanisms of volcanic tsunamis. *Philosophical Transactions of the Royal Society of London*, **A373**, 20140380, https://doi.org/10.1098/rsta.2014.0380

Paris, R., Switzer, A.D., Belousova, M., Belousov, A., Ontowirjo, B., Whelley, P. and Ulvrova, M. 2014. Volcanic tsunami: a review of source mechanisms, past events and hazards in Southeast Asia (Indonesia, Philippines, Papua New Guinea). *Natural Hazards*, **70**, 447–470, https://doi.org/10.1007/s11069-013-0822-8

Perrotta, A., Scarpati, C. and Luongo, G. 2006. Volcaniclastic resedimentation on the northern slope of Vesuvius as a direct response to eruptive activity. *Landslides*, **3**, 295–301, https://doi.org/10.1007/s10346-006-0057-9

Perttu, A., Caudron, C. *et al*. 2020. Reconstruction of the 2018 tsunamigenic flank collapse and eruptive activity at Anak Krakatau based on eyewitness reports, seismo-acoustic and satellite observations. *Earth and Planetary Science Letters*, **541**, 116268, https://doi.org/10.1016/j.epsl.2020.116268

Pierson, T.C. 1985. Initiation and flow behavior of the 1980 Pine Creek and Muddy River lahars, Mount St. Helens, Washington. *Geological Society of America Bulletin*, **96**, 1056–1069, https://doi.org/10.1130/0016-7606(1985)96<1056:IAFBOT>2.0.CO;2

Pierson, T.C. 1999. Transformation of water flood to debris flow following the eruption-triggered transient-lake breakout from the crater on March 19, 1982. *US Geological Survey Professional Paper*, **1586**, 19–36.

Pierson, T.C. 2005. Hyperconcentrated flow – transitional process between water flow and debris flow. *In*: Jakob, M. and Hungr, O. (eds) *Debris-flow Hazards and Related Phenomena*. Springer-Praxis, Berlin, 159–202.

Pierson, T.C. and Major, J.J. 2014. Hydrogeomorphic effects of explosive volcanic eruptions on drainage basins. *Annual Review of Earth and Planetary Sciences*, **42**, 469–507, https://doi.org/10.1146/annurev-earth-060313-054913

Pierson, T.C. and Scott, K.M. 1985. Downstream dilution of a lahar: transition from debris flow to hyperconcentrated streamflow. *Water Resources Research*, **21**, 1511–1524, https://doi.org/10.1029/WR021i010p0 1511

Pierson, T.C., Janda, R.J., Thouret, J.-C. and Borrero, C.A. 1990. Perturbation and melting of snow and ice by the 13 November 1985 eruption of Nevado del Ruiz, Colombia, and consequent mobilization, flow and deposition of lahars. *Journal of Volcanology and Geothermal Research*, **41**, 17–66, https://doi.org/10.1016/0377-0273(90)90082-Q

Pierson, T.C., Janda, R.J., Umbal, J.V. and Daag, A.S. 1992. *Immediate and long-term hazards from lahars and excess sedimentation in rivers draining Mt. Pinatubo, Philippines*. US Geological Survey Water-Resources Investigation Report **92-4039**.

Pierson, T.C., Daag, A.S., Delos Reyes, P.J., Regelado, M.T.M., Solidum, R.U. and Tubianosa, B.S. 1996. Flow and deposition of posteruption hot lahars on the east side of Mount Pinatubo, July–October 1991. *In*: Newhall, C.G. and Punongbayan, R.S. (eds) *Fire and Mud: Eruptions and Lahars of Mount Pinatubo, Philippines*. University of Washington Press, Seattle, 921–950.

Pierson, T.C., Pringle, P.T. and Cameron, K.A. 2011. Magnitude and timing of downstream channel aggradation and degradation in response to a dome-building eruption at Mount Hood, Oregon. *Geological Society of America Bulletin*, **123**, 3–20, https://doi.org/10.1130/B30127.1

Pierson, T.C., Major, J.J., Amigo, Á. and Moreno, H. 2013. Acute sedimentation response to rainfall following the explosive phase of the 2008–2009 eruption of Chaitén volcano, Chile. *Bulletin of Volcanology*, **75**, 723, https://doi.org/10.1007/s00445-013-0723-4

Pinel, V. and Albino, F. 2013. Consequences of volcano sector collapse on magmatic storage zones: insights from numerical modeling. *Journal of Volcanology and Geothermal Research*, **252**, 29–37, https://doi.org/10.1016/j.jvolgeores.2012.11.009

Procter, J., Cronin, S.J., Fuller, I.C., Lube, G. and Manville, V. 2010. Quantifying the geomorphic impacts of a lake-breakout lahar, Mount Ruapehu, New Zealand. *Geology*, **38**, 67–70, https://doi.org/10.1130/G30129.1

Pulgarín, B., Capra, L., Macías, J.L. and Cepeda, H. 2001. Depósitos de flujos de escombros gigantes (10 km^3) asociados a colapsos de edificios volcánicos: los casos de los volcanoes Nevado del Huila (Colombia) y Nevado de Colima (México). *Revista Geofisica*, **55**, 51–76.

Pulgarín, B., Cardona, C. *et al*. 2015. Erupciones recientes del Volcán Nevado del Huila: lahares asociados y cambios morfológicos del glaciar. *Boletin Geológico*, **43**, 75–87, https://doi.org/10.32685/0120-1425/boletingeo.43.2015.31

Punongbayan, R.S., Newhall, C.G. and Hoblitt, R.P. 1996. Photographic record of rapid geomorphic change at Mount Pinatubo, 1991–94. *In*: Newhall, C.G. and Punongbayan, R.S. (eds) *Fire and Mud: Eruptions and Lahars of Mount Pinatubo, Philippines*. University of Washington Press, Seattle, 21–66.

Pyle, D.M. 1989. The thickness, volume and grainsize of tephra fall deposits. *Bulletin of Volcanology*, **51**, 1–15, https://doi.org/10.1007/BF01086757

Rader, E., Geist, D., Geissman, J., Dufek, J. and Harpp, K. 2015. Hot clasts and cold blasts: thermal heterogeneity in boiling-over pyroclastic density currents. *Geological*

Society, London, Special Publications, **396**, 67–86, https://doi.org/10.1144/SP396.16

Reid, L.M. and Lewis, J. 2009. Rates, timing and mechanisms of rainfall interception loss in a coastal redwood forest. *Journal of Hydrology*, **375**, 459–470, https://doi.org/10.1016/j.jhydrol.2009.06.048

Reid, M.E. 2004. Massive collapse of volcano edifices triggered by hydrothermal pressurization. *Geology*, **32**, 373–376, https://doi.org/10.1130/G20300.1

Reid, M.E., Sisson, T.W. and Brien, D.L. 2001. Volcano collapse promoted by hydrothermal alteration and edifice shape, Mount Rainier, Washington. *Geology*, **29**, 779–782, https://doi.org/10.1130/0091-7613(2001)029<0779:VCPBHA>2.0.CO;2

Reid, M.E., Keith, T.E.C., Kayen, R.E., Iverson, N.R., Iverson, R.M. and Brien, D.L. 2010. Volcano collapse promoted by progressive strength reduction: new data from Mount St. Helens. *Bulletin of Volcanology*, **72**, 761–766, https://doi.org/10.1007/s00445-010-0377-4

Reyes-Dávila, G.A., Arámbula-Mendoza, R. *et al*. 2016. Volcán de Colima dome collapse of July, 2015 and associated pyroclastic density currents. *Journal of Volcanology and Geothermal Research*, **320**, 100–106, https://doi.org/10.1016/j.jvolgeores.2016.04.015

Richardson, D. 1968. Glacier outburst floods in the Pacific Northwest. *US Geological Survey Professional Paper*, **600D**, D79–D86.

Ritchie, L.J., Cole, P.D. and Sparks, R.S.J. 2002. Sedimentology of deposits from the pyroclastic density current of 26 December 1997 at Soufrière Hills Volcano, Montserrat. *Geological Society, London, Memoirs*, **21**, 435–456, https://doi.org/10.1144/GSL.MEM.2002.021.01.19

Roberti, G., Ward, B., van Wyk de Vries, B., Friele, P., Perotti, L., Clague, J.J. and Giardino, M. 2018. Precursory slope distress prior to the 2010 Mount Meager landslide, British Columbia. *Landslides*, **15**, 637–647, https://doi.org/10.1007/s10346-017-0901-0

Robinson, J.E., Bacon, C.R., Major, J.J., Wright, H.M. and Vallance, J.W. 2017. Surface morphology of caldera-forming eruption deposits revealed by lidar mapping of Crater Lake National Park, Oregon – implications for deposition and surface modification. *Journal of Volcanology and Geothermal Research*, **342**, 61–78, https://doi.org/10.1016/j.jvolgeores.2017.02.012

Robock, A. 2000. Volcanic eruptions and climate. *Reviews of Geophysics*, **38**, 191–219, https://doi.org/10.1029/1998RG000054

Roche, O., Buesch, D.C. and Valentine, G.A. 2016. Slow-moving and far-travelled dense pyroclastic flows during the Peach Spring super-eruption. *Nature Communications*, **7**, 10890, https://doi.org/10.1038/ncomms10890

Roche, O., Azzaoui, N. and Guillin, A. 2021. Discharge rate of explosive volcanic eruption controls runout distance of pyroclastic density currents. *Earth and Planetary Science Letters*, **568**, 117017, https://doi.org/10.1016/j.epsl.2021.117017

Rodolfo, K.S. 1989. Origin and early evolution of lahar channel at Mabinit, Mayon Volcano, Philippines. *Geological Society of America Bulletin*, **101**, 414–426, https://doi.org/10.1130/0016-7606(1989)101<0414:OAEEOL>2.3.CO;2

Rodolfo, K.S. and Arguden, A.T. 1991. Rain-lahar generation and sediment-delivery systems at Mayon Volcano, Philippines. *SEPM Special Publication*, **45**, 71–87.

Rodolfo, K.S. and Umbal, J.V. 2008. A prehistoric lahar-dammed lake and eruption of Mount Pinatubo described in a Philippine aborigine legend. *Journal of Volcanology and Geothermal Research*, **176**, 432–437, https://doi.org/10.1016/j.jvolgeores.2008.01.030

Romero, J.E., Moreno, H., Polacci, M., Burton, M. and Guzmán, D. 2022. Mid-Holocene lateral collapse of Antuco volcano (Chile): debris avalanche deposit features, emplacement dynamics and impacts. *Landslides*, **19**, 1321–1338, https://doi.org/10.1007/s10346-022-01865-z

Rose, W.I., Pearson, T. and Bonis, S. 1976. Nuée ardente eruption from the foot of a dacite lava flow, Santiaguito Volcano, Guatemala. *Bulletin Volcanologique*, **40**, 23–38, https://doi.org/10.1007/BF02599827

Roverato, M., Capra, L., Sulpizio, R. and Norini, G. 2011. Stratigraphic reconstruction of two debris avalanche deposits at Colima Volcano (Mexico): insights into pre-failure conditions and climate influence. *Journal of Volcanology and Geothermal Research*, **207**, 33–46, https://doi.org/10.1016/j.jvolgeores.2011.07.003

Roverato, M., Dufresne, A. and Procter, J. (eds) 2021. *Volcanic Debris Avalanches: from Collapse to Hazards*. Springer Nature, Switzerland.

Sasaki, H., Chiba, T., Kishimoto, H. and Naruke, S. 2016. Characteristics of the syneruptive-spouted type lahar generated by the September 2014 eruption of Mount Ontake, Japan. *Earth, Planets and Space*, **68**, 141, https://doi.org/10.1186/s40623-016-0516-z

Sassa, K., Dang, K., Yanagisawa, H. and He, B. 2016. A new landslide-induced tsunami simulation model and its application to the 1792 Unzen-Mayuyama landslide-and-tsunami disaster. *Landslides*, **13**, 1405–1419, https://doi.org/10.1007/s10346-016-0691-9

Satake, K. and Kato, Y. 2001. The 1741 Oshima-Oshima eruption: extent and volume of submarine debris avalanche. *Geophysical Research Letters*, **28**, 427–430, https://doi.org/10.1029/2000GL012175

Sato, H., Fujii, T. and Nakada, S. 1992. Crumbling of dacite dome lava and generation of pyroclastic flows at Unzen volcano. *Nature*, **360**, 664–666, https://doi.org/10.1038/360664a0

Saucedo, R., Macías, J.L., Bursik, M.I., Mora, J.C., Gavilanes, J.C. and Cortes, A. 2002. Emplacement of pyroclastic flows during the 1998–1999 eruption of Volcán de Colima, Mexico. *Journal of Volcanology and Geothermal Research*, **117**, 129–153, https://doi.org/10.1016/S0377-0273(02)00241-X

Schuster, R.L. 1983. Engineering aspects of the 1980 Mount St. Helens eruptions. *Bulletin of the Association of Engineering Geologists*, **20**, 125–143.

Scott, D.N. and Collins, B.D. 2021. Frequent mass movements from glacial and lahar terraces, controlled by both hillslope characteristics and fluvial erosion, are an important sediment source to Puget Sound rivers. *Water Resources Research*, **57**, e2020WR028389, https://doi.org/10.1029/2020WR028389

Scott, K.M. 1988*a*. Origins, behavior and sedimentology of lahars and lahar-runout flows in the Toutle-Cowlitz River system. *US Geological Survey Professional Paper*, **1447A**.

Scott, K.M. 1988*b*. Origin, behavior and sedimentology of prehistoric lahars at Mount St. Helens, Washington.

Geological Society of America Special Paper, **229**, 23–36.

Scott, K.M. 1989. Magnitude and frequency of lahars and lahar-runout flows in the Toutle-Cowlitz River system. *US Geological Survey Professional Paper*, **1447B**.

Scott, K.M., Vallance, J.W. and Pringle, P.P. 1995. Sedimentology, behavior and hazards of debris flows at Mount Rainier, Washington. *US Geological Survey Professional Paper*, **1547**.

Scott, K.M., Macías, J.L., Naranjo, J.A., Rodríguez, S. and McGeehin, J.P. 2001. Catastrophic debris flows transformed from landslides in volcanic terrains: mobility, hazard assessment and mitigation strategies. *US Geological Survey Professional Paper*, **1630**.

Scott, K.M., Vallance, J.W., Kerle, N., Macías, J.L., Strauch, W. and Devoli, G. 2005. Catastrophic precipitation-triggered lahar at Casita volcano, Nicaragua: occurrence, bulking and transformation. *Earth Surface Processes and Landforms*, **30**, 59–79, https://doi.org/10.1002/esp.1127

Scott, W.E. and McGimsey, R.G. 1994. Character, mass, distribution and origin of tephra-fall deposits of the 1989–1990 eruption of Redoubt Volcano, south-central Alaska. *Journal of Volcanology and Geothermal Research*, **62**, 251–272, https://doi.org/10.1016/0377-0273(94)90036-1

Scott, W.E., Hoblitt, R.P., Torres, R.C., Self, S., Martinez, M.M.L. and Nillos, T., Jr. 1996. Pyroclastic flows of the June 15, 1991, climactic eruption of Mount Pinatubo. *In*: Newhall, C.G. and Punongbayan, R.S. (eds) *Fire and Mud: Eruptions and Lahars of Mount Pinatubo, Philippines*. University of Washington Press, Seattle, 545–570.

Segerstrom, K. 1950. Erosion studies at Parícutin, State of Michoacan, Mexico. *US Geological Survey Bulletin*, **965-A**, 1–164.

Sekiya and Kikuchi 1889. The eruption of Bandai-san. *Tokyo Imperial University Collection of Science Journals*, **3**, 91–172.

Self, S. 1992. Krakatau revisited: the course of events and interpretation of the 1883 eruption. *GeoJournal*, **28**, 109–121, https://doi.org/10.1007/BF00177223

Self, S., Kienle, J. and Huot, J.-P. 1980. Ukinrek Maars, Alaska, II. Deposits and formation of the 1977 craters. *Journal of Volcanology and Geothermal Research*, **7**, 39–65, https://doi.org/10.1016/0377-0273(80)90019-0

Self, S., Rampino, M.R., Newton, M.S. and Wolff, J.A. 1984. Volcanological study of the great Tambora eruption of 1815. *Geology*, **12**, 659–663, https://doi.org/10.1130/0091-7613(1984)12<659:VSOTGT>2.0.CO;2

Shea, T., van Wyk de Vries, B. and Pilato, M. 2008. Emplacement mechanisms of contrasting debris avalanches at Volcán Mombacho (Nicaragua), provided by structural and facies analysis. *Bulletin of Volcanology*, **70**, 899–921, https://doi.org/10.1007/s00445-007-0177-7

Shea, T., Gurioli, L., Houghton, B.F., Cioni, R. and Cashman, K.V. 2011. Column collapse and generation of pyroclastic density currents during the A.D. 79 eruption of Vesuvius: the role of pyroclast density. *Geology*, **39**, 695–698, https://doi.org/10.1130/G32092.1

Shimokawa, E., Jitousono, T., Yazawa, A. and Kawagoe, R. 1989. An effect of tephra cover on erosion processes of hillslopes in and around Sakurajima Volcano. *Proceedings of the International Symposium on Erosion and Volcanic Debris Flow Technology*, July 31–August 3, Yogyakarta, Indonesia. Ministry of Public Works, Yogyakarta, Indonesia, V32-1–V32-35.

Shimokawa, E., Jitousono, T. and Tsuchiya, S. 1996. Sediment yield from the 1984 pyroclastic flow deposit covered hillslopes in Merapi volcano, Indonesia. *Journal of the Japanese Society of Erosion Control Engineering*, **48**, 101–107.

Siebe, C., Komorowski, J.-C. and Sheridan, M.F. 1992. Morphology and emplacement of an unusual debris-avalanche deposit at Jocotitlán volcano, Central Mexico. *Bulletin of Volcanology*, **54**, 573–589, https://doi.org/10.1007/BF00569941

Siebert, L. 1984. Large volcanic debris avalanches: characteristics of source areas, deposits and associated eruptions. *Journal of Volcanology and Geothermal Research*, **22**, 163–197, https://doi.org/10.1016/0377-0273(84)90002-7

Siebert, L. 1996. Hazards of large volcanic debris avalanches and associated eruptive phenomena. *In*: Scarpa, R. and Tilling, R.I. (eds) *Monitoring and Mitigation of Volcano Hazards*. Springer, Berlin, 541–572.

Siebert, L. and Roverato, M. 2021. A historical perspective on lateral collapse and volcanic debris avalanches. *In*: Roverato, M., Dufresne, A. and Procter, J. (eds) *Volcanic Debris Avalanches: from Collapse to Hazards*. Springer Nature, Switzerland, 11–50.

Siebert, L., Glicken, H. and Ui, T. 1987. Volcanic hazards from Bezymianny- and Bandai-type eruptions. *Bulletin of Volcanology*, **49**, 435–459, https://doi.org/10.1007/BF01046635

Siebert, L., Begét, J.E. and Glicken, H. 1995. The 1883 and late-prehistoric eruptions of Augustine volcano, Alaska. *Journal of Volcanology and Geothermal Research*, **66**, 367–395, https://doi.org/10.1016/0377-0273(94)00069-S

Sigurdsson, H. and Carey, S. 1989. Plinian and co-ignimbrite tephra fall form the 1815 eruption of Tambora volcano. *Bulletin of Volcanology*, **51**, 243–270, https://doi.org/10.1007/BF01073515

Sigurdsson, H., Carey, S.N. and Espindola, J.M. 1984. The 1982 eruptions of El Chichón volcano, Mexico: stratigraphy of pyroclastic deposits. *Journal of Volcanology and Geothermal Research*, **23**, 11–37, https://doi.org/10.1016/0377-0273(84)90055-6

Sigurdsson, H., Carey, S., Cornell, W. and Pescatore, T. 1985. The eruption of Vesuvius in A.D. 79. *National Geographic Research*, **1**, 332–387.

Simon, A. 1999. *Channel and drainage-basin response of the Toutle River system in the aftermath of the 1980 eruption of Mount St. Helens, Washington*. US Geological Survey Open-File Report **96-633**.

Simon, A. and Thorne, C.R. 1996. Channel adjustments of an unstable coarse-grained stream: opposing trends of boundary and critical shear stress and the applicability of extremal hypotheses. *Earth Surface Processes and Landforms*, **21**, 155–180, https://doi.org/10.1002/(SICI)1096-9837(199602)21:2<155::AID-ESP610>3.0.CO;2-5

Smith, D.M., Oommen, T., Bownman, L.J., Gierke, J.S. and Vitton, S.J. 2015. Hazard assessment of rainfall-induced landslides: a case study of San Vicente volcano in central El Salvador. *Natural Hazards*, **75**, 2291–2310, https://doi.org/10.1007/s11069-014-1422-y

Smith, G.A. 1987. The influence of explosive volcanism on fluvial sedimentation: the Deschutes Formation (Neogene) in central Oregon. *Journal of Sedimentary Petrology*, **57**, 613–629, https://doi.org/10.1306/212F8BBB-2B24-11D7-8648000102C1865D

Smith, G.A. 1991. Facies sequences and geometries in continental volcaniclastic sediments. *SEPM Special Publication*, **45**, 109–121.

Smith, G.A. and Fritz, W.J. 1989. Volcanic influences on terrestrial sedimentation. *Geology*, **17**, 375–376, https://doi.org/10.1130/0091-7613(1989)017<0375:VIOTS>2.3.CO;2

Smith, G.A. and Katzman, D. 1991. Discrimination of eolian and pyroclastic-surge processes in the generation of cross-bedded tuffs, Jemez Mountains volcanic field, New Mexico. *Geology*, **19**, 465–468, https://doi.org/10.1130/0091-7613(1991)019<0465:DOEAPS>2.3.CO;2

Smith, R.D. and Swanson, F.J. 1987. Sediment routing in a small drainage basin in the blast zone at Mount St. Helens, Washington, U.S.A. *Geomorphology*, **1**, 1–13, https://doi.org/10.1016/0169-555X(87)90003-1

Smith, R.L. 1960. Ash flows. *Geological Society of America Bulletin*, **71**, 795–841, https://doi.org/10.1130/0016-7606(1960)71[795:AF]2.0.CO;2

Sohn, C. and Sohn, Y.K. 2019. Distinguishing between primary and secondary volcaniclastic deposits. *Scientific Reports*, **91**, 12425, https://doi.org/10.1038/s41598-019-48933-4

Sohn, Y.K., Ki, J.S., Jung, S., Kim, M.-C., Cho, H. and Son, M. 2013. Synvolcanic and syntectonic sedimentation of the mixed volcaniclastic-epiclastic succession in the Miocene Janggi Basin, SE Korea. *Sedimentary Geology*, **288**, 40–59, https://doi.org/10.1016/j.sedgeo.2013.01.002

Sorem, R.K. 1982. Volcanic ash clusters: tephra rafts and scavengers. *Journal of Volcanology and Geothermal Research*, **13**, 63–71, https://doi.org/10.1016/0377-0273(82)90019-1

Sparks, R.S.J. and Wilson, L. 1976. A model for the formation of ignimbrite by gravitational column collapse. *Journal of the Geological Society of London*, **132**, 441–451, https://doi.org/10.1144/gsjgs.132.4.0441

Sparks, R.S.J., Moore, J.G. and Rice, C.J. 1986. The initial umbrella cloud of the May 18th, 1980, explosive eruption of Mount St. Helens. *Journal of Volcanology and Geothermal Research*, **28**, 257–274, https://doi.org/10.1016/0377-0273(86)90026-0

Sparks, R.S.J., Bursik, M.I., Ablay, G.J., Thomas, R.M.E. and Carey, S.N. 1992. Sedimentation of tephra by volcanic plumes. Part 2: controls on thickness and grain-size variations of tephra fall deposits. *Bulletin of Volcanology*, **54**, 685–695, https://doi.org/10.1007/BF00430779

Sparks, R.S.J., Barclay, J. *et al*. 2002. Generation of a debris avalanche and violent pyroclastic density current on 26 December (Boxing Day) 1997 at Soufrière Hills Volcano, Montserrat. *Geological Society, London, Memoirs*, **21**, 409–434, https://doi.org/10.1144/GSL.MEM.2002.021.01.18

Stoopes, G.R. and Sheridan, M.F. 1992. Giant debris avalanches from the Colima Volcanic Complex, Mexico: implications for long-runout landslides (>100 km) and hazard assessment. *Geology*, **20**, 299–302, https://doi.org/10.1130/0091-7613(1992)020<0299:GDAFTC>2.3.CO;2

Sulpizio, R., Mele, D., Dellino, P. and La Volpe, L. 2007. Deposits and physical properties of pyroclastic density currents during complex Subplinian eruptions: the AD 472 (Pollena) eruption of Somma-Vesuvius, Italy. *Sedimentology*, **54**, 607–635, https://doi.org/10.1111/j.1365-3091.2006.00852.x

Sulpizio, R., Dellino, P., Doronzo, D.M. and Sarocchi, D. 2014. Pyroclastic density currents: state of the art and perspectives. *Journal of Volcanology and Geothermal Research*, **283**, 36–65, https://doi.org/10.1016/j.jvolgeores.2014.06.014

Suryo, I. and Clarke, M.C.G. 1985. The occurrence and mitigation of volcanic hazards in Indonesia as exemplified at the Mount Merapi, Mount Kelut and Mount Galunggung volcanoes. *Quarterly Journal of Engineering Geology and Hydrogeology*, **18**, 79–98, https://doi.org/10.1144/GSL.QJEG.1985.018.01.09

Suwa, H. and Yamakoshi, T. 1999. Sediment discharge by storm runoff at volcanic torrents affected by eruption. *Zeitschrift für Geomorphologie Supplementary*, **114**, 63–88.

Swanson, F.J. and Major, J.J. 2005. Physical events, environments and geological-ecological interactions at Mount St. Helens: March 1980–2004. *In*: Dale, V.H., Swanson, F.J. and Crisafulli, C.M. (eds) *Ecological Responses to the 1980 Eruption of Mount St. Helens*. Springer, New York, 27–44.

Swanson, F.J., Collins, B.D., Dunne, T. and Wicherski, B.P. 1983. Erosion of tephra from hillslopes near Mount St. Helens and other volcanoes. *Proceedings of Symposium on Erosion Control Volcanic Areas*, July 6–9, 1982, Seattle and Vancouver, Wash, 183–221. Public Works Research Institute Technical Memorandum 1908. Tsukuba, Japan.

Swanson, F.J., Jones, J.A., Crisafulli, C.M. and Lara, A. 2013. Effects of volcanic and hydrologic processes on forest vegetation: Chaitén volcano, Chile. *Andean Geology*, **42**, 359–391, https://doi.org/10.5027/andgeoV40n2-a10

Swanson, F.J., Jones, J., Crisafulli, C., González, M.E. and Lara, A. 2016. Puyehue-Cordón Caulle eruption of 2011: tephra fall and initial forest responses in the Chilean Andes. *Bosque*, **37**, 85–96, https://doi.org/10.4067/S0717-92002016000100009

Taddeucci, J., Scarlato, P. *et al*. 2011. Aggregation-dominated ash settling from the Eyjafjallajökull volcanic cloud illuminated by field and laboratory high-speed imaging. *Geology*, **39**, 891–894, https://doi.org/10.1130/G32016.1

Takarada, S. and Hoshizumi, H. 2020. Distribution and eruptive volume of Aso-4 pyroclastic density current and tephra fall deposits, Japan: a M8 super-eruption. *Frontiers in Earth Science*, **8**, 170, https://doi.org/10.3389/feart.2020.00170

Takeshita, K. 1987. Influence of the change in soil infiltration due to large-scale tephra cover on erosional

processes of mountains. *Transactions Japanese Geomorphological Union*, **8**, 227–248 (in Japanese, with English abstr.).

Tanarro, L.M., Andrés, N., Zamorano, J.J., Palacios, D. and Renschler, C.S. 2010. Geomorphological evolution of a fluvial channel after primary lahar deposition: Huiloac Gorge, Popocatépetl volcano (Mexico). *Geomorphology*, **122**, 178–190, https://doi.org/10.1016/j.geomorph.2010.06.013

Tarasenko, I., Bielders, C.L., Guevara, A. and Delmelle, P. 2019. Surface crusting of volcanic ash deposits under simulated rainfall. *Bulletin of Volcanology*, **81**, 30, https://doi.org/10.1007/s00445-019-1289-6

Taylor, G.A.M. 1958. The 1951 eruption of Mount Lamington, Papua. *Australia Bureau of Mineral Resources Bulletin*, **38**, 1–117.

Teramoto, Y., Shimokawa, E. and Jitousono, T. 2006. Effects of volcanic ash on the runoff process in Sakurajima volcano. *Proceedings INTERPRAEVENT International Symposium*, 26 September, Nigata, Japan. Universal Academy Press, Tokyo, 303–310.

Thouret, J.-C., Abdurachman, K.E., Bourdier, J.-L. and Bronto, S. 1998. Origin, characteristics and behavior of lahars following the 1990 eruption of Kelud volcano, eastern Java (Indonesia). *Bulletin of Volcanology*, **59**, 460–480, https://doi.org/10.1007/s004450050204

Thouret, J.-C., Gupta, A., Lube, G., Chin Liew, S., Cronin, S.J. and Surono 2010. The 2006 pyroclastic deposits of Merapi Volcano, Java, Indonesia: high-spatial resolution IKONOS images and complimentary ground based observations. *Remote Sensing of Environment*, **114**, 1949–1967, https://doi.org/10.1016/j.rse.2010.03.016

Thouret, J.-C., Antoine, S., Magill, C. and Ollier, C. 2020. Lahars and debris flows: characteristics and impacts. *Earth-Science Reviews*, **201**, 103003, https://doi.org/10.1016/j.earscirev.2019.103003

Tibaldi, A. 2001. Multiple sector collapses at Stromboli volcano, Italy: how they work. *Bulletin of Volcanology*, **63**, 112–125, https://doi.org/10.1007/s00445010 0129

Tinti, S., Chiocci, F.L., Zaniboni, F., Pagnoni, G. and de Alteriis, G. 2011. Numerical simulation of the tsunami generated by a past catastrophic landslide on the volcanic island of Ischia, Italy. *Marine Geophysical Research*, **32**, 287–297, https://doi.org/10.1007/s11001-010-9109-6

Todesco, M. and Todini, E. 2004. Volcanic eruption induced floods. A rainfall-runoff model applied to the Vesuvian region (Italy). *Natural Hazards*, **33**, 223–245, https://doi.org/10.1023/B:NHAZ.0000037039.35228.c0

Tost, M., Cronin, S.J., Procter, J.N., Smith, I.E.M., Neall, V.E. and Price, R.C. 2015. Impacts of catastrophic volcanic collapse on the erosion and morphology of a distal fluvial landscape: Hautapu River, Mount Ruapehu, New Zealand. *Geological Society of America Bulletin*, **127**, 266–280, https://doi.org/10.1130/B31010.1

Tsuji, Y. and Hino, T. 1993. Damage and inundation height of the 1792 Shimabara landslide tsunami along the coast of Kumamoto Prefecture. *University of Tokyo Bulletin of the Earthquake Research Institute*, **68**, 91–176.

Tsunetaka, H., Shinohara, Y., Hotta, N., Gomez, C. and Sakai, Y. 2021. Multi-decadal changes in the relationships between rainfall characteristics and debris-flow occurrences in response to gully evolution after the 1990–1995 Mount Unzen eruptions. *Earth Surface Processes and Landforms*, **46**, 2141–2162, https://doi.org/10.1002/esp.5148

Ui, T. 1983. Volcanic dry avalanche deposits – identification and comparison with nonvolcanic debris stream deposits. *Journal of Volcanology and Geothermal Research*, **18**, 135–150, https://doi.org/10.1016/0377-0273(83)90006-9

Ulloa, H., Picco, L., Iroumé, A., Mao, L. and Gallo, C. 2014. Analysis of channel morphology and large wood characteristics through remote images in the Blanco River after the eruption of the Chaitén Volcano (Southern Chile). *In*: Lollino, G., Arattano, M., Rinaldi, M., Giustolisi, O., Marechal, J.C. and Grant, G. (eds) *Engineering Geology for Society and Territory*. Springer, **3**, 365–368.

Ulloa, H., Iroumé, A., Mao, L., Andreoli, A., Diez, S. and Lara, L.E. 2015. Use of remote imagery to analyse changes in morphology and longitudinal large wood distribution in the Blanco River after the 2008 Chaitén volcanic eruption, Southern Chile. *Geografiska Annaler, Series A, Physical Geography*, **97**, 523–541, https://doi.org/10.1111/geoa.12091

Ulloa, H., Iroumé, A., Picco, L., Mohr, C.H., Mazzorana, B., Lenzi, M.A. and Mao, L. 2016. Spatial analysis of the impacts of the Chaitén volcano eruption (Chile) in three fluvial systems. *Journal of South American Earth Sciences*, **69**, 213–225, https://doi.org/10.1016/j.jsames.2016.04.008

Umazano, A.M. and Melchor, R.N. 2020. Volcaniclastic sedimentation influenced by logjam breakups? An example from the Blanco River, Chile. *Journal of South American Earth Sciences*, **98**, 102477, https://doi.org/10.1016/j.jsames.2019.102477

Umazano, A.M., Melchor, R.N., Bedatou, E., Bellosi, E.S. and Krause, J.M. 2014. Fluvial response to sudden input of pyroclastic sediments during the 2008–2009 eruption of the Chaitén Volcano (Chile): the role of logjams. *Journal of South American Earth Sciences*, **54**, 140–157, https://doi.org/10.1016/j.jsames.2014.04.007

Umbal, J.V. 1997. Five years of lahars at Pinatubo volcano: declining but still potentially lethal hazards. *Journal of the Geological Society of the Philippines*, **52**, 1–19.

Umbal, J.V. and Rodolfo, K.S. 1996. The 1991 lahars of southwestern Mount Pinatubo and evolution of the lahar-dammed Mapanuepe Lake. *In*: Newhall, C.G. and Punongbayan, R.S. (eds) *Fire and Mud: Eruptions and Lahars of Mount Pinatubo, Philippines*. University of Washington Press, Seattle, 951–970.

Valentine, G.A. and Cole, M.A. 2021. Explosive caldera-forming eruptions and debris-filled vents: gargle dynamics. *Geology*, **49**, 1240–1244, https://doi.org/10.1130/G48995.1

Valentine, G.A., Fierstein, J. and White, J.D.L. 2021. Soft-sediment deformation in dry pyroclastic deposits at Ubehebe Crater, Death Valley, California. *Geology*, **49**, 211–215, https://doi.org/10.1130/G48147.1

Vallance, J.W. 2005. Volcanic debris flows. *In*: Jakob, M. and Hungr, O. (eds) *Debris-flow Hazards and Related Phenomena*. Springer-Praxis, Berlin, 247–274.

Vallance, J.W. and Iverson, R.M. 2015. Lahars and their deposits. *In*: Sigurdsson, H., Houghton, B., Rymer,

H., Stix, J. and McNutt, S. (eds) *The Encyclopedia of Volcanoes*. Academic Press, 649–664.

Vallance, J.W. and Scott, K.M. 1997. The Osceola Mudflow from Mount Rainier: sedimentology and hazard implications of a huge clay-rich debris flow. *Geological Society of America Bulletin*, **109**, 143–163, https://doi.org/10.1130/0016-7606(1997)109<0143:TOMFMR>2.3.CO;2

Vallance, J.W., Driedger, C.L. and Scott, W.E. 2002. Diversion of meltwater from Kautz Glacier initiates small debris flows near Van Trump Park, Mount Rainier, Washington. *Washington Geology*, **30**, 17–19.

Vallance, J.W., Bull, K.F. and Coombs, M.L. 2010. Pyroclastic flows, lahars and mixed avalanches generated during the 2006 eruption of Augustine Volcano. *US Geological Survey Professional Paper*, **1769**, 219–267.

Van Eaton, A.R., Mastin, L.G., Herzog, M., Schwaiger, H.F., Schneider, D.J., Wallace, K.L. and Clarke, A.B. 2015. Hail formation triggers rapid ash aggregation in volcanic plumes. *Nature Communications*, **6**, 7860, https://doi.org/10.1038/ncomms8860

Van Wyk de Vries, B. and Davies, T. 2015. Landslides, debris avalanches and volcanic gravitational deformation. *In*: Sigurdsson, H., Houghton, B., Rymer, H., Stix, J. and McNutt, S. (eds) *The Encyclopedia of Volcanoes*. Academic Press, 665–685.

Van Wyk de Vries, B. and Francis, P.W. 1997. Catastrophic collapse at stratovolcanoes induced by gradual volcano spreading. *Nature*, **387**, 387–390, https://doi.org/10.1038/387387a0

Van Wyk de Vries, B., Self, S., Francis, P.W. and Keszthelyi, L. 2001. A gravitational spreading origin for the Socompa debris avalanche. *Journal of Volcanology and Geothermal Research*, **105**, 225–247, https://doi.org/10.1016/S0377-0273(00)00252-3

Vázquez, R., Capra, L., Caballero, L., Arámbula-Mendoza, R. and Reyes-Dávila, G. 2014. The anatomy of a lahar: deciphering the 15th September 2012 lahar at Volcán de Colima, Mexico. *Journal of Volcanology and Geothermal Research*, **272**, 126–136, https://doi.org/10.1016/j.jvolgeores.2013.11.013

Vessell, R.K. and Davies, D.K. 1981. Nonmarine sedimentation in an active fore arc basin. *SEPM Special Publication*, **31**, 31–45.

Voight, B. 1981. Time scale for the first moments of the May 18 eruption. *US Geological Survey Professional Paper*, **1250**, 69–86.

Voight, B. and Elsworth, D. 1997. Failure of volcano slopes. *Géotechnique*, **47**, 1–31, https://doi.org/10.1680/geot.1997.47.1.1

Voight, B. and Elsworth, D. 2000. Instability and collapse of hazardous gas-pressurized lava domes. *Geophysical Research Letters*, **27**, 1–4, https://doi.org/10.1029/1999GL008389

Voight, B., Glicken, H., Janda, R.J. and Douglass, P.M. 1981. Catastrophic rockslide avalanche of May 18. *US Geological Survey Professional Paper*, **1250**, 347–377.

Voight, B., Janda, R.J., Glicken, H. and Douglass, P.M. 1983. Nature and mechanics of the Mount St. Helens rockslide-avalanche of 18 May 1980. *Géotechnique*, **33**, 243–273, https://doi.org/10.1680/geot.1983.33.3.243

Voight, B., Constantine, E.K., Siswowidjoyo, S. and Torely, R. 2000*a*. Historical eruptions of Merapi Volcano, Central Java, Indonesia, 1768–1998. *Journal of Volcanology and Geothermal Research*, **100**, 69–138, https://doi.org/10.1016/S0377-0273(00)00134-7

Voight, B., Young, K.D. *et al*. 2000*b*. Deformation and seismic precursors to dome-collapse and fountain-collapse nuées ardentes at Merapi Volcano, Java, Indonesia, 1994–1998. *Journal of Volcanology and Geothermal Research*, **100**, 261–287, https://doi.org/10.1016/S0377-0273(00)00140-2

Voight, B., Komorowski, J.-C. *et al*. 2002. The 26 December (Boxing Day) 1997 sector collapse and debris avalanche at Soufrière Hills Volcano, Montserrat. *Geological Society, London, Memoirs*, **21**, 363–407, https://doi.org/10.1144/GSL.MEM.2002.021.01.17

Wadge, G., Francis, P.W. and Ramirez, C.F. 1995. The Socompa collapse and avalanche event. *Journal of Volcanology and Geothermal Research*, **66**, 309–336, https://doi.org/10.1016/0377-0273(94)00083-S

Waitt, R.B. 1981. Devastating pyroclastic density flow and attendant air fall of May 18: stratigraphy and sedimentology of deposits. *US Geological Survey Professional Paper*, **1250**, 439–458.

Waitt, R.B. 2015. *In the Path of Destruction – Eyewitness Chronicles of Mount St. Helens*. Washington State University Press, Pullman, Washington.

Waitt, R.B. and Begét, J.E. 2009. Volcanic processes and geology of Augustine Volcano, Alaska. *US Geological Survey Professional Paper*, **1762**.

Waitt, R.B., Pierson, T.C., MacLeod, N.S., Janda, R.J., Voight, B. and Holcomb, R.T. 1983. Eruption-triggered avalanche, flood, and lahar at Mount St. Helens – effects of winter snowpack. *Science (New York, NY)*, **221**, 1394–1397, https://doi.org/10.1126/science.221.4618.1394

Walder, J.S. and Driedger, C.L. 1994. Rapid geomorphic change caused by glacial outburst floods and debris flows along Tahoma Creek, Mount Rainier, Washington, U.S.A. *Arctic and Alpine Research*, **26**, 319–327, https://doi.org/10.2307/1551792

Walder, J.S. and Driedger, C.L. 1995. Frequent outburst floods from South Tahoma Glacier, Mount Rainier, USA – relation to debris flows, meteorological origin and implications for subglacial hydrology. *Journal of Glaciology*, **41**, 1–10, https://doi.org/10.1017/S0022143000017718

Waldron, H.H. 1967. Debris flow and erosion control problems caused by the ash eruptions of Irazú Volcano, Costa Rica. *US Geological Survey Bulletin*, **1241-I**.

Walker, G.P.L. 1971. Grain-size characteristics of pyroclastic deposits. *Journal of Geology*, **79**, 696–714, https://doi.org/10.1086/627699

Walker, G.P.L. 1973. Explosive volcanic eruptions – a new classification scheme. *Geologische Rundschau*, **62**, 431–446, https://doi.org/10.1007/BF01840108

Ward, S.N. and Day, S. 2003. Ritter Island Volcano – lateral collapse and the tsunami of 1888. *Geophysical Journal International*, **154**, 891–902, https://doi.org/10.1046/j.1365-246X.2003.02016.x

Watson, E.J., Swindles, G.T., Lawson, I.T. and Savov, I.P. 2016. Do peatlands or lakes provide the comprehensive distal tephra records?. *Quaternary Science Reviews*, **139**, 110–128, https://doi.org/10.1016/j.quascirev.2016.03.011

Watt, S.F.L. 2019. The evolution of volcanic systems following sector collapse. *Journal of Volcanology and*

Geothermal Research, **384**, 280–303, https://doi.org/10.1016/j.jvolgeores.2019.05.012

Watt, S.F.L., Gilbert, J.S., Folch, A., Phillips, J.C. and Cai, X.M. 2015. An example of enhanced tephra deposition driven by topographically induced atmospheric turbulence. *Bulletin of Volcanology*, **77**, 35, https://doi.org/10.1007/s00445-015-0927-x

Waythomas, C.F. 2001. Formation and failure of volcanic debris dams in the Chakachatna River valley associated with eruptions of the Spurr volcanic complex, Alaska. *Geomorphology*, **39**, 111–129, https://doi.org/10.1016/S0169-555X(00)00097-0

Waythomas, C.F. 2014. Water, ice, and mud: lahars and lahar hazards at ice- and snow-clad volcanoes. *Geology Today*, **30**, 34–39, https://doi.org/10.1111/gto.12035

Waythomas, C.F. 2015. Geomorphic consequences of volcanic eruptions in Alaska: a review. *Geomorphology*, **246**, 123–145, https://doi.org/10.1016/j.geomorph.2015.06.004

Waythomas, C.F., Scott, W.E. and Nye, J.C. 2010. The geomorphology of an Aleutian volcano following a major eruption: the 7–8 August 2008 eruption of Kasatochi Volcano, Alaska, and its aftermath. *Arctic, Antarctic and Alpine Research*, **42**, 260–275, https://doi.org/10.1657/1938-4246-42.3.260

Waythomas, C.F., Pierson, T.C., Major, J.J. and Scott, W.E. 2013. Voluminous ice-rich and water-rich lahars generated during the 2008 eruption of Redoubt Volcano, Alaska. *Journal of Volcanology and Geothermal Research*, **259**, 389–413, https://doi.org/10.1016/j.jvolgeores.2012.05.012

Wentworth, C.K. 1922. A scale of grade and class terms for clastic sediments. *Journal of Geology*, **30**, 377–392, https://doi.org/10.1086/622910

White, J.D.L. and Houghton, B.F. 2006. Primary volcaniclastic rocks. *Geology* , **34**, 677–680, https://doi.org/10.1130/G22346.1

White, J.D.L. and Riggs, N.R. (eds) 2001. *Volcaniclastic Sedimentation in Lacustrine Settings*. International Association of Sedimentologists Special Publication 30. Blackwell Science, Oxford.

White, J.D.L., Houghton, B.F., Hodgson, K.A. and Wilson, C.J.N. 1997. Delayed sedimentary response to the A.D. 1886 eruption of Tarawera, New Zealand. *Geology*, **25**, 459–462, https://doi.org/10.1130/0091-7613(1997)025<0459:DSRTTA>2.3.CO;2

Wilcox, A.C., O'Connor, J.E. and Major, J.J. 2014. Rapid reservoir erosion, hyperconcentrated flow, and downstream deposition triggered by breaching of 38 m tall Condit Dam, White Salmon River, Washington. *Journal of Geophysical Research – Earth Surface*, **119**, 1376–1394, https://doi.org/10.1002/2013JF003073

Wilson, C.J.N. 1985. The Taupo eruption, New Zealand II. The Taupo ignimbrite. *Philosophical Transactions of the Royal Society of London A*, **314**, 229–310, https://doi.org/10.1098/rsta.1985.0020

Wilson, C.J.N. 1986. Pyroclastic flows and ignimbrites. *Science Progress*, **70**, 171–207.

Wilson, C.J.N. 2001. The 26.5 ka Oruanui eruption, New Zealand: an introduction and overview. *Journal of Volcanology and Geothermal Research*, **112**, 133–174, https://doi.org/10.1016/S0377-0273(01)00239-6

Wilson, C.J.N. and Hildreth, W. 1997. The Bishop Tuff: New insights from eruptive stratigraphy. *The Journal of Geology*, **105**, 407–439, https://doi.org/10.1086/515937

Wilson, L., Sparks, R.S.J. and Walker, G.P.L. 1980. Explosive volcanic eruptions – IV. The control of magma properties and conduit geometry on eruption column behaviour. *Geophysical Journal of the Royal Astronomical Society*, **63**, 117–148, https://doi.org/10.1111/j.1365-246X.1980.tb02613.x

Wolf, T. 1878. Geognostische Mitteilungen aus Ecuador: Der Cotopaxi und seine letzte Eruption am 26 Juni 1877. *Neues Jahrbuch für Mineralogie, Geologie, Paleontologie*, 113–167.

Woods, A.W., Sparks, R.S.J., Ritchie, L.J., Batey, J., Gladstone, C. and Bursik, M.I. 2002. The explosive decompression of a pressurized volcanic dome: the 26 December 1997 collapse and explosion of Soufrière Hills Volcano, Montserrat. *Geological Society, London, Memoirs*, **21**, 457–465, https://doi.org/10.1144/GSL.MEM.2002.021.01.20

Worni, R., Huggel, C., Stoffel, M. and Pulgarín, B. 2012. Challenges of modeling current very large lahars at Nevado del Huila Volcano, Colombia. *Bulletin of Volcanology*, **74**, 309–324, https://doi.org/10.1007/s00445-011-0522-8

Wright, H.M.N., Lesti, C., Cas, R.A.F., Porreca, M., Viramonte, J.G., Folkes, C.B. and Giordano, G. 2011. Columnar jointing in vapor-phase-altered, non-welded Cerro Galán ignimbrite, Paycuqui Argentina. *Bulletin of Volcanology*, **73**, 1567–1582, https://doi.org/10.1007/s00445-011-0524-6

Yamakoshi, T. and Suwa, H. 2000. Post-eruption characteristics of surface runoff and sediment discharge on the slopes of pyroclastic-flow deposits, Mount Unzen, Japan. *Transactions Japanese Geomorphological Union*, **21**, 469–497.

Yamakoshi, T., Ishida, T., Nakano, M. and Yamada, T. 2002. Characteristics of sediment movement phenomena caused by rainfall after the 2000 eruption of Usu volcano. *Proceedings of INTERPRAEVENT 2002 Pacific Rim International Congress*, October 14–18, Matsumoto, Japan, **1**, 145–151.

Yamakoshi, T., Doi, Y. and Osanai, N. 2005. Post-eruption hydrology and sediment discharge at the Miyakejima volcano, Japan. *Zeitschrift für Geomorphologie Supplementary*, **140**, 55–72.

Yamamoto, T., Takarada, S. and Suto, S. 1993. Pyroclastic flows from the 1991 eruption of Unzen volcano, Japan. *Bulletin of Volcanology*, **55**, 166–175, https://doi.org/10.1007/BF00301514

Yamamoto, T., Nakamura, Y and Glicken, H. 1999. Pyroclastic density current from the 1888 phreatic eruption of Bandai volcano, NE Japan. *Journal of Volcanology and Geothermal Research*, **90**, 191–207, https://doi.org/10.1016/S0377-0273(99)00025-6

Ye, L., Kanamori, H., Rivera, L., Lay, T., Zhou, Y., Sianipar, D. and Satake, K. 2020. The 22 December 2018 tsunami from flank collapse of Anak Krakatau volcano during eruption. *Science Advances*, **6**, eaaz1377, https://doi.org/10.1126/sciadv.aaz1377

Yoshida, H. 2013. Decrease of size of hummocks with downstream distance in the rockslide-debris-avalanche deposit at Iriga volcano, Philippines: similarities with

Japanese avalanches. *Landslides*, **10**, 665–672, https://doi.org/10.1007/s10346-013-0414-4

Yoshida, H., Sugai, T. and Ohmori, H. 2012. Size–distance relationships for hummocks on volcanic rockslide-debris avalanche deposits in Japan. *Geomorphology*, **136**, 76–87, https://doi.org/10.1016/j.geomorph.2011.04.044

Zehfuss, P.H., Atwater, B.F., Vallance, J.W., Brenniman, H. and Brown, T.A. 2003. Holocene lahars and their by-products along the historical path of the White River between Mount Rainier and Seattle. *In*: Swanson, T.W. (ed.) *Western Cordillera and Adjacent Areas*. Geological Society of America Field Guide, **4**, 209–223.

Zernack, A.V. and Procter, J.N. 2021. Cyclic growth and destruction of volcanoes. *In*: Roverato, M., Dufresne, A. and Procter, J. (eds) *Volcanic Debris Avalanches: from Collapse to Hazards*. Springer Nature, Switzerland, 311–355.

Zernack, A.V., Cronin, S.J., Neall, V.E. and Procter, J.N. 2011. A medial to distal volcaniclastic record of an andesite stratovolcano: detailed stratigraphy of the ring-plain succession of south-west Taranaki, New Zealand. *International Journal of Earth Sciences*, **100**, 1937–1966, https://doi.org/10.1007/s00531-010-0610-6

Zheng, S., Wu, B., Thorne, C.R. and Simon, A. 2014. Morphological evolution of the North Fork Toutle River following the eruption of Mount St. Helens, Washington. *Geomorphology*, **208**, 102–116, https://doi.org/10.1016/j.geomorph.2013.11.018

Zimanowski, B., Büttner, R., Dellino, P., White, J.D.L. and Wohletz, K.H. 2015. Magma – water interaction and phreatomagmatic fragmentation. *In*: Sigurdsson, H., Houghton, B., Rymer, H., Stix, J. and McNutt, S. (eds) *The Encyclopedia of Volcanoes*. Academic Press, 473–484.